MICROFLUIDIC SYSTEM FOR THROMBOSIS UNDER

MULTIPLE SHEAR RATES AND PLATELET THERAPIES

A Thesis
Presented to
The Academic Faculty

by

Melissa Li

In Partial Fulfillment
of the Requirements for the Degree
Doctor of Philosophy in the
School of Biomedical Engineering

Georgia Institute of Technology
August 2013

MICROFLUIDIC SYSTEM FOR THROMBOSIS UNDER MULTIPLE SHEAR RATES AND PLATELET THERAPIES

Approved by:

Professor Craig R. Forest, Advisor
Woodruff School of Mechanical
Engineering
Georgia Institute of Technology

Professor Jeremy D. Ackerman
School of Medicine
Emory University

Professor David N. Ku
Woodruff School of Mechanical
Engineering
Georgia Institute of Technology

Professor Rudolph L. Gleason
Wallace H. Coulter Department of
Biomedical Engineering
Georgia Institute of Technology

Professor Manu O. Platt
Wallace H. Coulter Department of
Biomedical Engineering
Georgia Institute of Technology

Date Approved: 1 May 2013

ACKNOWLEDGEMENTS

This work is indebted to the contributions of many. Foremost to my advisor, Craig R. Forest, for his guidance and boundless enthusiasm throughout this project. It's been a pleasure to be part of his research team and to share in its growth and success over the years. Craig's passion for innovation, improvement, and collaboration coupled with his enthusiasm and support have been a huge part of the success of this work. Thanks to Prof. David Ku for providing his academic acumen and formidable knowledge and expertise in this field to the project. Thanks also to my committee members Prof. Jeremy Ackerman, Prof. Rudy Gleason, and Prof. Manu Platt for their thoughtful comments, suggestions, and discussion.

Thanks to the past and present researchers of the Precision Biosystems Laboratory over the years from its graduate students (Christopher Phaneuf, Nikita Pak, Suhasa Kodandaramaiah, Curtis Saunders, Gregory Holst, Caitlin Henegar, John Glisson, and William Stoy) to its undergraduate students (Michael Dergance, Daniel Shenoda, Matthew Emerick, Nicholas Sondej, Michael McKinnon, and Jamison Go), all of whom I care deeply for and who have all been great friends and teachers. Of these, special thanks to Nikita Pak for design advice, machining assistance, and for constituting the best part of Team Half-Human Half-Walrus. To Curtis Saunders for sage counsel and historical un-trivia. To Suhasa for assistance with optics fabrication and his devotion to the scientific life. To PBL's founding member, lab manager, and mainstay of Black Rock City, Christopher Phaneuf for patient instruction and assistance in CAD, CAM, machining, exceptional design sense, pragmatism, and bicycle advocacy. To "Team Heart-Thromb" (Randy Hefelfinger, Siddharth Gurnani, Oscar Martinez, Pranav Ghandhi, and Nicholas Turitto) for their hard work and amazing progress on

TABLE OF CONTENTS

LIST OF TABLES

LIST OF FIGURES

SUMMARY

Thrombosis is the pathological formation of platelet aggregates that cause stroke and heart attack—the leading causes of death in developed nations. Determining effective dosages for platelet therapies (e.g. aspirin, Integrilin, and Plavix) to prevent thrombosis is a persistent medical challenge (studies estimate up to 45% of patients exhibit insufficient responses to these drugs) and recent studies have implicated pathological flow conditions of high shear rates and stenosis morphology as primary factors. However, there are currently no diagnostic instruments able to recapitulate a range of such pathological flow conditions for evaluating thrombosis with and without these drugs.

In this work, a microfluidic device and associated optical system were designed and fabricated for simultaneous measurement of platelet aggregation at multiple initial wall shear rates within multiple stenotic channels in label-free whole blood and used to characterize thrombosis at varying dosages of two platelet therapies: acetyl-salicylic acid (aspirin) and eptifibatide (Integrilin).

Results from our studies show the effects of pathologically high shear rates on enhancing platelet thrombosis and demonstrate the widely varied, shear-dependent efficacy of each therapy. This study lays the foundation for the future development of a medical diagnostic for optimizing the type and dosage of patient platelet therapy and to better understand their mechanisms of action.

CHAPTER I

INTRODUCTION

Thrombosis is the pathological formation of platelet aggregates that occlude blood flow causing stroke and heart attack —the leading causes of death in developed nations. Heart attacks, also known as myocardial infarction, are caused when platelet aggregates, or thrombi, are formed within the coronary arteries to occlude flow. Stroke, or cerebrovascular accident, are often caused when thrombi migrate to the small vessels of the brain and occlude flow.

Each of these thrombosis-induced conditions presents a dramatic burden to mortality, morbidity, and health care costs. In mortality, recent reports have estimated that in 2007 alone 785,000 Americans experienced a new coronary attack, 470,000 experienced recurring attacks, and an additional 195,000 may have experienced silent attacks. The same report estimates morbidity from 610,000 new, 185,000 recurring, and 195,000 silent stroke cases in the same year. While not all of these heart attacks and strokes were fatal, they still accounted for an estimated 1 in every 3 deaths in the United States, approximately 813,804 [7].

Resultant costs of prevention and care for stroke, heart attack, and related cardiovascular conditions for affected Americans was estimated at $286 billion for the same year of 2007, a figure which includes direct cost of medical care and indirect costs due to lost productivity. This figure far exceeds its closest competitor, cancers and benign neoplasms, whose direct and indirect costs are estimated at $228 billion [7].

With such costs, improved instrumentation for diagnosing and treating pathological platelet aggregation has the potential for major clinical impact. Currently, the

mainstay for thrombosis prevention without other treatable causes or risk factors is therapy including aspirin and/or an additional anti-platelet agent (e.g. eptifibatide, clopidogrel), a choice that balances the patient's risk of severe thrombotic events against the risk of GI discomfort and bleeding. This choice is often made empirically and without measurement of dosing or efficacy (i.e. appropriate platelet inhibition). Patients are determined to have failed therapy if they have a vascular event while being treated; then either increased dosing or combination therapy is initiated.

Thus this section of the thesis will review the structure and function of platelets and key receptors targeted in anti-platelet therapies. It will then provide a survey of the current methods for measuring and understanding platelet behavior, and finally it will outline the goals that we aim to achieve in this study.

1.1 Platelets

Although platelets compose only 1% or less of blood (by volume), they are vital to wound healing, during which they adhere to the site of injury and participate in the complex cascade of events involved in blood clotting. Under normal conditions, circulating platelets are discoid, anuclear cells 2-3 μm in diameter and are present in concentrations on the order of of 200,0000—400,000 cells per milliliter of blood. Platelets originate from megakaryocyte cells within bone marrow, each of which can produce thousands of platelets that will remain in circulation for approximately ten days. Key features of the platelet's structure and function include a variety of externally presented surface receptors as well as internally stored clotting factors. External surface receptors such as GPIb and GPIIb/IIIa allow platelets to rapidly adhere to sites of injury and to one-another, respectively. Specifically, adhesion is primarily mediated by the bond between GPIb and von Willebrand Factor ("vWF", located suspended in blood serum and released from other platelets) and collagen (a common structural protein in blood vessels and extra-cellular matrix). In contrast, GPIIb/IIIa

is thought to primarily bind to fibrinogen and vWF, both found in other platelets as well as suspended in blood serum. In addition to these surface receptors, platelets also internally store and release clotting factors in alpha- and dense- type vesicles (also known as granules for their appearance under electron microscopy) each of which store different types of factors. Alpha granules predominantly store fibrinogen, cytokines, growth factors, and von Willebrand Factor (vWF) while dense granules store adenosine diphosphate (ADP), serotonin, and calcium. Release of these factors from the interior of the platelets induces other nearby platelets to release their granules in a positive feedback wave. The contents of these granules has been observed to induce shape changes in platelets from their normally smooth and discoid shapes, to activated states in which they flatten and form pseudopod spines [8].

Platelets can stop the flow of blood by two different methods: coagulation and thrombosis. Coagulation occurs primarily under conditions of low fluid shear (below 1500 s^{-1}) and requires the activity of a number of clotting factors found in blood serum to form nets of fibrin which entrain platelets and red blood cells, in a red clot. In contrast, thrombosis generally occurs at higher shear rates (exceeding 1500 s^{-1}), and is mediated primarily by platelets in a white clot. Under these high shear conditions, this process has been shown to occur in three phases: (I) initial adhesion of platelets to a substrate, (II) the rapid accumulation of platelets binding to other platelets and (III) the final stabilization and contraction of the platelets into a solid mass that occludes flow [9, 10]. Thus it is clear that a deeper understanding of how flow affects these different methods of platelet activity is necessary to optimize therapy and prevention.

1.2 Platelets in flow

Blood is a complex fluid with some novel hemodynamic properties based on its particulate nature. First, the viscosity of blood varies with local shear rate, and as flow

rate and shear rate increase, the viscosity of the blood will decrease. Additionally, blood can separate into two phases, one particle-rich layer filled with cells, and the other a relatively acellular plasma layer near the vascular wall [11].

This layer is not completely acellular, however, and is sometimes populated with platelets and leukocytes which have been displaced from centerline flow by red blood cells, whose deformability allows them to centrally migrate. This process of "margination" enhances platelet adhesion to the walls of the vessel and to other platelets. While many researchers are aware of this phenomenon, it remains difficult to account for in experimental assays. In this study, we assume constant viscosity (Newtonian fluid), and acknowledge the under-estimation errors associated with the assumption.

Under this Newtonian assumption, we can calculate a parameter frequently used to characterize flow is shear rate, γ, as:

$$\gamma = \frac{\delta V}{\delta x} \tag{1}$$

Where V indicates local velocity and x indicates distance from the wall. Previous work has described three specific shear flow regimes within the body and their associated binding mechanisms. The lowest range, from 100 to 1500 s^{-1} found in unobstructed veins and arteries, is primarily governed by fibrinogen, coagulation factors, and the GPIIb/IIIa (also known as integrin $\alpha_{IIb}\beta_3$). Next, from 1500 to 4000 s^{-1} found in arterioles, primarily governed by GPIb, GPIIb/IIIa, and soluble agonists such as ADP. And the final regime describing higher pathologic shear found in stenotic or obstructed arteries with shear rates above 4000 s^{-1} and above, primarily governed vWF and GPIb [12, 4, 13]. Such conditions are found in constricted arteries, such as those commonly observed in clinical cases of coronary artery disease and atherosclerosis, conditions which affect more than 17 million Americans [10, 9, 14, 15, 16].

High shear rates are thought to affect thrombosis in the following ways. First, it regulates how many platelets, soluble coagulation factors, and fibrinogen molecules pass near the adhesive surface of the vessel wall over a period of time. Second, high

4
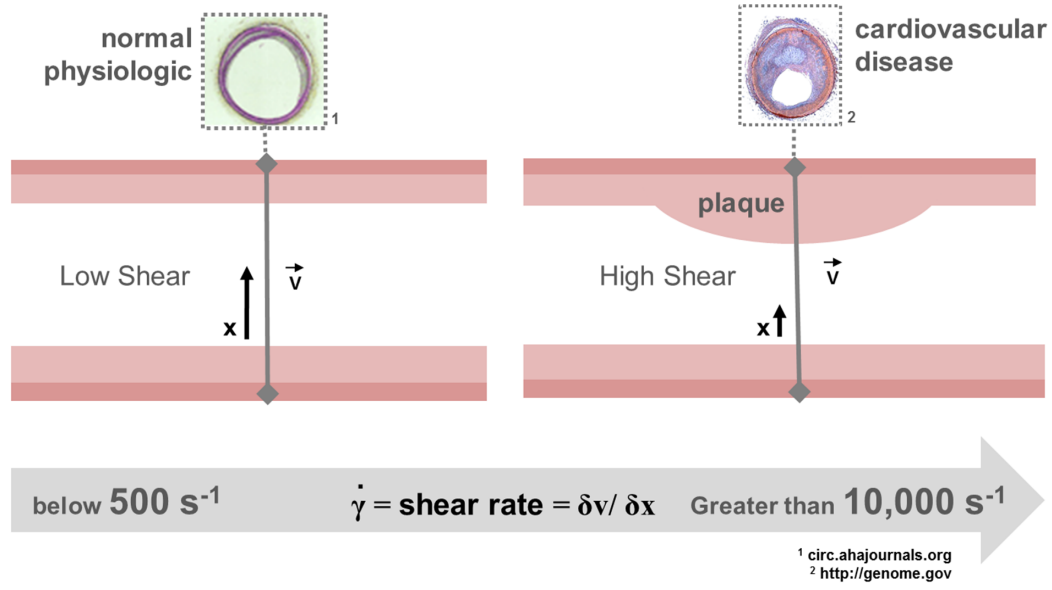
Figure 1: Normal, physiologic flow conditions in healthy, non-constricted arteries exhibit lower shear rates compared with pathological flow conditions induced by local constrictions commonly caused by coronary artery disease and atherosclerosis. Shear rate can be expressed by the change in velocity, v, over the change in radius, x, shown in the diagram.

shear rates have been found to enhance the adhesive behavior of specific proteins such as the GPIb receptor and von Willebrand Factor [17, 18, 19]. Next, it determines the residence time during which reactive soluble factors and related species can affect one another. Finally, increased shear rates and increased shear forces can detach platelets from eachother or from surfaces such as the vessel wall, creating an embolus.

1.3   Platelet therapy

A number of different types of therapeutics have been developed for the treatment of thrombosis according to the previously discussed flow regimes. Platelet drug therapies have been developed to disable specific targets of each of these aforementioned three mechanisms including: GPIIb/IIIa inhibitors (eptifibatide, abciximab), soluble agonist inhibitors (clopidogrel, acetylsalicylic acid), and anti-coagulants (heparin,

citrate) [4]. A multi-shear approach to screening anti-platelet efficacy could thus provide salient information on shear-dependence to guide clinicians to choose appropriate drugs and dosages for patients with potential arterial pathologies, or to aid in the process of industrial drug candidate screenings [4].

Thus local shear conditions and flow patterns can enhance or diminish specific mechanisms affected by anti-platelet therapies. Investigations in this area can lead to enhanced knowledge of both platelet behavior and to pre-clinical drug efficacy screenings.

These drugs have provided invaluable rapid therapy, but they have a major flaw: patient responses vary widely, leading to potentially severe consequences. Under- and over- dosing of these medications can result in ineffective treatment, excessive bleeding, severe gastric discomfort, or death. Despite these dangers, clinicians are unable to determine how effective a medication is and thus employ a generic solution when prescribing these drugs.

As a result, out of the current 68 million Americans taking anti-platelet drugs, more than 15 million are misdiagnosed with the dosage or the wrong drug and constitute one of the four top drug types causing hospitalization in senior citizens [7, 20, 21]. Thus what is needed is a method to quantify platelet function to measure the efficacy of these drugs and their varying dosages. Currently a number of companies are attempting to commercialize such diagnostic methods, discussed in detail in the next section . While their efforts have tested poorly in clinical trials, they have demonstrated a market size of $3 billion for anti-platelet diagnostics [2, 11, 22, 23].

A rapid, inexpensive, clinical test for efficacy of anti-platelet therapies would be desirable for a variety of reasons. First, a test of efficacy may allow improved dosing of these agents, since dosing of these agents is done in fixed amounts that are not dependent on blood volume or platelet activity. Second, such a test would help to

identify patients that do not respond to anti-platelet therapy. Although this population has been identified in the literature, the mechanism of unresponsiveness is unclear—whether due to under dosing, misuse (or non-compliance) of medication, or underlying physiologic differences.

1.4   Platelet function testing

As outlined by the previous sections, platelets not only play a crucial role in wound healing and primary hemostasis, but are also a key part of a growing public health burden presented by thrombosis [7]. Thus methods for measuring and assessing platelet function are an area of significant interest. To this end, a wide variety of platelet function tests exist, although none have been developed.

The goal of this section is to provide a description of each method, identify the strengths and weaknesses of each, and to provide a brief history on its clinical successes and failures.

1.4.1   Flow cytometry

Flow cytometry is a popular method for measuring platelet function since the whole blood cytometer can be used for such a wide variety of standardized clinical laboratory measurements. This technique is often used for targeted cell or receptor counts after the administration of fluorescently labelled monoclonal antibodies. The method works by flowing a thin, focused stream of single cells through a laser beam, which evaluates cell types through forward scattering, which provides information on the shape of each passing cell. Additional fluorescence detectors can provide information on additional targets of interest.

The platelet function assays using flow cytometry and antibody labelling include the popular VASP kit (BioCytex, Marseilles, France) which can provide absolute quantification of the number of receptors and the ability of therapeutic drugs to bind them using only a small amount of blood (less than 1 mL) for each test [24]. The

VASP (vasodilator–stimulated phosphoprotein) phosphorylation assay, which is used to test whether therapeutic drugs can bind the P2Y12 receptor, the main target of clopidogrel (Plavix) through the conversion of the vasodilator-stimulated phosphoprotein phosphorylation (VASP) protein to its phosphorylated form (VASP–P), determined using an antibody for the latter and measuring the resultant fluorescence [20]. Recent studies have demonstrated PRI cutoff values of 48-53% as prognostic indicators for stent thrombosis following coronary percutaneous interventions, and others have reported that clopidogrel loading doses adjusted according to PRI values $< 50\%$ decreased the rate of major adverse cardiovascular events after PCI [25]. However, results from the VASP kit tests have shown poor correlations with results from other popular testing methods (i.e. the VerifyNow, and light transmission aggregometry), suggesting that the definition of "clopidogrel resistance"is very test dependent. Thus a more clinical testing and tracking of patient outcomes may be required for future development and validation of this method [26].

Unlike other methods, flow cytometry allows for integrated measurements of other important elements of blood including vWF titers, levels of coagulation factors in the blood, platelet count, mean platelet volume, mean corpuscular volume, red blood cell count, hemoglobin concentration, white blood cell count, etc. The machine enables the acquisition of a wide variety of platelet metrics for a very complete set of clinical data.

The disadvantages of method are its lack of clinical correlates for patient outcomes, or for correlates with similar platelet function analysis methods. In addition, flow cytometry faces additional challenges from its requirements for trained personnel, and from time–consuming and labor–intensive sample preparation. [24].

1.4.2 Bleeding time

Bleeding time is one of the oldest assays for platelet function, and is performed completely in-vivo. A small blade (often spring loaded or otherwise mechanically enabled to make standardized cut sizes), makes a small incision into the skin and blood pressure at the wound site is monitored to indicate when bleeding ceases due to platelet activity. The output of the test is the time needed for the wound to stop bleeding, and is typically performed in triplicate.

Clinically, the BT assay has shown poor sensitivity to platelet therapies and is not often recommended for use in most clinical settings due to its aforementioned variability. However it has shown great clinical utility for the diagnosis of vascular disorders such as Ehlers Danlos (a condition which affects collagen production), as well as low platelet count or hematocrit [27].

Advantages of the method are its simplicity and low associated costs. Its *in–vivo* application makes it one of the only test methods able to reflect the interactions of the vessel wall with a subject's platelets and results are thus very physiologically relevant [28, 20].

Disadvantages of the method are thus its low responsiveness to platelet therapies, poor reproducibility, invasiveness, and the numerous sources of variability including skin temperature, skin thickness, consistency of wound depth, and subjective measurement of bleeding cessation [29].

1.4.3 Light transmission aggregometry

Light transmission aggregometry (LTA) was first developed in the 1960s by Born, who noted visible turbidometric changes in a solution of PRP (platelet rich plasma) after the addition of the agonist adenosine diphosphate (ADP).

The method requires a sample of platelet rich plasma (PRP), which is prepared by centrifuging a sample of whole blood. The resultant platelet rich plasma is placed

in a clear, heated (37°C) cuvette with a small stir bar atop a magnetic stirring plate. Platelets are activated through the addition of an agonist (e.g. ADP, ristocetin, botrocetin, collagen, arachidonic acid, thrombin, epinephrine), after which the stir plate begins to rotate the stir bar to generate shear forces and to mix the contents of the cuvette. Platelets first change shape, causing a small increase in sample turbidity, and then begin to aggregate and precipitate out of solution, reducing the turbidity of the solution. These platelet-platelet bonds underlying aggregate formation are thought to be due primarily to the activation of the GPIIb/IIIa receptors [20].

Currently the oldest and most tested method of platelet function testing, and is a general comparison standard against which results from all other methods are compared [24, 20, 4]. Advantages of this method are the preponderance of clinical data describing its clinical efficacy, the ability to make dynamic measurements in real-time, and the ability to discern multiple important binding events (platelet cohesion and platelet shape change). The advanced age of this method has allowed long term studies to document statistically significant, nearly threefold increases in endpoint risks of major adverse effects associated with aspirin resistance as diagnosed using LTA with ADP and arachidonic acid agonists [30]. Additional studies have shown the utility of the LTA method to diagnose platelet disorders and generalized "bleeding disorders" [31].

Disadvantages of the method are primarily due to the need for PRP instead of whole blood–a process which is time consuming, labor intensive, potentially detrimental to the sample, non-physiological use of small enclosed cuvette volumes, poorly reproducible, requires large sample volumes, and results lack standardization for stir speed, size of stir bar, size of cuvette, etc. Furthermore, the stirring activity creates variable shear rates within the cuvette which may skew results $\sim 300\text{s}^{-1}$ [20, 25, 4, 32]

These disadvantages have led to more user-friendly devices aimed at point-of-care applications including the VerifyNow, and the impedance-based Whole Blood

Analyzer, both of which are discussed in greater detail below.

1.4.4 VerifyNow

To date, Accumetric's VerifyNow is perhaps the most commercially successful point-of-care platelet diagnostic. Founded in 1996, the product has been successfully marketed as a point-of-care diagnostic for small clinics and hospitals. The device is a modified form of the LTA assay which addresses some of the LTA's greatest weaknesses with the ability to use whole blood samples, and does not require additional pipetting due to its use of enclosed cartridges pretreated with reagents and able to perform automated aspiration steps.

Like the LTA method, the VerifyNow depends on the platelet-platelet cohesion. Unlike LTA, whole blood is able to be used in this device due to the addition of fibrinogen coated glass or latex particles whose wavelength is measured over time to indicate aggregation. Thus when platelets bind to the fibrinogen coated beads, they begin to precipitate the beads out of solution and transmission increases. Testing only requires the addition of a small volume of blood (<1 mL) anticoagulated using citrate and a cartridge loaded into the machine to begin. Blood is automatically aspirated up into the machine, and a magnetic bead stirs the blood with the cartridge-specific agonist and coated beads, and light transmission readings begin. Results are available within only 2-5 minutes. Outputs of the test are "platelet reactive units" (PRU) which use cutoff values for a binary detection of "high on" or "normal". Currently, the test sells three different types of cartridges for the detection of GPIIb/IIIa antagonists (using thrombin-receptor-activated protein (TRAP)), aspirin (using Arachidonic Acid), and clopidogrel (using ADP/PGE1). In addition, the test has shown some utility for detection of [25, 20].

The VerifyNow has an extensive background of clinical studies to back up its *in-vitro* results for GPIIb/IIIa, aspirin/ASA, and clopidogrel. Its GPIIb/IIIa assay kit,

the first of its cartridges on the market, has shown results with excellent agreement to other methods including LTA and flow cytometry, and good consistency in its results from site to site [33, 34]. The GOLD center study, a large scale clinical trials of over 500 human subjects, showed a high correlation between adverse patient outcomes and low response values from the VerifyNow using the GPIIb/IIIa test kit with long-term patient major adverse cardiac events (MACE's: composite of death, myocardial infarction, and urgent target vessel revascularization), implying that the assay might be useful for diagnosing resistance to GPIIb/IIIa drugs [35].

The VerifyNow aspirin assay uses arachidonic acid as agonist and to detect resistance to acetyl salicylic acid (ASA) effects. The test has been shown correlates well with AA-induced LTA [36] and is associated with an increased risk of adverse clinical outcomes in stable patients with coronary artery disease [37].

The VerifyNow clopidogrel assay is a two channel cartridge which measures P2Y12 platelet activity using the agonists ADP and prostaglandin–1 (PGE1) in one cartridge channel, and measures global platelet activity using TRAP (thrombin receptor activating peptide) and PAR4-AP (PAR4 activating peptide) in a second cartridge channel.

In prospective study the PRU values on clopidogrel (12 h post-loading of 600 mg) of 380 patient undergoing PCI were used to derive a optimal cut-off value of ≥ 235 PRU for post-treatment reactivity in predicting six month out-of-hospital cardiovascular (CV) death, non-fatal MI, or stent thrombosis [38]. Using the clinical cut-off, patients with high post-treatment reactivity had significantly higher rates of CV death, stent thrombosis, and the combined endpoint. These results were confirmed by a study in 683 patients with acute coronary syndrome undergoing dual-antiplatelet therapy during a percutaneous coronary intervention [39]. With the optimal cutoff value of ≥ 240 PRU could be used to predict significantly higher rates of cardiovascular death, stent thrombosis, or non-fatal myocardial infarction during a twelve month

post-treatment observation period [39].

Despite these success, other trials have not been as positive. The GRAVITAS clinical trial examined over 1100 human subjects over a six month period after surgical intervention and subsequent treatment with Plavix. The VerifyNow was used to determine whether it could successfully predict an optimal patient dosage (high or standard concentration treatment). Results showed that there was no significant difference in patient outcomes between VerifyNow's predicted optimal treatment and the standard concentration treatments. This was a disappointing development both for platelet function analyzers, for whom the VerifyNow has been the strongest demonstration of potential capabilities, and for the manufacturers of Plavix, who had hoped to demonstrate enhanced product efficacy [38, 40].

In summary, the advantages of the method are its small sample volumes, user-friendly interface, and easy to interpret results. Standardization of results is also much improved from LTA due to its extra automation and minimal sample handling. Clinically, it has shown some predictive ability for adverse MACE's in some patients using ASA, GPIIb/IIIa inhibitors, and clopidogrel. However, it has not shown the ability to adjust patient dosages to optimal amounts to avoid these adverse events.

There are a number of disadvantages to the test as well. First, the method itself does little to recapitulate the pathological conditions that it attempt to diagnose. Like the LTA, the device is only able to measure low– or no– shear flow conditions due to its enclosed cartridges. This means that it ignores several key bonding evens including vWF to GPIb, one of the primary mediators of high shear thrombosis [4]. The test also requires the use of non-physiological agonist agents, which may confound or distort correlations with clinical results. Additional disadvantages of the method are its high per–test cost ($\sim$ \$ 40-60 per single cartridge) likely due to its user-friendly features including the enclosed, automation-friendly, reagent storage and specialized bead manufacture, especially in comparison to the cost of a single cuvette and stir

bar required for similar results from an LTA assay. Similar to other tests, the test is also limited to a specific defined range of hematocrit and platelet count [20].

1.4.5 PFA-100

With these concerns over flow integration into the assay in mind, we address the platelet function analyzer for the high shear regime, the Platelet Function Analyzer (PFA–100), developed by Siemens Healthcare Diagnostics.

The PFA–100 tests platelet function under high shear rates ($\sim$4000-6000 s^{-1}) within different disposable cartridges, and is intended for a laboratory/research environment. The machine consist of a number of integrated parts including a capillary, a sample reservoir and a porous membrane. During a test, 800 μL of whole blood with 0.109 or 0.129 mol/l buffered sodium citrate is aspirated at a constant pressure from the sample reservoir through a capillary ($\sim$ 500 μm) blocked by a the disposable biochemically active porous cellulose membrane with a central aperture of 100 μm (P2Y) or 150 μm (Col/ADP, Col/EPI). Part dimensions are defined by information provided by the company [41], but further information on tolerances for dimensions are not available. A variety of different disposable biochemically active membranes are available, including: collagen and ADP (Col/ADP), collagen and Epinephrine (Col/EPI), and ADP, prostaglandin, and calcium chloride (P2Y).

At the beginning of each test, trigger solution is dispensed on the membrane to dissolve the reagents. The blood sample is then aspirated up through the capillary and through the aperture and the membrane. As the sample passes through the aperture, platelets will begin to adhere to the coated cellulose surface. Due to the interaction with the membrane and the dissolved reagents, platelets become activated, release their granule contents, and start to aggregate. Over the duration of the test (300 seconds, or 5 minutes), platelets will continue to form a plug until occlusion of flow.

14

These activators and cartridge conditions cause platelet adhesion to the membrane, activation of the platelets and aggregation, followed by a platelet plug formation in the area of the aperture. Thus, the test end point is the time to aperture occlusion and the resulting cessation of blood flow, closure time (CT), or non-closure (NCT) when CT is greater than 300 seconds.

The PFA–100 allows a simple and standardized test performance. However, different concentrations of anticoagulants, sample collection, transportation, conditions and time window between sampling and testing may influence CT [42]. Thus, establishing individual reference values has been recommended.

Moreover, CT values inversely correlate with a decreasing hematocrit less than 30% and a decreasing number of circulating platelets of less than 100×10^9 . Therefore, knowledge of the actual platelet count and hematocrit are essential for the interpretation of the CT results . Furthermore, it is important to realize that CT values increase with decreased vWF activity. Apart from any disease entity, this may be related to the effect of the ABO-blood group system on vWF activity (lowest activity can be observed in patients with blood group O) [39].

The PFA-100 is one of the most widely used and studied platelet function tests with more than 600 publications in peer review journals. It offers tests for diagnosing the following: clopidogrel (using the agonist adenosine diphospate —ADP), ASA (using the agonist arachidonic acid), GPIIb/IIIa antagonists (using the agonist Thrombin Receptor Agonist Peptide—TRAP), general thrombosis disorders (using collagen), and von Willebrand's disease (using the agonist ristocetin) [25].

Due to the low cost and accessibility of aspirin, it has been a primary target of numerous studies with this instrument [43, 44]. Although aspirin does show increases in average CT values [45] it is still far less specific than other marketed devices at detecting "aspirin resistance". In fact, the prolongation effects observed may be closer

related to patients taking other types of anti-inflammatory drugs, and not to specifically anti-platelet effects [30]. This deficiency has been a high hurdle for acceptance of this instrument in the healthcare community, especially given the relative successes of other methods such as the previously discussed LTA, VerifyNow, and WBA units. Notably, the use of epinephrine in the C-EPI cartridge for the detection of aspirin uncommon in contrast to the use of arachidonic acid assays, the agonist which is used in the aforementioned competitors' assays. Some studies have shown that arachidonic acid is ineffective as an agonist in their assay, supporting the theory that inhibitors of soluble factors have little effect at high shear rates such as those within their device [46]. The company has embarked on a number of large scale clinical studies on thousands of subjects [47, 48] attempting to find correlations of their test with aspirin sensitivity, but to date has not been very successful. They have, however, identified what they believe to be various independent factors influencing non-response as defined by C-EPI, specifically old age, an acute vascular event, chronic ASA usage, the ASA dosage, diabetes mellitus, the concentration of buffered sodium citrate, and cut-off time used to determine abnormal CT.

The second most popular target is clopidogrel (Plavix). The detection of platelet inhibition by clopidogrel has not been shown to be reliable for both the C-EPI and the C-ADP activation, but a new cartridge for the assessment of the anti —P2Y12 effect will be available for broad clinical applications [49]. However, the PFA-100 may help to monitor therapy with GP IIb/IIIa antagonists [50].

Although the PFA-100 has not been able to match current competitors on the detection of aspirin and clopidogrel, it has been successful in detection of von Willebrand disease (vWD), with an estimated 90% sensitivity [51] Additionally, very short or shortened Col/ADP CT has also been identified as a potential marker for platelet hyperreactivity or hyperfunction, which is present in patients suffering from

16

an acute myocardial infarction, an acute coronary syndrome or stable angina, stable cardiovascular disease patients with increased risk of major adverse events, ASA non-responders or patients with genetic polymorphisms associated with a heightened platelet reactivity.

Close monitoring of the successes and failures of the high-shear PFA–100 are especially valuable to this project, which seeks to characterize shear-induced effects on anti-platelet efficacy. Combined with information on low- or zero- shear devices like the LTA and VerifyNow, their studies often span large populations of subjects which are often inaccessible to academic researchers, thus their efforts have to the potential to advise directions for our work.

1.4.6   Impedance aggregometry

Impedance aggregometers measure changes in electrical impedance due to the buildup of platelets on the surface of two noble metal electrodes after the administration of select platelet agonists. Currently, the most popular commercial impedance aggregometers are the Whole Blood Analyzer (Chronolog, Haverton PA) and the Multiplate system (Dynabyte, Munich, Germany). Each unit is available in a multichannel format (1-4 channels from Chronolog, 1-5 channels from Dynabyte). The process of testing is the same as LTA, although measurements are electrical instead of optical. The Whole Blood Aggregometer is composed of a pair of electrodes, a stirring element, and a heating element. A 500 μL blood sample is added to an equal amount of saline, an electrode, and a small stir bar in a cuvette, and warmed for approximately five minutes at 37°C. The sample is then ready to be placed in the testing chamber, which has a rotating magnet that will spin the stir bar in the cuvette. The test will be able to begin when the electrode has been able to establish a consistent baseline. At that point, a chosen agonist is added to the cuvette, and the stir bar both distributes the agonist throughout the sample, and also provides a local shearing force on the

17

blood. Activated platelets then adhere to the electrode, and the impedance will rise in accordance with the coverage of the electrode by platelets in the sample. The machine has three primary outputs used to describe its measurements of impedance due to platelet adhesion over time: Lag Time (the time period before impedance passes 2 Ohms), Amplitude (the maximum change in impedance over the timecourse of the trial), and Area Under the Curve (the integral of the impedance over time) also called the "AUC". The Multiplate system shares the basic characteristics and limitations with the whole-blood laboratory-based aggregometer systems. This system is nearly identical to the Whole Blood Analyzer, except that it does not require washing of the electrodes and also adds computerized electronic pipetting of the activators and adds duplicate measurements to enhance reproducibility.

A primary advantage of the device is able to use whole blood instead of the PRP required for LTA, thus avoiding additional sample handling and potential activation of the platelets and improves method standardization. Second, the multichannel formats offered provide exceptional experimental throughput. The method also provides outputs on the dynamics of aggregation, unlike the VerifyNow or PFA–100 which simplifies its measurements to a single number. Finally, many of these methods offer affordable base unit costs ($\sim$\$4000-7000) and similarly affordable per-test costs (\$0.03 − \$5.24).

Disadvantages of the method are its poor ability to assess surface binding, its closed volumes, and its non-physiological flow conditions. Additionally, each test requires some cleaning of electrodes, and electrodes which have been improperly cleaned can lead to errors in results (see Chapter 5), although this problem has been remedied in the Multiplate through the use of disposable ready-to-use test cells with two independent sensor units consisting of two silver-coated copper electrodes.

Despite these disadvantages, the WBA has been quite successful in detecting congenital and acquired platelet disorders and in monitoring the familiar anti-platelet

targets of aspirin and clopidogrel. In a study including 182 patients after PCI those identified as dual non-responders to acetylsalicylic acid and clopidogrel by WBA induced by ADP and collagen were at higher risk (relative risk 2.57; 95% CI 1.185.61; log-rank p= 0.03) to suffer from a combined primary endpoint of myocardial infarction, target vessel revascularization, late stent thrombosis, or cardiac death. A number of tests are available including: clopidogrel (ADPtest and ADPtest HS), acetylsalicylic (arachidonic acid), GPIIb/IIIa antagonists (TRAPtest), general activity tests using collagen (COLtest), and von Willebrand's disease (vDWD) [25].

1.4.7   Perfusion chambers

Unlike the methods discussed thus far, perfusion chambers attempt to incorporate biomimetic flow conditions into their assays. Generally they can be categorized as cylindrical tubes or rectangular channels. The former were popularized by H. R. Baumgartner's *ex-vivo* studies with human blood taken from the antecubital vein, or *in-vivo* in rabbits [52]. In contrast to simple collagen coatings of glass surfaces, perfusion chambers often use biological substrates such as subendothelium of rabbit aorta, human renal arteries, or human umbilical arteries. Popular end-point measurements are radiometry of deposited radio-labelled platelets on thrombus forming surfaces while continuous tests often monitor pressure drop over a segment of interest in testing for thrombus formation [18]. More recently, this principle has been applied to the Badimon chamber, a flow channel lined with porcine vascular tissue which is examined by microscopy and/or post-testing histology for platelet accumulation [53].

In rectangular cross-section flow channels, the parallel plate chamber is a popular tool for characterizing shear induced behaviors. The first parallel-plate perfusion system was developed in the early 1980s by K. S. Sakariassen and colleagues [18], and remains a popular method for drug efficacy screenings in the early development stage [54]. This device has been employed in many studies with human and animal in vitro

anti-coagulated blood, in ex vivo studies in man and in in vivo studies in dogs. A rectangular flow slit with different heights, allows studies at different wall shear rates at a constant flow rate, thus analogous to the annular chamber. During the mid-1990s, R. M. Barstad and colleagues introduced various eccentric stenoses into the flow channel of the chamber [55]. This results in rapidly increasing wall shear rates from 420 up to 32,000 s^{-1}. A variation to be mentioned is the so called Hele-Shaw perfusion chamber developed by S. Usami and colleagues [56] which allows studies at continuous shear variation from virtually 0 to 20,000 s^{-1} in one perfusion run. Common measurements using this instrument are radiometry of radio-labelled platelets, en-face morphometry, confocal microscopy, standard morphometry, computer-assisted morphometry and immunologic quantification of deposited fibrin and platelets following plasmin digestion of the thrombotic deposits. A variety of biomarkers released by activated platelets, protease cleaved activation peptides from coagulation factors, FPA, and TAT complexes are usually sampled downstream to the thrombus forming area during the individual perfusion runs. Also, activated platelet GPIIb-IIIa, platelet pro-coagulant activity (annexin V binding) and platelet microparticle formation are assessed downstream to the site of thrombus formation [16].

However, one of the greatest drawbacks of the perfusion chamber is its general lack of flexibility to achieve specific channel morphologies. Additionally, their large sizes tend to use up unecessarily large volumes of samples. Thus, customizable, microscale versions of these flow chambers have become the obvious next evolution of platelet analysis.

1.4.8 Microfluidic platelet assays

The field of microfluidics has provided high throughput, low volume methods well suited for the development of tools to study platelet function in the research community. Low volumes enable not only high throughput from regular sample volumes,

but also allows screening of small samples volumes from mouse models, which may be used to study protein knockouts. Microfluidics also allows the selective manipulation and observation of cellular-level interactions between platelets and their surroundings, or even to study single platelet behavior. It has also allowed the construction of highly customized flow channels to aid in our understanding of how the biomechanics of flow influence thrombosis. Finally, it allows systematic studies of large numbers of parameters, a key element in the study of the closely intertwined events of the coagulation pathway. This section will review some of the standout contributions of microfluidics to the field of platelet research.

A demonstration of the application of microfluidics to both murine thrombosis models and to microfluidic channel design comes from the Jackson group, who along with Ruggeri have presented significant research in the area of shear induced platelet activity [17, 12]. In one of their more recent works, they showed the development of a mouse injury model for observing thrombosis *in-vivo* uses a mild crush injury of the wall of the mesenteric artery of a mouse under DIC microscopy to observe platelet aggregate formation. The induction of this local stenosis creates a rapid local increase in downstream platelet accumulation, which forms cycles of aggregation and disaggregation [57]. Microfluidic fabrication allowed the group to attempt to recapitulate this aggregation behavior in a microchannel to investigate the effects of the shear gradient on thrombus formation with and without the influence of anti-platelet drugs. The designed microchannels were approximately 20 μm in height, very close to the size of a single platelet (1-2 μm), and induced peak shear rates of (20000 s $^{-1}$). Results showed that thrombi formed specifically in the area downstream of the constriction in "discoid aggregates" within a deceleration zone. The stability and formation of these aggregates was highly receptor specific, with GPIb providing a vital link to allow the formation of stable thrombi. In contrast, the effects of soluble agonists such as ADP, TXA2, and thrombin proved ineffective at preventing formation

of aggregates at these high shear rates, but was successful at reducing the stability of formed thrombi. The researchers attribute this to the formation of "membrane tethers" formed with the help of extracellular calcium addition. This work, headed by the Jackson research group, provides a thorough experimental demonstration of their previous theories and techniques on the different adhesive mechanisms at play using in-vivo and in-vitro demonstrations.

Effects of channel morphology on thrombosis have been further characterized using microfluidic models by Tovar-Lopez [58], who measured thrombus formation in multiple configurations of stenosis from a step-like constriction to a straight channel. His work concluded that the step configuration was most effective at creating stable thrombi, while the straight channel was unable to form stable thrombi even at shear rates twice as high as the constricted channel, a finding supported by the work of others [59, 57]. However, it is notable that thrombi within his channels formed strictly downstream of the step-like stenosis, not within the constriction itself in the same manner noted by others [59]. Also, although both Nesbitt and Tovar-Lopez investigate the effects of channel morphologies on platelet activation, their studies do not compare activity differences due to changing shear rate while keeping morphology constant.

Another work that took advantage of the small volume requirements of microfluidics to study murine platelet behavior came from Gutierrez in 2008 [60]. This work compared thrombosis in two different strains of knockout mice–one completely lacking the $\alpha IIb\beta3$ receptor, and the other with a domain mutation. Device channels were straight (i.e. non-constricted) 24 x 200 μm in height x width over its cross-section and examined shear rates from 13 to 1300 s^{-1}. Due to the small size of the channels, small sample volume, and the researchers' desire to keep shear constant, they examined only the adhesion step alone in 40 μL over a 10 minute period, quantified by the number of fluorescently labelled stationary platelets on the device's inner surface.

Results showed that even at this lower shear regime, platelets with no $\alpha IIb\beta3$ receptor were unable to form aggregates. The work validated the utility of microfluidics for phenotyping genetic knockouts and provided new information on the structure and function of a key protein in the process of thrombosis. Similar to Gutierrez, the Diamond research group has also employed microfluidics for phenotypic knockout mice. In 2008, they showed the role of the $\alpha IIb\beta3$ receptor protein in binding collagen by comparing the platelet adhesion in receptor knockout mice to controls. Like the Gutierrez group, they used non-constricted channels with focal regions of patterned collagen at low shear rates (400, 1000 s^{-1}). Thrombosis was quantified by the measured intensity of fluorescence from the labelled platelets. While both of these approaches have proven effective for research oriented evaluations of small blood volumes, this volume constraint has prevented them from more in-depth investigations of the effects of high shear rates on platelet activity seen in human pathologies.

Microfluidics have also been useful for creating controlled environments for cellular level studies, such as the Lam group's studies on single platelet spreading over micropatterned collagen regions (simulating focal vessel injuries) [61], or platelets adhering to microchannels seeded with endothelial cells (simulating intact, healthy vasculature) [62]. They applied this approach to study the synergistic effects of endothelial inflammatory signaling, platelet adhesion, and sickle cell flow mechanics on vascular occlusion in these engineered microvascular environments.

Recently, a company called Bioflux has begun attempts to bring microfluidic platelet assays to the commercial world with the BioFlux Live Cell imaging system. The system consists of a PDMS flow chamber integrated with a well plate and microscopy system for examinations of cells under various flow conditions. The group has focused on applying the system to platelets and vascular cells, although it also advertises applications with stem cells and immune cells. The testing apparatus uses

fluorescent platelet labelling and microscopy to perform adhesion screenings, similar to the devices and techniques of Gutierrez [60] and Neeves [63] discussed above, but with greater throughput and higher equipment reliability/repeatability. While the system does offer similar capabilities to the aforementioned researchers, the cost of each study unit is near $80,000 (personal correspondence) due to the cost of the associated microscopy and cell culture equipment. Recently Bioflux has released a Journal of Visualized Experiments (JOVE) video detailing the applications of their system to screening GPIIb/IIIa drug efficacy on a platelet sample [3].

1.4.9 Conclusions on current platelet function tests

The preceding section has provided a survey on the current state of the art in platelet function measurement and analysis and identified some of the strongest competitors and their defining features, strengths, and weaknesses. Key failings of current methods are inconsistencies in results due to sample handling requirements, inconsistencies between testing methods, and (most importantly) lack of consistent clinical evidence that such diagnostics are able to predict major adverse clinical outcomes (MACE) and/or reduce these adverse effects through optimized treatment. As stated by others in the field, there is distinct need in the field for an easy bedside assay with consistent and clinically validated metrics which can be used to monitor patients during disease and therapy [4].

These points are echoed in an overview report put forth in a 2006 report by the International Society on Thrombosis and Hemostasis, the head oversight committee for the science and engineering of this area of medical technology. Their report summarizes many the key design features for an optimal commercial platelet function diagnostic, the main points of which are summarized in the list below. [11].

The diagnostic should incorporate dynamic flow to simulate vascular conditions in order to address the different bonding mechanisms observed under flow [17, 9, 10, 15].

24

This perfusion region should have an eccentric stenosis to simulate pathological flow conditions that have been shown to stimulate specific thrombus growth patterns [57, 58]. Next, flow conditions should be able to reach both pathological high shear rates, and physiological low shear rates to recapitulate the range of flow conditions which may be present in a patient [17, 9, 10, 15]. Additionally, it should also be sensitive to the addition of a variety of anti-platelet drugs, such as the GPIIb/IIIa, P2Y12, and aspirin tests currently on the market. The device should also be able to detect clinically relevant events of thrombus detachment, or embolism, for enhanced clinical relvance. The report also acknowledges that antibody or fluorescence labelling and microscopy are very effective for measuring platelet thrombosis, their high cost and size makes them difficult to use in point-of-care diagnostics. Finally, the diagnostic should provide continuous, real-time monitoring on the kinetics of thrombus formation. Currently there is no commercial device able to address all of these criteria. Most commercialized methods for platelet function analysis are only able to perform testing on single samples at a single shear rate under flow conditions—including high speed bead mixing, forced flow through a membrane, cone-and-plate flow that are not relevant to biological flow through blood vessels.

For comparison, this design criteria has been charted against representatives from the previous section (Fig. 2): the VerifyNow for point-of-care, user-friendly development of some of the most well-studied methods in the field from light transmission aggregometry (LTA); the PFA-100, the first high shear platelet analysis device which has been aggressively marketed to medical laboratories but seen mixed success; and the Bioflux system whose specialty in cell-level assays using high end research equipment represents much of the microfluidics community. Since there is not yet a device able to satisfy the listed categories, a multi-faceted approach combining their information is required, and recommended by some [4, 20].

Recent advances in platelet research have added additional concerns to methods

	VerifyNow	PFA-100	Fluxion
Perfusion/flow		Yes	Yes
Eccentric stenosis			
Tests high shear		Yes* (est. 4000 s^{-1})	Yes+ (est. 0-4000 s^{-1})
Tests low shear	Yes* (est. 1000 s^{-1})		Yes+ (est. 0-1000 s^{-1})
Drug sensitivity	Yes* (GPIIbIIIa, aspirin, P2Y12)	Yes* (GPIIbIIIa, aspirin)	Yes+ (GPIIbIIIa)
Detect emboli			Yes
Microscope-free	Yes	Yes	
Label-free		Yes	
Continuous monitoring			Yes

Figure 2: Comparison of current commercial platelet function analysis methods [2] (*) and [3] (+) based on criteria from the International Society on Thrombosis and Hemostasis (ISTH) 2006 oversight report [4]. These three entries represent the current state of the art in the field. The VerifyNow leverages its technology from Light Transmission Aggregometry, one of the oldest platelet analysis methods, in a more user-friendly package aimed at the point of care market. The PFA-100 is the first high shear platelet analysis device which has been aggressively marketed to medical laboratories and despite going through extensive clinical tests has seen mixed diagnostic efficacy. Finally, the Bioflux company specializes in custom miniaturized flow assays and vasculature cell assays using high-end research equipment, and represents the commercial side of the microfluidics community.

for platelet function testing, including measurement methods for platelet aggregation. As discussed previously, the formation of a thrombus occurs in three phases: (I) initial adhesion of platelets to a substrate, (II) the rapid accumulation of platelets binding to other platelets and (III) the final stabilization and contraction of the platelets into a solid mass that occludes flow [9, 10]. However, most studies to date have been conducted only on the initial adhesion phase [14, 15], using fluorescence microscopy and are not well suited to volumetric measurements in real time. Microscopy methods are limited by small measurement areas, poor depth measurement, the need for image post-processing, and often require sample pre-treatment.

The field of microfluidics has provided high throughput, low volume methods well suited for the development of tools to study platelet function in the research community. Recently, Gutierrez et al. [60] showed the importance of platelet receptor integrin αIIβ3 in genetically modified mice platelets adherence to collagen (thrombosis phase I) at low shear rates 50-1410 s^{-1} in a multichannel microfluidic device. While this device was able to address multiple shear rates in multiple channels simultaneously, these tests did not include pathologically relevant high shear behavior or the later stage of rapid platelet-platelet bonding known as "rapid platelet accumulation" (thrombosis phase II). Other recent work by Tovar-Lopez et al. [58] has shown the importance of stenotic geometry to high-shear platelet aggregation using microscale devices. While this study and device thoroughly analyzed changes in platelet aggregation downstream of the stenosis, it did not examine aggregation within the stenoses nor explore aggregation at varying shear rates in identical stenoses.

Thus current methods have been limited by one or more of the following parameters: limited relevance to physiological flow [41, 20], need for external cell labeling,[60, 64] platelet fractionation and washing for imaging and analysis [65, 31] non-pathologically relevant low shear rates [66, 14, 10], small measurement area limited by microscopy [67, 10, 14], channel sizes insufficient to observe rapid platelet

accumulation, and large volumes of blood [68]. Additionally, many in vitro models have not attempted to address aspects of specific clinical pathologies relevant to thrombosis including high shear rates and stenotic morphology [69, 9, 14, 10].

There is presently no instrumentation able to simultaneously examine individual trials of a wide range of fluid shear rates including those exceeding 10000 s^{-1}, with simultaneous platelet aggregation to occlusion measurement, which is important given the time dependent effects of clotting and anticoagulants. The creation and application of such high throughput instruments could enable essential, large scale, comprehensive studies which would inform research on cardiovascular pathologies and their appropriate anti-platelet therapies. The field could benefit from a low volume, high throughput, short analysis time, and low cost system while minimizing sample handling.

Finally, and perhaps most importantly, the greatest failing of most of these methods is in their inability to consistently predict clinical outcomes and to effectively guide improvements in therapy. Without such clinical evidence, these devices are unlikely to succeed in commercialization, and may instead be best suited as tools for research and development for the next design iteration [4, 20, 70].

1.5   Thesis outline

This work has three primary aims:

- Aim 1: Design, fabricate, and test a microfluidic device capable of inducing shear rates ranging from 500-20000 s^{-1} in stenotic channels.

- Aim 2: Development of an optical sensor for label-free, non-contact, multi-channel, high temporal resolution measurement of platelet-based thrombus formation.

- Aim 3: Apply the integrated system to measure platelet aggregation as a function of shear rates dosed with platelet therapies

This thesis outlines the design, fabrication, testing, and application of a microfluidic device and associated optical system for simultaneous measurement of platelet aggregation at multiple initial shear rates within four stenotic channels in label-free whole blood and its applications to platelet therapy.

CHAPTER II

MICROFLUIDIC DEVICE

This chapter describes the design, fabrication, and testing of a microfluidic device for measurement of *in-vitro* platelet aggregation for a wide range of different shear rates.

2.1 Design and modelling

The design for an optically-clear, multichannel, microfluidic device was developed to induce a spectrum of shear rates while permitting direct optical measurement of formation of occlusive blood clot formation in porcine blood. Specifically, we desired to address shear rates of 500, 1500, 4000, 7000, 10000, and 13000 s^{-1} within the channels high-shear stenotic regions. These shear rates were chosen to represent the physiological conditions in veins and arterioles (500-1500 s^{-1}), pathological shear rates (4000 s^{-1}), and high pathological shear rates (10000 s^{-1} and above), as discussed in the preceding Chapter.

As a design consideration, while other work [57, 60] has limited the minimum channel dimension to 20-50 μm, we chose a minimum dimension of 250 μm to enable observation of aggregates on the order of millions of platelets (100s of microns) during rapid platelet accumulation, for comparison with prior work [59]. Rapid platelet accumulation is also significant because it presents a potentially unique set of binding events which are not present during the formation of smaller aggregates on the order of hundreds of platelets (e.g. the platelet adhesion and early platelet aggregation events) [59, 5]. Another consideration was the design of the stenosis to reflect pathologically relevant geometry. Thus we designed the diameter reduction from the channel region to the stenosis region to be 53%, near to the 50% reduction often used as an indicator for surgical intervention in the left main coronary artery [71]. In

the channels upstream and downstream of the high-shear stenotic regions, we require that the maximum shear rates not exceed 1500 s^{-1}, the upper bound of physiological shear rates. In our initial designs, we tested thrombosis in channels with dimensions of 250, 500, 750, and 1000 μm, and empirically determined that the 750 μm wide channel was the widest channel able to induce thrombotic occlusion using less than 10 mL of porcine blood. This wider channel was preferable to the narrower channels, which would often be occluded by artefact debris or preformed aggregates common in unfiltered porcine blood used in early experiments.

Early chip designs used different stenosis geometries and a common inlet and outlet to increase the range of shear rates obtainable from one channel (Fig. 6). This design was changed in later experiments to four identical stenosis geometries with independent outlets. The use of identical stenoses removed the potentially confounding effects of comparing occlusion in channels with very different surface area to volume ratios and overall cross-sectional areas. Separate outlets were used to prevent "cross talk" between channels as occlusion events change local pressure drops. An *en–face* view of the final chip design is shown in Fig. 3.

In order to obtain a wide range of initial wall shear rates in multiple identical microchannels sharing a single flow input, we passively controlled channel flow resistance downstream of the stenotic region through the use of 50SHL Tygon tubing (Saint Gobain, Valley Forge, PA), a formulation rated for blood handling which exhibits low cell adhesion. Thus determination of shear rates within the stenosis required fluid modelling efforts combined the effects of the channel and tubing resistances. While other groups have used on-chip resistive channels for controlling flow rates [60], this off-chip resistive tubing design enables simple shear rate control over two orders of magnitude from an array of identical microchannels, simplifies fabrication, and interfaces easily with weighing scales for flow rate measurement

In this work, we calculated initial estimates for resistance tubing dimensions using
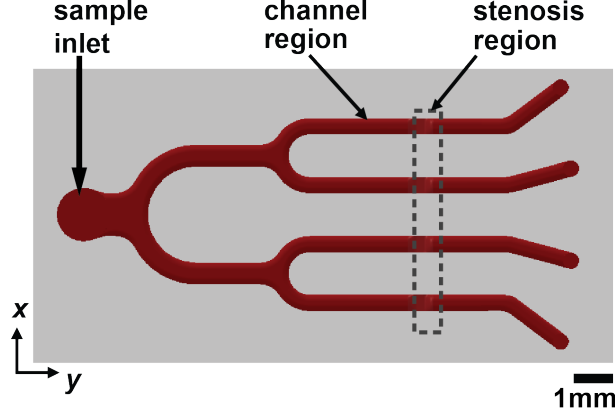
Figure 3: Schematic showing top view of the design of the microfluidic device for inducing platelet aggregation at four distinct initial wall shear rates in whole blood within the high shear stenosis regions. An off-chip suspended syringe (not shown) connected to the sample inlet provides a pressure driven flow through the channel regions (750 μm wide by 750 μm high) and through the locally constricted stenosis regions (750 μm wide by 250 μm high) then back into channel regions of the same dimensions prior to egress from four separate outlets and their respective resistance tubing. Dimensions of the four stenoses were identical to one-another, the use of varying downstream tubing lengths and dimensions (not shown) enables the study of a wide range of initial wall shear rates.

an analytical method, then refined the estimates using a computational method. These methods are discussed in the following sections.

2.1.1 Analytical modelling

Analytical modelling was used for initial estimates of resistance tubing dimensions based on target wall shear rates. First, wall shear rate values and pressure drops were chosen, and used to determine the target overall resistance within each flow path (defined from fluid reservoir inlet to flow outlet). Then, using a circuit model assuming Poiseuillar laminar flow, the requisite length for each outlet tubing section was determined.

The wall shear rate, γ of a flow channel can be calculated as:

$$\gamma = \frac{32Q}{\pi d_h^3} \tag{2}$$

Where Q is the volumetric flow rate, d_h is the hydraulic diameter of the channel

32

(in the case of a channel with rectangular cross-section) [10]. Hydraulic diameter of a channel with a cross section of width w and height h is defined as $d_h = 2hw/(h + w) \times f(Re)$, where $f(Re)$ is an adjustment factor based on the aspect ratio and the Reynolds number describing flow within the channel [72]. Having set the dimensions of the stenosis at $h = 250$ μm and $w = 750$ μm as discussed in the previous section, the resultant hydraulic diameter of the stenosis with adjustment factor for aspect ratio is $d_h = 351$ μm. This specific hydraulic diameter was desirable for its similarity to previous work examining platelet-platelet aggregation [73, 59]. We may then input desired values for γ to solve for the target volumetric flow rate Q.

Next, this Q value is used to solve for the target length of resistance tubing. In general, the overall flow rate and resistance within a flow path from flow inlet to flow outlet can be defined as:

$$\Delta P = R_{\text{total}}Q \tag{3}$$

Where R_{total} is the total resistance in the flow path. Using a circuit model, resistance within the flow path is additive [74] and thus can be calculated by:

$$R_{\text{total}} = 128\mu \left(\frac{L_{in}}{d_{in}^4} + \frac{L_{ch}}{d_{ch}^4} + \frac{L_t}{d_t^4} + \frac{L_{st}}{d_h^4} \right) \tag{4}$$

Where $\mu = 0.00385$ Pa $\times$ s is the average dynamic viscosity of blood [75], L_{in} is the length of the inlet tubing, L_{ch} is the length of the channel, L_t is the length of the outlet resistance tubing, L_{st} is the length of the stenosis, d_{in} is the diameter of the inlet tubing d_{ch} hydraulic diameter of the channel, d_t is the diameter of the tubing, and d_h is the hydraulic diameter of the stenosis. We set all of these values except the L_t and d_t based on our materials and previously discussed dimensions (L_{in}=150 mm, $L_{ch} = 15$ mm, $L_{st} = 300$ μm, $d_{in} = 1.75$ mm, $d_{ch} = 750$ μm, $d_h = 351$ μm). Commercial vendors of the preferred tubing formulation, Tygon S50HL, provide tubing with inner diameters d_t of 0.79, 1.27, 1.58, and 2.38 mm, from which we could calculate preferred values of L_t which were convenient for interfacing with

downstream flow measurement using weighing scales, whose use is further discussed later in this Chapter.

This method was used for initial estimations only. Researchers in this field have noted that wall shear estimates using such analytical equations may have significant inaccuracies due to particle margination-based local changes in viscosity [10]. Further efforts were pursued for refinement of tubing length calculations based on computational models, discussed in the following section.

2.1.2   Computational modelling

Measurements of shear rate γ in the remaining body of this work were determined finite volume fluid modelling using ANSYS (ANSYS Inc., Canonsburg, PA).

Simulations of flow in the model used the following settings. Blood viscosity, μ, and density, ρ, were assumed constant (valid for shear rate <6 s^{-1} [75]) at 0.00385 Pa·s and 1.080 g/mL, respectively [75]. Particulate fluid effects were not considered due to the relative dimensions of the channel in relation to cell size (approximately 50 to 150 times). However, findings on platelet margination effects due to particulate flow indicated that such models have potential value [76], and is an area for future investigations. Boundary conditions were for pressure P=0 at all outlet faces, and all no-slip walls on all other surfaces. The boundary to the inlet was consdered as having a set pressure of 1400 Pa, determined by ρgh. Flow was assumed to be laminar, and solutions convergence was set at $1e^{-6}$ or 500 iterations. Mesh elements used minimum side lengths of 2 μm within the stenosis region to approximate the boundary layer region in which a platelet (2-20 μm diameter) binds. Optimal meshing conditions were achieved by modeling long resistance tubing sections by smaller tube formations with equivalent resistance, calculated using the relationship $\dfrac{L_r}{d_r^4} = \dfrac{L_m}{d_m^4}$

We applied this model to select resistive tubing lengths ranging from L=60 cm, d= 0.79 mm to L=30 cm, d=2.38 mm (for experiments where input ΔP was set at 1400
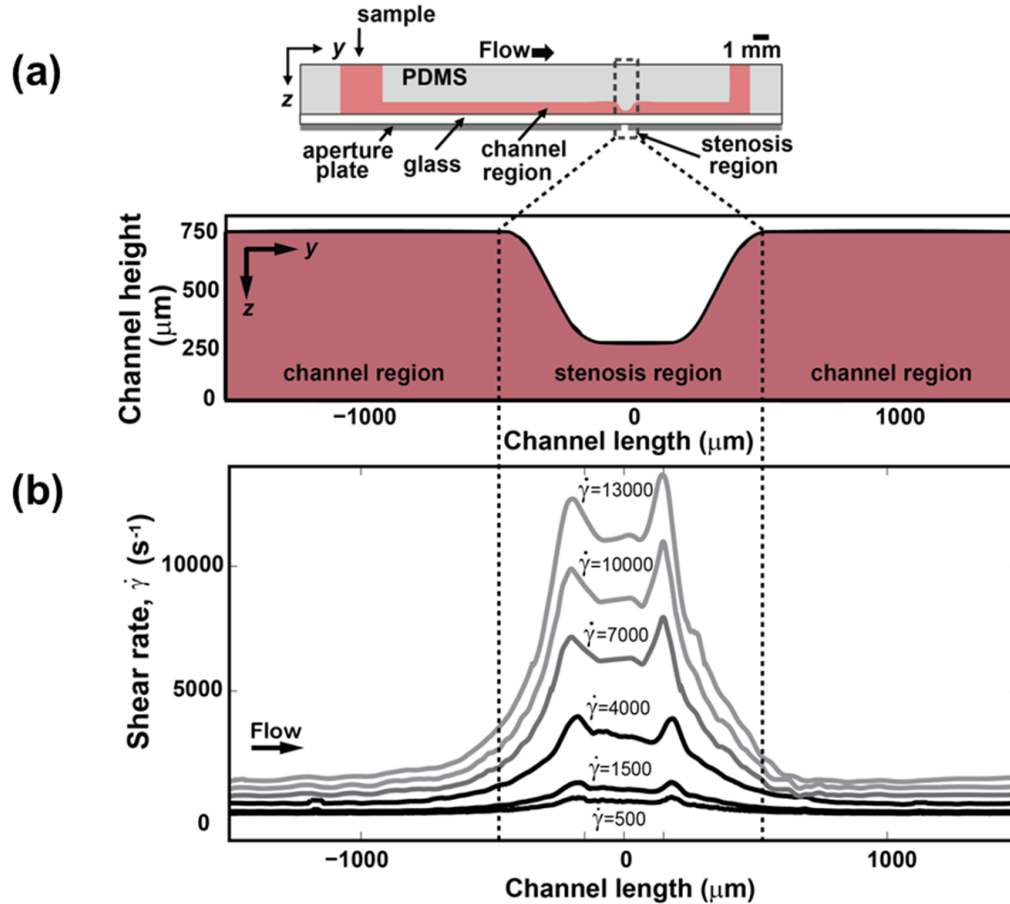
Figure 4: Six shear rate profiles were computed and were obtained experimentally by varying outlet tubing geometry connected to a uniform channel geometry (a). The maximum shear rate outside of the stenoses regions is within physiological range <1500 s^{-1}, while maximum shear rate within the stenoses were designed for a variety of physiological and pathological shear rates (500-13000 s^{-1}) (b).

Pa). Modeled wall shear stress measurements were extracted from the solved simulation and imported into Matlab, where the values were averaged over the perimeter to obtain the local shear rate γ at discrete points over the length of the channel to produce the data shown below in Fig. 4.

Notably the shear rate peaks at the borders of the stenosis region, a region where initial aggregates appeared in microscopy studies. Others in the field have examined the effects of adjusting stenosis angles, and such adjustments to mitigate the local peaks may be of interest. However, the dimensions of vascular occlusions vary widely

over patients, and in this work we have adhered to the primary criteria of percent occlusion by area >50%, eccentric formation, and hydraulic diameter of 350 μm.

Having calculated the *initial* wall shear rate, we were interested in the changes in wall shear rate over the time course of occlusion. We conducted simulations of channel occlusion using a solid model created in SolidWorks, and analyzed corresponding changes in initial wall shear rate using an ANSYS finite volume fluid model. In these simulations, we assumed thrombus growth was uniformly distributed over the entire inner surface of the stenosis and thus modelled channel occlusion by thrombus growth as a localized reduction in the height and width of the stenosis cross section.

$$\text{Stenosis\%} = 100 * \frac{d_0 - d_i}{d_0} \tag{5}$$

These simulations were analyzed in ANSYS with the same settings described earlier in this section. In order to reflect clinical concerns, local stenosis dimensions are shown here by stenosis %, which is defined by Equation 5, where d_0 is the initial diameter, and d_i is the constricted diameter. Flow rate results were as expected from 2, with an exponential relationship of $Q \sim d_h^{-4}$. Results showed that as stenosis % increased, shear rate increased to a maximum of nearly 4-fold (19260 s^{-1}) its initial amount for increases from 66 to 90 stenosis % until falling precipitously as flow rates approach zero. Notably shear rate increases most rapidly between 80-90 stenosis %, which may be instrumental in the "rapid platelet accumulation" phase observed in later stage thrombosis. Other experimental methods have used constant flow models and shown increases in shear rate of approximately 21-fold for a similar increase in stenosis % (80 to 93%) [5]. In contrast, the model developed in this work uses constant pressure, and thus increases in shear are much more modest, but perhaps more physiologically relevant since the heart is not able to provide infinite pressure required to produce a constant flow condition.

Thus with the desired dimensions determined, we next describe the methods used

(a)

(b)
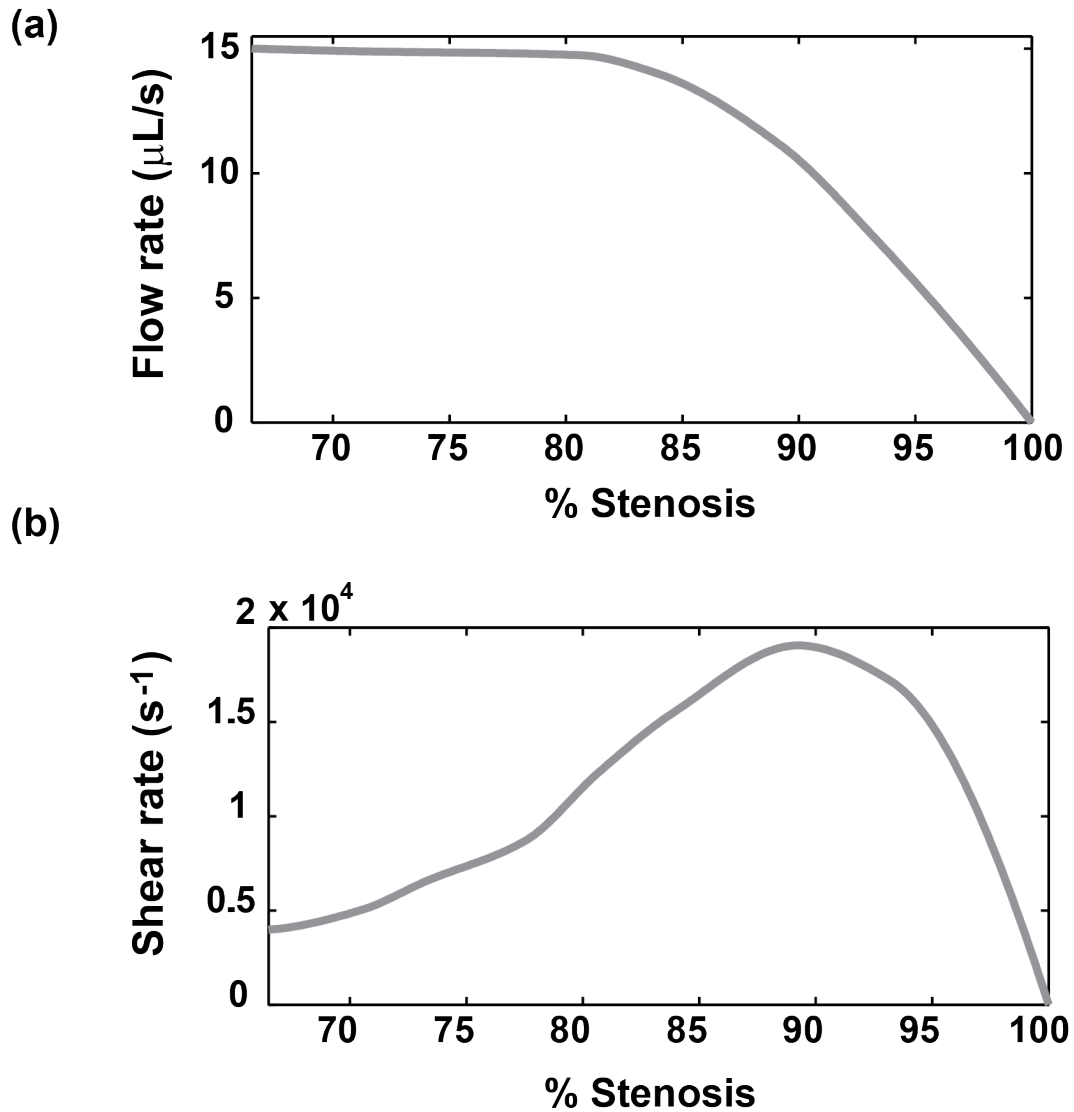
Figure 5: Simulations of channel occlusion using a solid model of the channel with initial shear rate 4000 s^{-1} in our device. The model was created in SolidWorks, and analyzed corresponding changes in wall shear rate using an ANSYS finite volume fluid model. shear rate increased to a maximum of nearly 4-fold (19260 s^{-1}) its initial amount for increases from 66 to 90 stenosis % until falling precipitously as flow rates approach zero. Notably shear rate increases most rapidly between 80-90 stenosis %, which may be instrumental in the "rapid platelet accumulation" phase observed in later stage thrombosis. Other experimental methods have used constant flow models and shown increases in shear rate of approximately 21-fold for a similar increase in stenosis % (80 to 93%) [5].

to fabricate these devices.

2.2   Device fabrication

The desired dimensions described above presented distinct challenges. First, the requisite device feature sizes ranged from 250 to 1000 μm, an atypical size range for traditional semiconductor methods used for soft-lithography microfluidic devices. Second, the device was designed with three-dimensional curved surfaces at the edges of the stenosis (designed to blunt the sudden increases seen in Fig. 4) and the fillets on the upper border of the non-stenotic channel regions (implemented to help prevent areas of stagnant flow which might entrain passing soluble factors and thus skew results). While these regions were curved, the stenosis region itself retained a rectangular cross section in order to prevent optical measurement errors.

Traditional semiconductor fabrication methods of photolithography on silicon are commonly limited to hydraulic diameters of 5-200 μm and relatively large effort is necessary to obtain curved, three-dimensional topographies. Thus, in order to fabricate a microfluidic device with the requisite change in hydraulic diameters (300-1000 μm) as well as the gradual transition to the stenosis from the non-stenotic channel region, we utilized an unconventional microfabrication technique. We first created a mold in aluminum 6013 using a vertical milling machine (Haas, OM-1a, Oxnard, CA). The milling process used square endmills with diameters D=0.25-1.57 mm and a ball endmill with D=125 μm operated at a spindle speed of 30000 rpm (See Fig. 7). For all tools, feed rates were 50.8 mm/min; depths of cut were D/3. Unattended mold machining time was approximately 30 hr, attended user- operation time was approximately 2 hours. Mold surface average roughness, Ra, measured by white light interferometry (Zygo, NewView 200, Middlefield, CT), was approximately 150 nm, less than the 2 μm platelet diameter, and so was deemed sufficient. Absolute dimensions of our device were measured using high resolution (0.762 μm) 3D digital
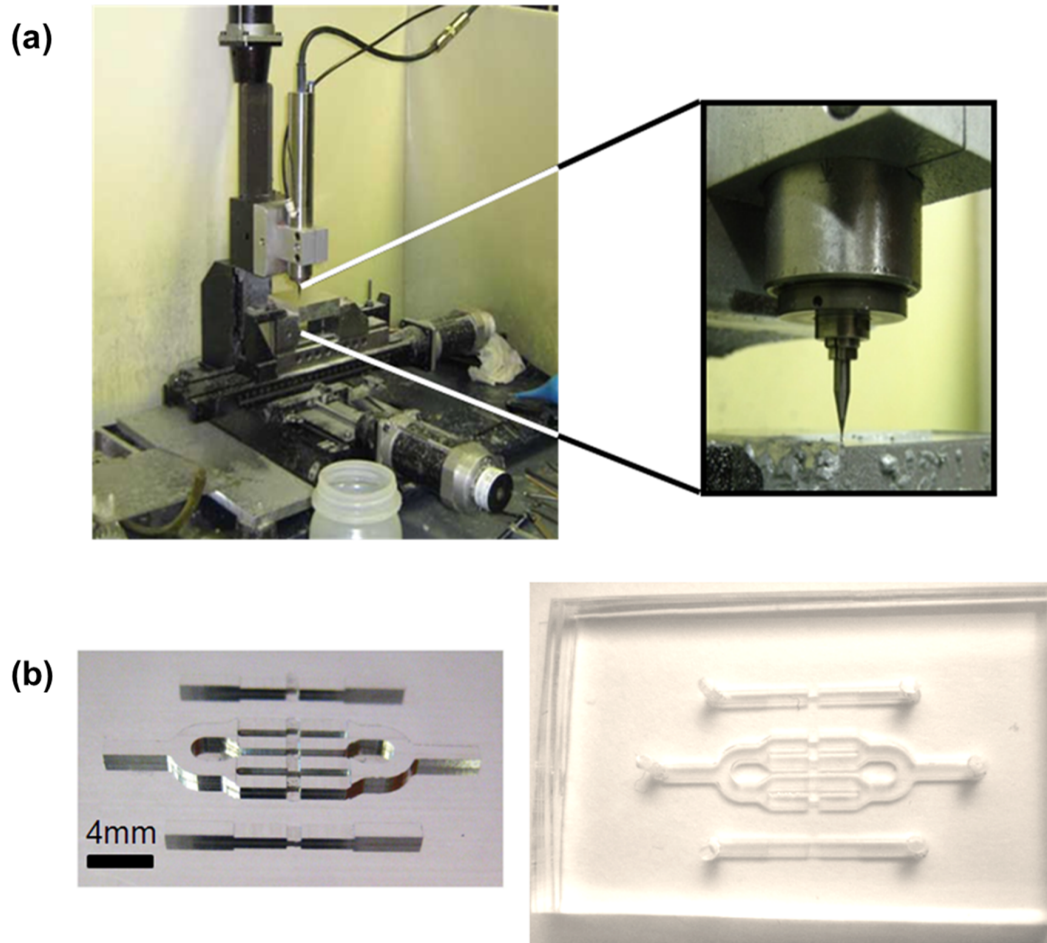
Figure 6: An early version of the device mold was constructed using a customized Sherline mini milling machine (a). The mold geometry was milled using square end-mills ranging from 150-1000 μm in diameter (a, inset) at spindle speeds of 80000 rpm. The completed mold is shown on the bottom left (b), and the molded PDMS device layer on the bottom right (b, inset).

microscopy (Keyence VHX-600) as 250 μm in height and 750 μm in width at the stenosis region, and 751 μm at peak height at the channel regions

While this method was used to create devices with some curved features but rectangular cross-section stenoses, we questioned what the effects of changing the shape of the stenosis had on subsequent platelet aggregation. In order to answer this question, we needed to develop a fabrication method for creating stenosis cross sections of widely varied shapes and sizes.
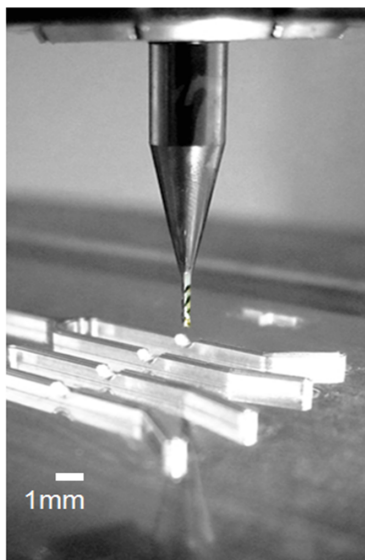
Figure 7: Fabrication of the final device mold was achieved in 6013 Aluminum using an vertical milling machine with square endmills with diameters D=0.25-1.57 mm at a spindle speed of 30000 rpm.

2.2.1 Circular cross-section channels

Recent intravascular angiographic clinical studies of human coronary arteries affected by atherosclerosis have shown that affected vessels exhibit localized constricted cross sections with predominantly eccentric elliptical or circular cross sections. Overall area reductions in cases of patients characterized as extremely high risk for thrombosis from myocardial infarct were reported in the range from 50-84% [77, 78]. Thus there is great interest in designing instruments to better understand how and why these conditions of altered artery shapes impact patients risk for thrombosis.

The ability to accurately, inexpensively, quickly and repeatably fabricate sub-millimeter scale features has made soft-lithography based microfluidics a vital tool for the biomedical research and lab-on-a-chip assays. However, traditional methods used in this field, such as photolithography, deposition, and etching are generally limited to creating features with rectangular cross-sections, low aspect ratios, and feature heights below 200 μm [79]. These limitations cause several problems in the application of

microfluidics to biological assays. Specifically, rectangular cross sections induce non-physiological gradients in fluid shear rate, velocity, and pressure in contrast with the rounded cross-sections found in most natural physiological systems, such as blood vessels and airways. Further, fabrication of features with multiple heights is complex and costly. Finally, casting and releasing around complex features can be problematic. Thus the development of methods for fabricating a wide range of heights and cross-sections within the same device would provide a valuable complement or replacement to standard microfabrication techniques.

Although previous groups have formulated methods for obtaining rounded channels such as reflow of photoresist during photolithography of the device mold, molding through the use of small wires, or by using additional coating hexanes within square channels, all of these methods have shown poor control over the resultant geometries and are unable to vary shapes and aspect ratios [79, 80]. In contrast, micromilling channel molds is an option which can address a wide range of features and dimensions.

We next present a technique for the fabrication of an array of micro-scale channels of varying cross-sectional shape and areas with dimensions from $100 - 750$ μm. In addition, we demonstrate the utility of these channels for investigating effects of varying local flow conditions on thrombosis.

To study the effects of vessel shape, we designed an array of microchannels to study clot formation within four constricted regions with distinct cross-sectional areas: circular, square, semicircular, and eccentric (elliptical). Square and semicircular cross sections were chosen to represent the dynamics of traditionally fabricated microchannels, while the circular and eccentric channels were chosen to represent the clinical conditions described previously.

Square and circular cross sections had equal hydraulic diameters, while eccentric and circular cross sections had the same area constrictions were reduced in area by 50 – 84% relative to the rest of the channel to correspond to patients at very high risk

for thrombotic stroke [81, 82]. We first used micromilling to construct a mold from which we cast parts which were subsequently aligned, and bonded to create enclosed channels with the desired cross sectional areas.

Device dimensions and added downstream resistance elements were chosen such that each channel would experience identical average shear rates of 7000 s^{-1}, an amount representative of conditions in patients at high risk for thrombosis and one which we have verified to cause clot formation in previous experiments. In order to address such high shear rates for small volumes (less than 5 mL) of blood per trial, we required a wide range of feature heights and widths from 100   750 μm. These dimensions were modeled and verified using both an analytical Poiseuillar flow analysis in conjunction with finite volume characterizations using Navier-Stokes equations (ANSYS Fluent).

The mold was cut from brass alloy 385 on a vertical milling machine (Haas OM-1) using square endmills from 1.57 mm to 254 μm in diameter and a 508 μm ball endmill at spindle speeds from 5,000 - 30000 rpm. For all tools, feed rates were 50.8 mm/minute with depth of cuts set to 1/3 the tool diameter. Surface milled toolpaths were generated using MasterCAM X3 software. After machining, the mold was treated for eight hours with a silanizing agent (UCS Chemicals) to facilitate polymer release during the casting step.

Verification of the molds dimensions was performed using high-resolution (0.762 μm) digital microscopy (Keyence VHX-600), which was used to measure the mold height over the cross-sectional profile of the stenosis region. Results of metrology on these areas were characterized by "figure error" [83], which was calculated as the mean of the absolute value of the difference between the height profile measured using the Keyence and the desired profile. Results are shown in Table 1. Surface roughness along the flat face of the channel was sub-micrometer, and provided a sufficiently smooth surface for bonding castings of PDMS to PDMS along these regions.
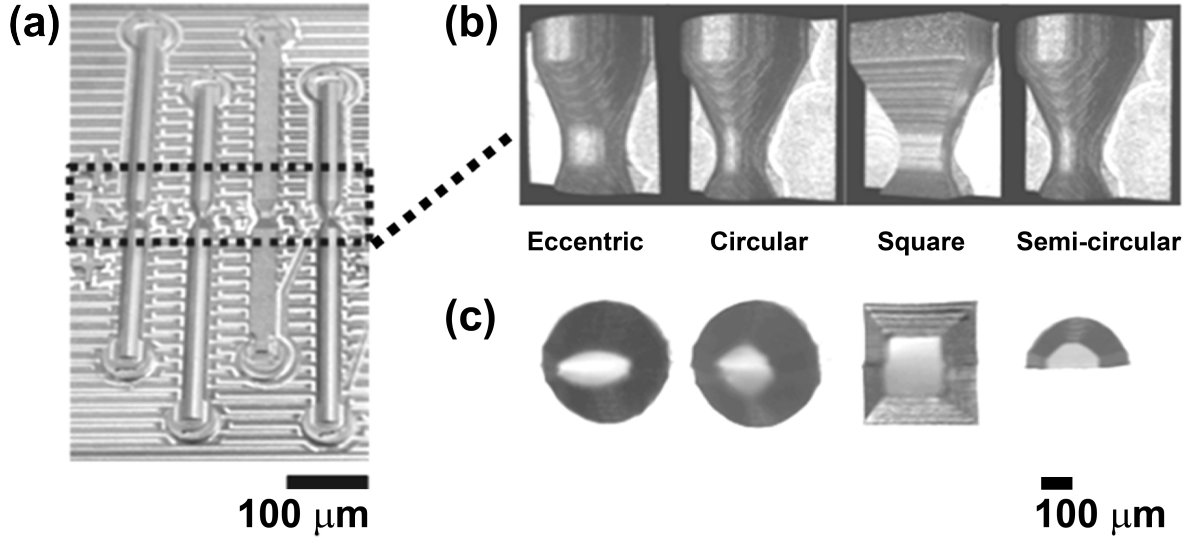
Figure 8: (a) Image of the device mold with four different types of cross-sections. (b) Images of the milled microchip mold with enlarged images of the constricted regions of interest of varying cross sectional areas within the mold: elliptical, round, square, and semicircular. Images captured using digital microscopy. (c) Cross-section of the fabricated two layer PDMS device. Images taken using a dissection microscope. For a diagram showing the viewing angle and fabrication process of (c), see Fig. 9.

Table 1: Comparison between designed and fabricated mold dimensions, and their total calculated figure error within the stenosis region, measured using 3D digital microscopy. Designed and fabricated total device heights are also included.

	Eccentric	Circular	Square	Semicircular
Figure Error (μm)	6.60	2.60	10.2	3.20
Designed mold height (μm)	106	150	150	150
Measured mold height (μm)	106	152	160	151
Designed mold width (μm)	424	300	300	300
Measured mold width (μm)	468	328	303	342
Designed device height (μm)	212	300	300	150
Measured device height (μm)	212	304	320	152

We have developed a method for achieving a variety of three-dimensional features unachievable by traditional soft-lithography semiconductor fabrication processes. Employing this method, we demonstrated the creation of a single device mold containing four different cross sectional areas, with smoothly transitioning feature sizes ranging from 100 to 750 μm and aspect ratios ranging from 2:1 to 1:1. Variations in clotting time reveal the differential behavior of clot formation and nucleation over a range of cross-sectional areas.

The device fabricated in this work demonstrates the ability of micromilling to address hereto-unattainable feature dimensions. Analysis of the milled mold showed a wide range of heights and a surface shapes with "figure error" within 10 μm and absolute dimensions within 44 μm. Width dimensions showed the largest feature errors due to artefacts of the metrology method. The limiting factor for the entire fabrication method occurs in the manual alignment of the two molded parts, which could be improved through inclusion of specialized techniques such as temporary methanol bonding and the use of a mechanical stage [84].

Despite the physiological relevance of channels with circular cross-sections, we decided to use rectangular cross-sections for larger porcine and human studies in Chapters 4 and 5 due to ease of imaging and current manufacturing capabilities. Also, the presence of errors in alignment risks unintended local increases in shear rate or flow streamlines, both factors of great concern in the study of shear induced thrombosis. However, we did perform limited evaluations of thrombosis in porcine blood in these different stenosis cross-sections, which are discussed later in this Chapter's thrombosis validation section.

2.2.2 Device bonding and interfacing

From this mold, we cast devices using the high fidelity, transparent polymer poly-dimethylsiloxane (PDMS) (Sylgard 184, Dow Chemical). The poured polymer was

then placed in a vaccuum chamber at -15-25 psi gauge pressure to eliminate air bubbles. Degassed polymer was then cured at 70°C for at least 1.5 hours, and the polymer gently peeled away from the mold. Devices were cast for thicknesses of 5 mm–a height which allows firm anchoring of fluid interconnects from the device to attach with resistance tubing.

Next, input and output interfacing holes were punched in PDMS at the inlets and outlets using a 14 gauge Luer needle with a beveled edge. Use of a non-beveled needle will result in interfacing holes with small pieces of PDMS debris which may dislodge and occlude channels during testing. Beveled edges can easily be created by gentle pressure with a Dremel's grinding tip. Inlet and outlet tubing was attached to the device using small (∼1 cm long) sections of PTFE 16 gauge light wall tubing (Zeus, Orangeberg, SC). This material is preferable to metal due to its exceptional smoothness and low affinity for cellular adhesion. The 16 gauge PTFE tubing formed a tight seal with 1/16" inner diameter tygon tubing, while tubing of smaller inner diameter than the PTFE was attached using an outer "sleeve" cut from 1.5 cm of Tygon tubing of the next size up, or in some cases sealed with heat shrink. However, the latter method should be avoided if possible, since the melting point of Tygon is fairly close to the activation temperature of the heat shrink.

Devices with elliptical, circular, and square cross-sections whose mold fabrication was previously described were and plasma bonded using high frequency corona bonding (Electrotechnic, Chicago, IL). Alignment of the layers before bonding was achieved manually under a stereomicroscope. All channels except the semicircular channel were bonded to a mirror image. The complete process of milling and alignment is shown in Fig. 9.

In contrast to the mirror image alignment and bonding used to create elliptical, circular, and square cross-sections, normal rectangular cross-section devices were instead bonded it to coverglass (thickness #1.5—0.17 mm). Devices were bonded to
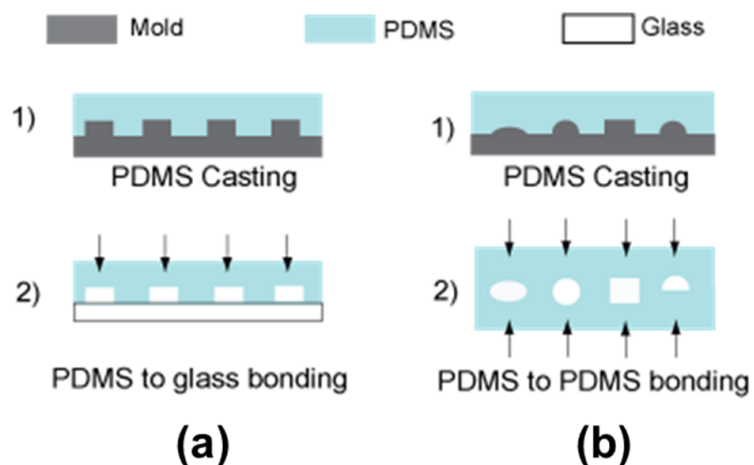
Figure 9: A comparison between (a) conventional microfluidic channel fabrication, and (b) our method for forming microfluidic round channels using micromilling and manual alignment.

coverglass using a PDC-32G plasma cleaner (Harrick Plasma, Ithaca, NY). Bonding using this machine is mediated through saturating the normally hydrophobic PDMS surface with oxygen radicals created by high radio frequencies within the cleaner's chamber to form a temporarily hydrophilic surfaces able to bond to other similarly treated surfaces. Scotch tape was used to prevent the adhesion of dust particles to the device, and/or to remove them prior to bonding. Earlier experiments, such as the construction of circular cross-sections described later in this Chapter, used a corona cleaner for surface treatment and subsequent bonding. However, the bond formed by this method was inconsistent and weak, and we found that the use of the plasma cleaner produced a much stronger, more consistent bond between the coverglass and the microfluidic device. In accordance with the plasma cleaner manufacturer, devices and coverglass were treated with plasma gas for 1.5 minutes on high RF setting with their bonding faces towards the top of the chamber, then immediately removed and their surfaces pressed firmly together within the optimal bonding time window of 20 seconds after the plasma RF has been switched off. Bonded devices were then placed

in a 70°C oven to assist in the bonding process and to allow unbonded, treated surfaces to revert to their original hydrophobic state for a minimum of two hours prior to filling with collagen solution. This timed step is important, since injection of collagen into the device directly after plasma treatment can lead to the temporarily hydrophilic surface pulling the fluid between the PDMS and coverglass, interfering with the bond between the two. After the requisite two hours in the oven, devices were bonded firmly enough to inject collagen into the channels. Collagen in a concentration of 100 μg/mL was injected into the channels to fill the entire device [85]. Next, a piece of Scotch tape was placed over the inlet and outlet holes of the device to prevent evaporation of the solution. Devices were used for platelet assays a minimum of eight hours after the bonding process, since plasma surface treatment has been found to enhance platelet aggregation [86].

The aluminum mold has been used for molding in excess of two hundred times without notable degradation in performance. Later versions of the device used in Chapter 5 were cast into acrylic frames and aligned during the molding step with a customized molding chamber to enable fast, accurate, and repeatable alignment of the stenosis region to the CCD (x,y = $\pm$46 μm for N=6 trial measurements).

2.2.3 Fluid delivery

Flow control in our device was achieved through gravity pressure head. Many previous experimental systems for evaluating platelet activity have used syringe pumps to control volumetric flowrates, and thus shear rates [59, 63]. However, such methods are problematic for studies of full thrombotic occlusion of flow channels, which would necessitate the use of high pressures unachievable by the human circulatory system. Additionally, the use of tubing Thus our system controls flow using gravity pressure head. In our experiments, we used pressures, P, of 1400 Pa, which were implemented by elevating the fluid input reservoir – an open, suspended 60-100 mL polypropylene
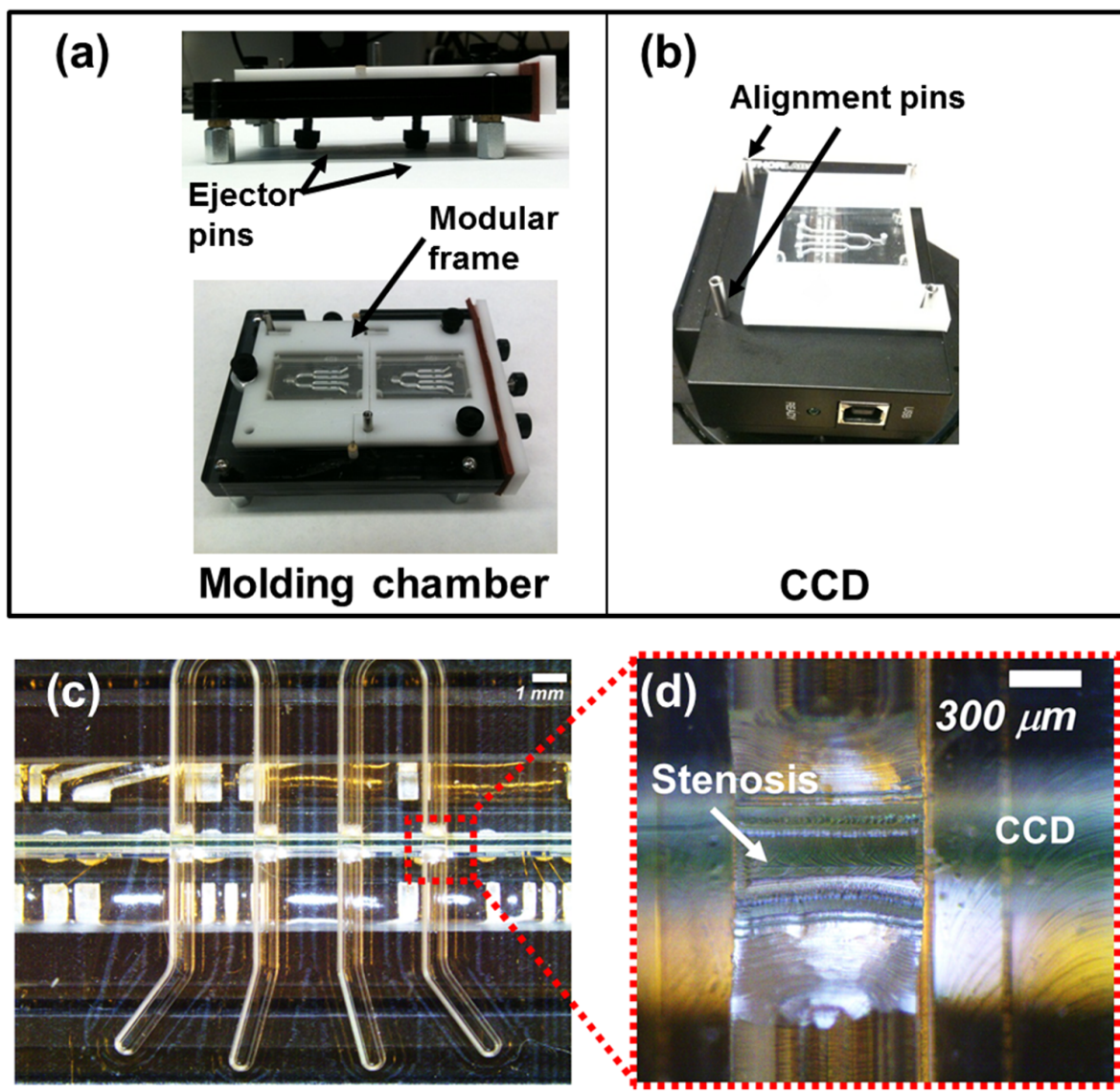
Figure 10: Alignment of the stenosis region to the CCD was enabled by the use of laser cut acrylic frames. Each frame was aligned to the mold and polymer poured and set so that the stenosis feature was a known distance from the frame. Next, the cast devices within the frame were bonded and coated with collagen. The completed devices were then aligned to the CCD through metal posts ("alignment pins") attached to the surface of the CCD. The system enabled fast, consistent alignments within ± 25 μm of the centerline of the CCD without the need for manual stage adjustment.

syringe (Monoject, Mansfield, MA) to the height h, calculated as $P = \rho g h$, where $g = 9.81$ m/s^2, and ρ is the average density of blood, 1080 kg/m^3 [75]. Thus suspension height used was thus 132 mm of gravity pressure head. Pressure head was monitored either manually or using an automated system. Manual monitoring produced average height differences of approximately 3 mm within the desired height setpoint, while the automated system was able to maintain heights within sub-millimeter resolution of the desired setpoint. These errors corresponded with 10-31 Pa of uncertainty.

The automated system operates by detecting the location of the top of the fluid reservoir. A laser light (Optodiode, Newbury Park, CA) is shone through the transparent syringe reservoir and detected on the other side by a photodiode (US-Lasers, Baldwin Park, CA). When the light is interrupted by the presence of blood within the syringe, the signal detected by the photodiode is interrupted, and a linear actuator (Firgelli, Victoria, Canada) incrementally moves the syringe up by 1 mm increments. Voltage input from the photodiode and output to the actuator are provided by a Labview script.

2.3   *Experimental validations of flow rate and platelet thrombosis*

In this section the validation of the computational modelling previously discussed is shown using experimental flow rate tests. Next we validated the ability of the device to form platelet-rich aggregates using brightfield microscopy and histological staining.

2.3.1   Flow rate validation

Experimental flow rate tests were used to validate that the device was able to achieve the desired stenotic shear rates. Flow rate tests were performed using two fluids: a 43% glycerol/phosphate buffered saline (Sigma Chemical, St. Louis, MO) [87], viscosity matched at μ=3.85$\times 10^{-3}$ Pa· s [75] prior to flowing blood, and porcine blood anticoagulated with 40 Units/mL of heparin. Interestingly, porcine blood with this

Table 2: Modeled and experimentally verified steady flow rates in the microfluidic device. For both glycerol and heparinized blood, flow rates match the model well at all shear rates well. Measured flow rates are shown as averages $\pm$ standard deviation. Instrument (weighing scale) measurement uncertainty is 0.3 μL/s.

Shear rate γ (s^{-1})	Q_{model} (μL/s)	$Q_{glycerol}$ (μL/s)	Q_{blood} (μL/s)
500	1	0.5$\pm$0.4	0.6$\pm$0.3
1500	5	3$\pm$1	3$\pm$1
4000	15	13$\pm$1	13$\pm$1
7000	19	17$\pm$1	17$\pm$1
10000	24	27$\pm$2	27$\pm$2
13000	40	39$\pm$7	39$\pm$3

level of anti-coagulant did undergo platelet thrombosis in our devices, while human blood did. This difference may be attributable to the use of acid-soluble collagen to coat the devices used with these porcine samples.

Volumetric flow rates Q were measured using weighing scales (Ohaus, Parsipanny, NJ or Adams Equipment, Danbury, CT) with 0.01 g resolution. The open end of each channel's outlet tubing was taped into place onto Petri dish, each of which was placed on an independent scale (four in total, one for each channel). Mass, m, as a function of time, t, data from the weighing scales was acquired at 1Hz and written to file using a Labview acquisition program. Mass over time was then converted to Q according to $Q = \dfrac{\Delta m}{\rho \Delta t}$, where ρ is the density of the fluid (1.11 kg/m^3 for 43% glycerol [88], 1080 kg/m^3 for blood [75]), and Δt is a 10 second window of time.

2.3.2 Thrombus histology

Next we needed to verify that these flow conditions and devices were able to consistently form thrombus. We also needed to confirm that the contents of the thrombus were platelets, as hypothesized.

To verify the platelet composition of the occlusive thrombus, we used Carstairs histological staining method. To perform Carstairs staining, we excised the PDMS layer containing attached thrombi, preserved them with formalin for 48 hours, dehydrated them in a series of xylene washes, fixed them in paraffin, microtome sectioned
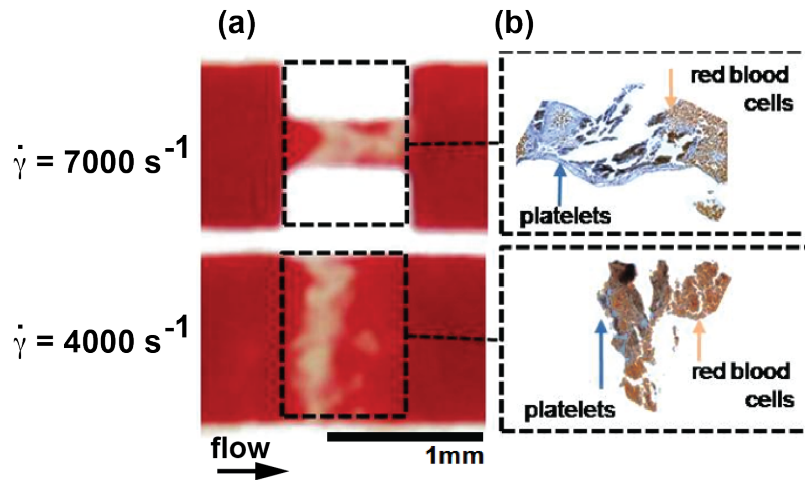
Figure 11: Microscopy images (a) of thrombi formed within device stenoses at higher shear rate, 7000 s^{-1} (top) and lower shear rate, 4000 s^{-1} (bottom). Subsequent histology (b) via Carstairs staining reveals expected platelet thrombi (stained blue) at high shear rate and red blood cells (stained orange/red) mixed with platelets in thrombi at the lower shear rate. Images were taken *en-face* at 4X magnification.

them into 5 μm slices, and stained them. The stain colors platelets blue and red blood cells orange/red. Thrombus volume within the stenosis was estimated by multiplying its cross-sectional area by the height of the stenosis.

Thrombus histology results using Carstairs staining method (Fig. 11) indicate that thrombi formed within the stenosis region of our devices showed high concentrations of platelets with low concentrations of fibrin at high shear rates and greater numbers of red blood cells in thrombi at low shear rates, as expected and consistent with previous reports [15, 89]. Further evidence towards the formation of larger, more platelet-rich thrombi at high shear rates was shown in optical results detailed in Chapter 3. Thrombi formed at the higher shear values of 4000 and 10000 s^{-1} showed larger changes in SNR of Volumes of thrombi were estimated at 0.0256 μL (N=7), approximately 55% of the stenosis volume.

Table 3: Experimental measurements of times for blood flow to occlude microchannels for varying cross-sectional shapes under conditions of identical shear rates (N=3 for all cross-sections).

	Eccentric	Circular	Square	Semi-circular
Time to Occlusion $\mu \pm \sigma(s)$	78±48	313±55	170±42	66±48

2.3.3   Thrombosis in stenoses of varying cross-sectional shapes

The fabricated devices were used to assess the effects of variations in cross-sectional area on the formation of clots. Tests were run by flowing blood under specific shear rate conditions and monitoring the time it takes for clots to form and stop flow within each microchannel. This quantity is defined as the time to occlusion. Flow was monitored through the use of video microscopy and mass flow measurements with 10 μL resolution.

Our results showed that the time to occlusion for the circular channel was higher than within the square channel by almost three standard deviations (Fig. 12). Since both channels had nearly identical hydraulic diameters and shear rates, we conclude that this effect may be due to differences in shear effects between square and circular cross-sectional shapes. One explanation may be due to the larger inner surface area of the square channel to allow adhesion of platelets (1.3X larger in the square than the circular). Although this surface area is larger, it is notable that the two still have similar area:perimeter ratios of 78.5 for circular and 77.5 for square cross sections, respectively. It may also be possible that platelet margination patterns may vary between the two cross-sectional shapes, although this topic will require additional investigation and is beyond the scope of this work. Although these results show large differences in occlusion times, further investigation should be performed on these test results due to low number of experimental trials and inherent variability of porcine blood samples used.

Thus the estimation of hydraulic diameter for square cross-sections, a common
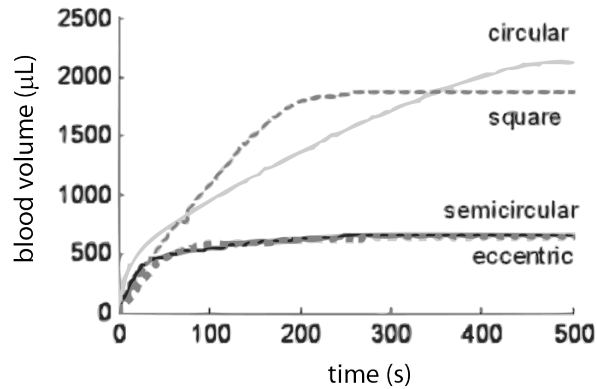
Figure 12: Channel occlusion was measured by mass flow of blood through the microchannels of different cross-sectional areas at equal shear rates. The circular channel required the most blood volume to occlude, followed by the square channel, while the semi-circular and eccentric channels occluded with nearly the same sample blood volume.

practice in microfluidics, may not accurately predict fluid behavior for shear-dependent applications. Additional evidence for the importance of hydraulic diameter is provided by comparing the circular channels time to that of the eccentric channel with the same percentage constriction and cross-sectional area. These variations in clotting time for channels of similar shear rates demonstrate the importance of both cross-sectional channel shape as well as hydraulic diameter and may provide substantial differences in thrombosis assays. These initial findings underscore the importance of developing methods for improved manufacturing techniques in microfluidic assays and also suggests that the common clinical assessment of arterial constriction by area may be insufficient to assess patient risk for thrombosis. However, it is again worthy to note that although these initial results show large differences in occlusion times, this finding may be due to low number of experimental trials and inherent variability of porcine blood samples used.

2.4 Conclusions

This chapter describes the design, fabrication, and testing of a microfluidic device for measurement of in-vitro platelet aggregation for a wide range of different shear rates.
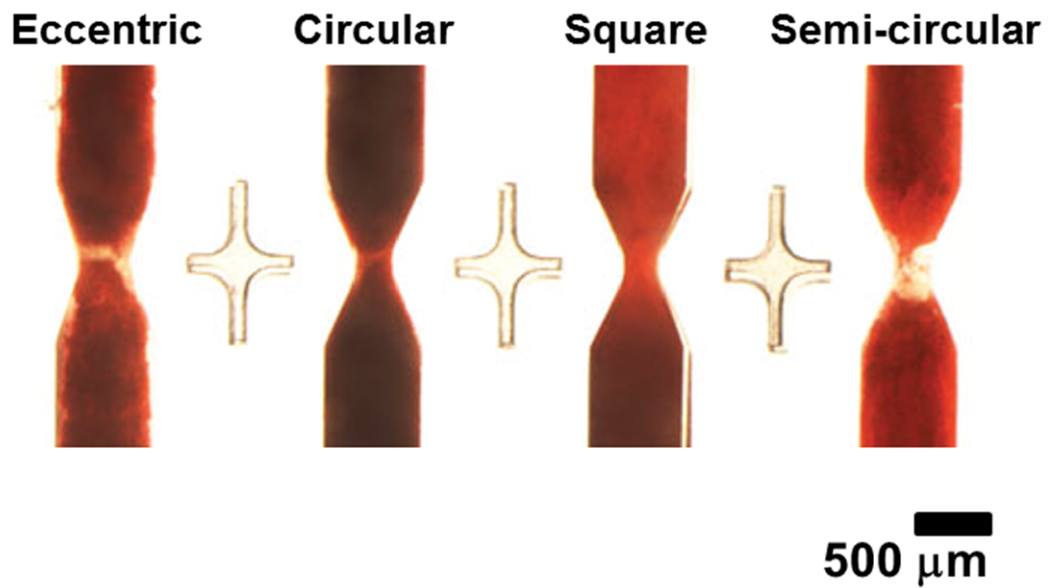
Figure 13: Images of formed platelet thrombi in channels of varying cross section morphologies (eccentric, circular, square, and semi-circular) on a single device after 500 seconds.

Analytical and computational modelling have shown the system's ability to address specific initial wall shear rates over two orders of magnitude, from 500 to 13000 s^{-1} a within a single device trial, simultaneously. Also described is a method for adjusting this range of shear rates using resistance tubing and input pressure.

We have also discussed novel methods for device fabrication. Unlike other traditional soft lithography microfluidics which are best for producing simple planar features of 200 μm or less in height, we have demonstrated the use of micromilling techniques to produce a variety of complex shapes over feature sizes from 250 to 1000 μm, and channel cross sections of various shapes.

Finally, we demonstrated the ability of these designed and fabricated channel arrays to experimentally address the correct shear rates and to form platelet thrombi, and showed that hydraulic diameter alone is insufficient to determine thrombosis times and dynamics. Although rounded channels provide an interesting prospect for future work, there are significant problems with achieving these shapes. First, the alignment

of these shapes to one another could be achieved with maximum accuracy of 31 to 64 μm, which in this case constitutes up to 21% of the width of the channel. This can also create shape discontinuities that could incur unwanted flow dynamics. In addition to this level of inaccuracy, the method also requires a high degree of manual dexterity due to the natural compliance of the PDMS material, short timescale allowed for optimal PDMS-PDMS bonding (approximately 30 seconds), and difficulty with visual and manual alignment using a dissection microscope. Findings on the effects of channel cross-sectional shape on occlusion time suggest that the square approximation of rounded or eccentric channels may be very inaccurate. Thus it is suggested that contribution of the latter two shapes to fluid dynamics leading to thrombosis might outweigh potential errors induced by shape [59], and should thus be pursued in future device designs provided that the tests shown here can be robustly replicated in similar studies.

Future development of the device for commercial or clinical applications should focus on the reduction of sample volume and sample handling required for users, especially in the area of drug screenings (discussed further in Chapter 5). Although the volumes used in this study are suitable for research applications such as these, multiplexing of these tests would require volumes of blood which may prove difficult for subjects to provide.

CHAPTER III

OPTICAL DETECTION OF PLATELETS

This chapter describes the development of an optical sensor for label-free, non-contact, multi-channel, high temporal resolution measurement of platelet-based thrombus formation. First, we describe the theoretical basis for our transmission-based sensing method. Next, the implementation and capabilities of this system in a variety of wavelengths and light sources is discussed. Finally, verification and comparison between this method and traditional microscopy methods is presented.

3.1   Design and modelling

As previously noted, current methods for measuring platelet aggregation have been predominantly conducted using microscopy. However, microscopy methods are problematic due to limitations of small measurement areas, poor depth measurement, need for image post-processing, and often require sample pre-treatment and/or fluorescence capabilities. Alternative methods have used flow, but such methods can be bulky and costly. Yet other methods have used electrical impedance, but the use of electrodes requires the exposure of blood to a non-physiological metal surface.

Thus for our microfluidic system, our goals were to construct an optical sensing system that was able to detect thrombus kinetics in real time (including clinically relevant measurements of thrombus buildup, occlusion, and detachment events), scalable to detect thrombosis in many channels, and able to perform such tasks with capabilities similar to conventional microscopy techniques.

The gross differences between large platelet thrombi, a semi-transparent white, and whole blood, an opaque red cellular suspension are immediately noticeable by eye, thus measurement of light transmission through the thrombus mass was an attractive

candidate to measure thrombosis. The transmissive properties of blood's components varies widely. Platelets are less scattering and less absorbing to visible light (250-850 nm) than red blood cells due to differences in their index of refraction and lack of hemoglobin [1, 6]. Therefore, as platelet–rich thrombus accumulates in the stenosis, otherwise filled with blood, light transmitted through it increases.

To quantify the differences in light transmission through these different tissue types, we applied a Monte Carlo radiative transport optical model for simulating large numbers of photon "packets" propagating through turbid tissues at calculated trajectories. The simulations are based on macroscopic optical properties of tissues which extend uniformly over step sizes of 10-1000 μm, and are thus most appropriate for a tissue-level evaluation, and not one at the cellular level. At each of these step distances, photon packet trajectory is calculated based on the local tissue's ability to scatter it (α_s) in a direction determined by its anisotropy of scattering (g), while the energy which keeps the packet moving is determined by the local ability to absorb the photons' energy (α_a). The point at which the number of photons which are able to propagate drops below a certain point due to absorptive energy loss or scattering to a different direction is the penetration depth of the light source, and the number of photons able to reach a depth z over the original number incident at the surface of the tissue is the transmission. Thus these simulations are commonly used in modelling the capabilities of medical imaging methods such as magnetic resonance imaging (MRI)[90]. In this work, we seek to use this method to predict the changes in light transmission as the layers of "tissue" within the stenosis change their percentages of composition, from 0% thrombus and 100% whole blood when the stenosis is first exposed to the sample, to 100% thrombus and 0% blood at full occlusion, as shown in the schematic of Fig. 14.

The software package which runs these simulations is called the "Monte Carlo model of steady-state light transport in multi-layered tissues" (MCML), written by
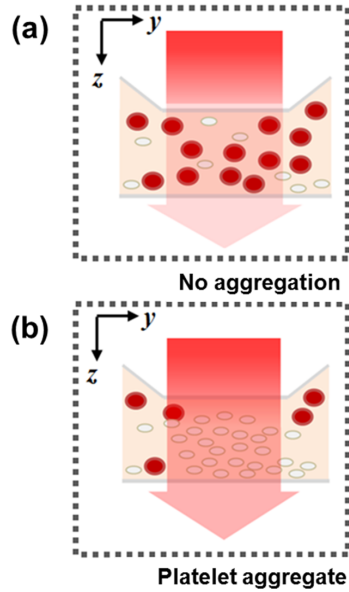
Figure 14: Platelets are less scattering and less absorbing to visible light (250-850 nm) than red blood cells due to differences in their index of refraction and lack of hemoglobin [1, 6]. Therefore, as platelet–rich thrombus accumulates in the stenosis (otherwise filled with blood, (a)) light transmitted through it increases (b).

Prof. Lihong Wang and Prof. Stephen Jacques [91]. The program's client input is provided through the .mci file, which allows the user to specify the properties of the tissue layers throughout each of the δz depth steps. This input file interfaces with a command-line based C program called mcml.exe, which uses it to perform the stochastic simulations, and writes the outputs of the simulations to an output .mco file.

Notably, the MCML software package also offers additional capabilities beyond what has been explored in this thesis. In particular, it offers a conv.exe program, which can account for different beam profiles (Gaussian, "top hat", etc.) defined by the user. Thus for the LED light sources, which may not have as many beams incident with the surface of the sample as the previous laser sources, use of a custom beam shape to refine estimates of changing transmission may be beneficial.

In our Monte Carlo optical model input file, we needed to provide inputs for the bulk optical properties of the scattering coefficient, α_s, the absorption coefficient,

α_a, anisotropy of scattering, g, and refractive index, n for the two layers of interest–platelet thrombus and whole blood (we assumed hematocrit, Hct=0.41). Since all of these three properties vary over different wavelengths, they are difficult to study without the use of specialized equipment including an integrating sphere to capture and characterize the angle of scattered light. However, previous work has measured and tabulated these parameters in whole blood, as well as in diffuse concentrations of platelets [1, 92]. However, we sought to characterize the second layer as a layer of concentrated platelet thrombus, not diffuse platelets. For these more concentrated layers, we would at least need to know the new scattering coefficient, which is often nearly two orders of magnitude larger than the absorption coefficient [1]. However, such measurements on concentrated thrombus optical properties was not available. Thus we needed a method to determine α_s for concentrated platelet-rich thrombus in order to run these Monte Carlo simulations.

To address this issue, we identified a widely used technique for characterizing the scattering coefficient at a specific wavelength using rCSLM (reflectance Confocal Scanning Laser Microscopy) [93, 94]. This method uses experimental measurements of the intensity of reflected light I_r(z) vs. scanning depth z within the tissue of interest to calculate α_s using the following exponentially decaying function (Equation 6):

$$I_r(z) = I_0 exp(-2\alpha_s \times z) + C \tag{6}$$

Where I_0 is the incident intensity of the confocal light source before entering the tissue and C is a fitting constant. Reflected light intensity at a specific depth is determined using image processing, here performed using an automated custom written Matlab script.

Measurements were performed using a Zeiss LSM Vis microscope using a Plan Apo 20X objective (NA = 0.75), 71 μm diameter pinhole (1 Airy Unit), 1.61 μs pixel dwell over a depth range of 44 μm. Acquired images were 450 x 450 4 μm over 16

line averages. Master gain was set at 867, digital offset to 0.1, digital gain to 1.0. Our wavelength range of interest for this study was 632.8 - 650 nm (representing the HeNe laser and the diode laser), thus our reflectance measurements were obtained using the a 633 nm wavelength (set at 17% power in these experiments).

We verified that the method was successful after confirming its accuracy by using it to verify the known α_s for Intralipid-20% (Sigma-Aldrich, St. Louis, MO). Intralipid-20% is a fat emulsion clinically used as an intravenous food source in hospitals, but also commonly used as a substitute for human tissue (also known as an "imaging phantom") for medical imaging since the fat droplets resemble the lipid bilayers of cellular tissues. Briefly, samples of 1% v/v Intralipid-20% were freshly mixed and vortexed for 30 seconds before being injected into a microfluidic device. Devices were bonded to No. 1.0 thickness (0.13-0.16 mm) coverglass to account for the working distance (1 mm) of the confocal objective. Images were acquired over a depth of 120 μm, with measurements beginning 10 μ into the sample from the coverglass surface, which was detected by a sudden spike in reflected light intensity. Measurements were taken at two regions of interest within the stenosis.

Previous work has used this rCSLM method to characterize Intralipid-20 at 1% v/v concentrations and 633 nm wavelength as 22-48 cm^{-1} [95]. In our N=2 trials, we determined values of 22.75 and 23.86 cm^{-1}, thus verifying that we had successfully executed the rCSLM protocol.

After verifying the rCSLM protocol, we went on to characterize the scattering coefficient of concentrated occlusive platelet thrombi. Samples of thrombi were formed within microfluidic devices (again, bonded to No. 1 thickness glass) under shear conditions of 10000 s^{-1}, and rCSLM experiments were characterized within two hours of their formation.

To ensure that our measurements of depth vs. reflected intensity were taken in areas of high platelet density, we labelled platelets were labelled with the fluorophore

mepacrine for location purposes. This was a necessary step since post-processing of images was required to obtain the image contrast necessary to determine the location of a platelet thrombus. Mepacrines 525 nm emission was spectrally excluded from the platelet aggregation measurement wavelength bandpass through the use of a long pass 560 nm filter. Mepacrine was not used in any other experiments.

A sample image stack (450×450 μm) is shown in Fig. 15. It is notable from the image that the penetration depth into the stenosis is poor. This is due to the high degree of scattering from the thrombus and the red blood cells. The image stack shown was not used for the calculations of thrombus scattering due to its low density. Empirically we noted penetration depths of only 50 - 100 μm. We had originally planned to use this method to evaluate the volume of formed thrombi, as employed by others in literature [96]. However, this was not possible with the 250 μm tall stenosis used in this work.

Image stacks were then processed by selecting 100×100 μm regions of interest, and summing their pixel values to obtain local intensity as a function of depth z into the stenosis. This data could then be plotted as depth z vs. reflected light intensity, $I_r(z)$, and fit to Equation 6, as shown below in Fig. 16. The experimentally determined scattering coefficient for platelet thrombus is shown along with published optical properties of whole blood and platelets in Table 4 (α_s=184-203, for N=3).

Thus with the determination of the scattering properties of the platelet thrombus, we were able to provide all of the necessary inputs to the Monte Carlo optical model. All of the properties used in the model are listen in Table 4.

Using this information, we were then able to run the MCML depth simulations to calculate expected increase in transmitted light intensity as a function of platelet thrombus thickness within the channel. The model examined eleven different "runs", each of which were defined as a different thrombus height (and corresponding reduction in the size of the whole blood layer). Depth step sizes, δz were 10μm, and we
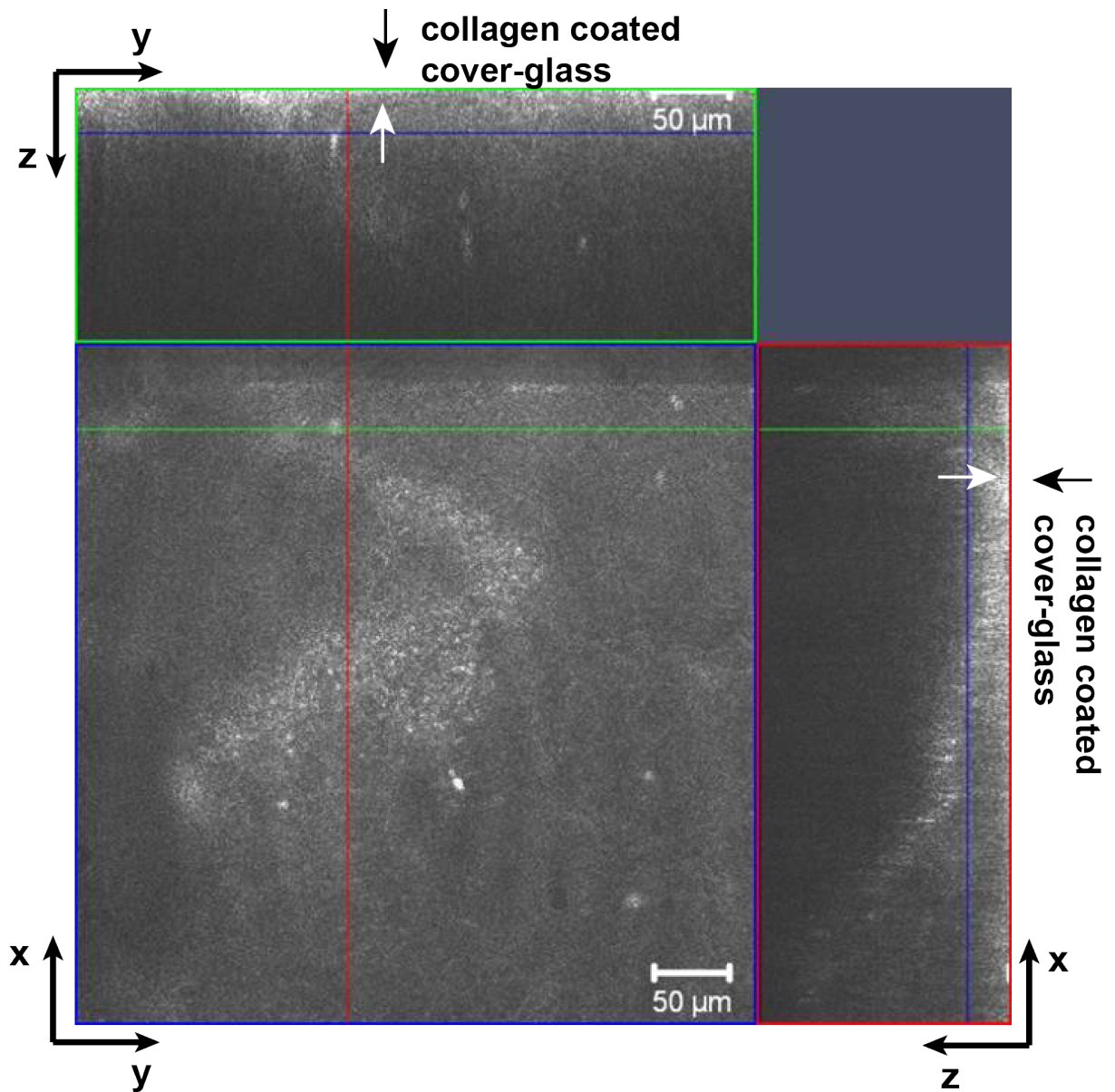
Figure 15: Fluorescence imaging using confocal microscopy was used to locate the regions of interest of highest thrombus concentration. As is evident from this image, the light is not able to penetrate through the entire depth of the stenosis, and reaches only about 50-100 μm in depth. Image acquisition began 10 μm away from the surface of the coverglass in order to avoid reflectance artefacts. These measurements were used to select the region of interest with the highest local thrombus thickness in order to calculate the scattering coefficient of concentrated platelet thrombus.
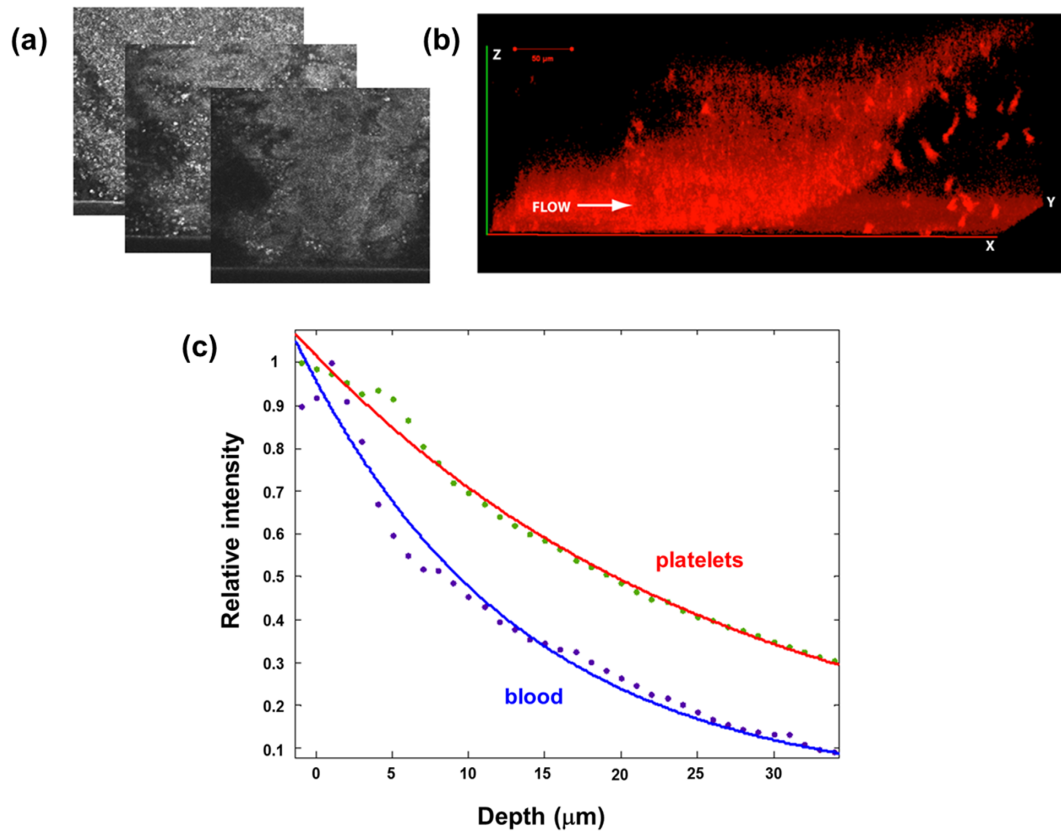
Figure 16: (a),(b) Reflectance measurements as a function of depth within the platelet thrombus were acquired using confocal microscopy. These values were then used to calculate the scattering coefficient of platelet thrombus by fitting the data (c) to the equation: $I_r(z) = I_0 exp(-2\alpha_s \times z) + C$ to determine the value of the scattering coefficient, α_s.

Sample	α_s (cm^{-1})	α_a (cm^{-1})	n	g
Blood (Hct 41%)	794*	7.92*	1.42*	0.99*
Platelet thrombus	193 †	1.21*	1.35*	0.96*

Table 4: Cited ([1] (*)) and measured (†) optical properties scattering coefficient α_a, refractive index n, absorption coefficient α_a, and anisotropy of scattering g, for whole blood and platelet thrombus at 633 nm were used to calculate changes in light transmission during thrombus growth.
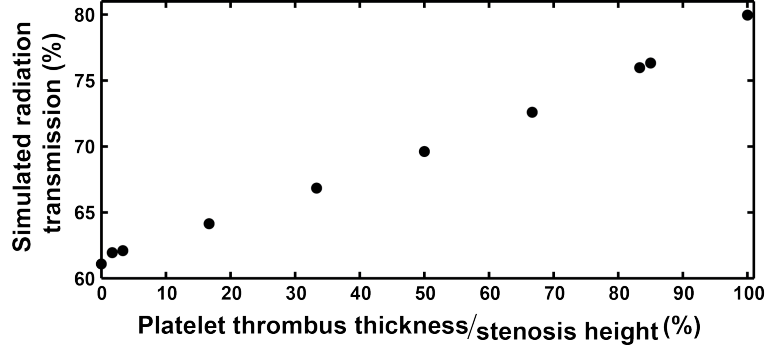
Figure 17: A Monte Carlo simulated relationship was calculated using cited and measured optical properties of blood and platelet thrombus. Values from the simulation were used to calculate of the percentage of 633 nm light transmitted through a platelet thrombus of varying thicknesses within a 250 μm stenosis filled with blood. Light transmitted is predicted by the model to increase by 19% from whole blood (0%) to fully occlusive thrombus (100%).

assumed $1e^5$ photons of incident light. Varying this number of photons had no effect on the overall percentages of light transmitted.

Model results returned the percentage of light transmitted through both layers (blood, thrombus) within the sample (Fig. 17). They predict a nearly linear increase proportional to thrombus height, up to a 19% change in light transmitted at full occlusion in which the thrombus thickess equals the full channel stenosis height. These results are supported by experimental results, which show increases in absolute light intensity of $24 \pm 10.2\%$ (N=68) for a thrombus whose thickness spans the entire stenosis height.

A significant limitation to our optical model is that it is not able to account

for changes in bulk optical properties over the course of thrombosis. However, observation of the thrombosis using brightfield microscopy seems show that thrombus density appears to change visibly from round to elliptically shaped clumps of non-contiguous platelet aggregates (10-100 μm in diameter) into a larger, more dense, semi-transparent mass of combined thrombus. (exceeding 100 μm in diameter) However this early, diffuse state of independent platelet aggregates is difficult to maintain for measurement. Often it was observed that even though tests were stopped partway to attempt to preserve these aggregates in their current state, their appearance would gradually change to the semi-transparent state seen in more advanced, denser stages. The observed change in state may be due to platelet shape change, which would create a surface that would more easily scatter light and thus appear more white than semi-transparent.

In fact, the scattering properties of growing aggregates have been used for platelet detection [97]. This principle provides the output measurements for platelet aggregation in the technique known as Light Transmission Aggregometry (LTA), one of the oldest methods for measuring platelet activity and the remaining "gold-standard" for such techniques [4, 20, 98]. Such measurements are made possible by the requirement that the test be run in Platelet Rich Plasma (PRP), a step which requires the slow, gentle centrifugation of blood to separate its components. Although it remains the gold standard, it is hampered by the need for this extra sample processing step, as well as the addition of non-physiological agonists to induce shape change and aggregation in platelets, by the potential activating effects of centrifuging the blood and the additional sample handling, and finally by the removal of native elements of whole blood which may play a role in thrombus development. Such scattering effects in developing thrombi in whole blood may be of interest for future optical studies.

3.2　Optical system fabrication

The optical system measures platelet aggregation through increases in light transmission comprises a monochromatic (laser) or quasi-monochromatic (light-emitting diode) light source coupled to a photodiode detector, or charge-coupled device (CCD) array of such detectors. In this work, we evaluated a variety of light sources including a 0.95 mW gas HeNe laser at 632.8 nm (SpectraPhysics, Bozerman, MT), a 0.9 mW diode laser at 650 nm (Melles Griot, Albuquerque, NM), and an adjustable power (up to 150 mW) LED source at 590 nm (Thorlabs, Newton, NJ). Power levels of all light sources were more than sufficient to detect thrombus formation–non-adjustable laser sources required the use of neutral density filters to prevent saturation of the CCD.

When using the laser light sources (at 632.8 and 650 nm), the size of the beam was typically near 0.75 mm in diameter. Thus it was necessary to expand the beam size to simultaneously interrogate all of the channels. To do so, we first removed spatial noise from the beam using a filter comprised of a small objective lens for focusing the beam into a pinhole of 20 μm in diameter. The resultant filtered beam was expanded in one direction using a cylindrical lens. The beam covered the width of each stenosis and the transmission of the light was measured with a 3000 pixel 12-bit linear CCD with pixel dimensions 7 μm x 200 μm (Thorlabs, Newton NJ) placed beneath the beam. Optical cross–talk between channels was mitigated with sufficient channel spacing and the use of an aperture plate, made from laser cut cardstock coated in mylar foil (Fig. 18).

Due to difficulties with the alignment, the gas laser system above was later replaced with a more robust and durable fixturing system which included a variable Galilean beam expander (Thorlabs, Newton, NJ) and the 650 nm diode laser. The beam expander created a circular spot size of approximately 25 mm in diameter–wide enough to cover all stenoses with a variation of 4.5% across the stenosis regions of the beam. Such differences in initial intensity incident on the stenosis regions did
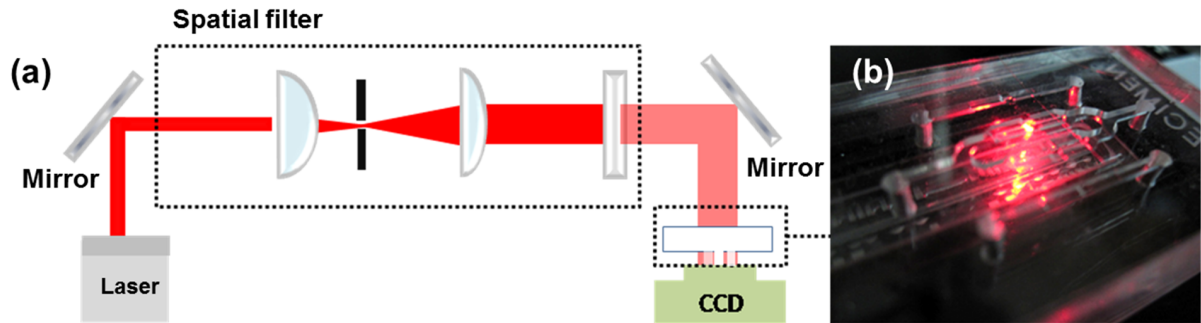
Figure 18: (a) The first generation of the optical system comprised a 632.8 nm HeNe gas laser whose beam was spatially filtered through a 20 μm diameter aperture and expanded unidirectionally by a cylindrical lens. The resultant linear beam then encounters a mylar aperture, underneath which the stenoses of the device are aligned (Device shown in (b)). The beam then shines through each stenosis, and transmitted light is detected by a linear CCD.

not appear to affect the overall change in transmission due to thrombus formation. The large spot size was not necessary, but convenient since it did not require special alignment procedures, and negated the requirement for an additional neutral density filter. This configuration was used for the experiments described in Chapter 4.

Although our modelling efforts had been focused on laser light in the 632-650 nm range, we had not yet determined whether this wavelength range was optimal. Furthermore, the use of a LED sources in place of lasers might be able to provide a lower cost alternative and wider areas of effect. Thus, we next use spectrometry to determine optimal testing wavelength and constructed the system using an LED source.

3.3   Wavelength optimization

Previous work has shown the detectable differences in light transmission through dilute platelet solutions vs. whole blood are greatest at 500-600 nm [1]. In this work, we experimentally verified these transmission-based differences through concentrated platelets thrombi formed inside a microdevice vs. whole blood using spectrometry and two quasi-monochromatic optical systems. Platelet thrombi were formed within
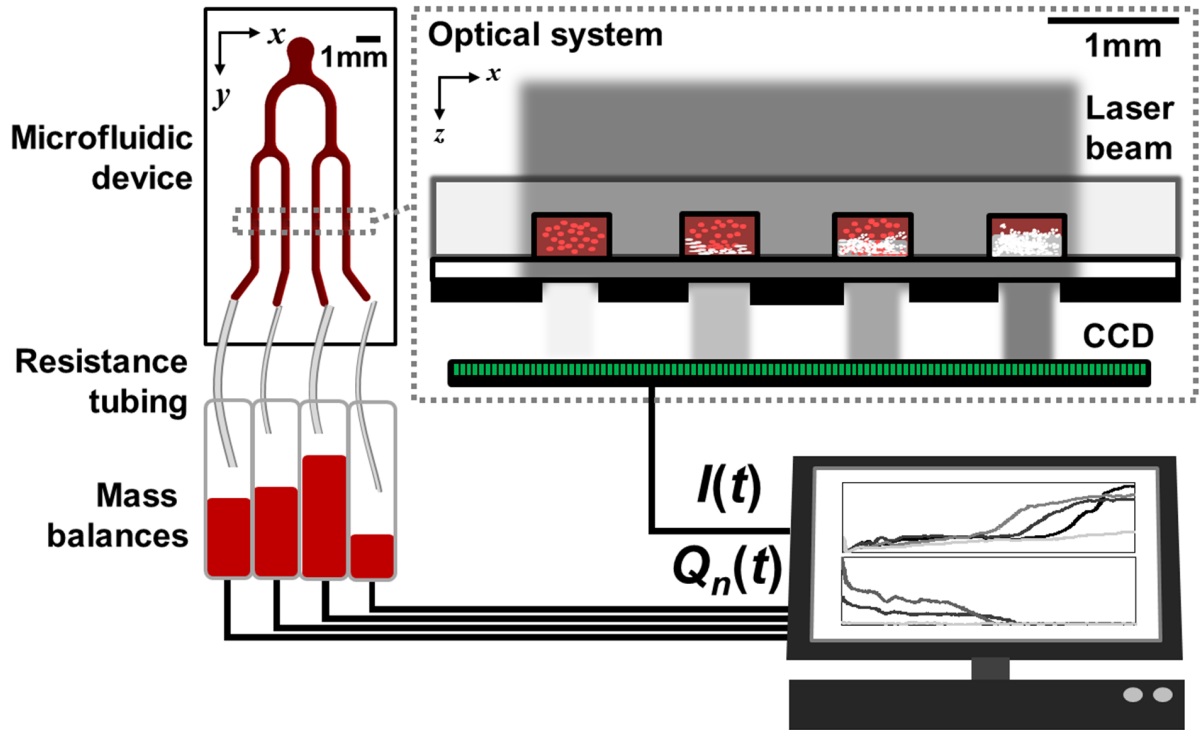
Figure 19: The microfluidic system comprises the microfluidic device and optical system. The optical system measures an increase in light transmission (from the laser to the CCD), $I_{\mathrm{laser}}(t)$, as the platelet aggregation in the stenotic regions increases during shear-mediated thrombosis. The shear rates in each stenotic region are controlled by resistance tubing, which terminates in independent weighing scales to measure flow rates $Q_n(t)$. Light transmission $I_{\mathrm{laser}}(t)$ and flow rates $Q_n(t)$ are acquired automatically in Labview and processed in Matlab.

PDMS microfluidic devices from whole porcine blood as described Chapter 4. Since the optical fiber used for spectroscopy (Ocean Optics, Dunedin, FL) is only 300 μm in diameter, and the thrombus is near the same size, the two needed to be precisely aligned to obtain accurate spectroscopy readings (Fig. 20). To align the two, a custom-built base plate made to fit onto a on a microscope stage which held the device with thrombus inside the stenoses. Next a custom built stage fixture which holds the optical fiber upright was attached to the microscope base plate. The microscope stage could be used to align the thrombus sample with the microscope objective. Then the focus could be switched in the z-direction and the optical fiber positioned directly above the thrombus using a crosshair overlay avaiable through our Nikon Elements NIS software. Thus the optical fiber would be precisely aligned to take accurate spectroscopy images from samples with microscale dimensions.

Using this system, we measured relative changes in light transmission (ΔT) through platelet thrombi vs. through whole blood (N=18 samples) were measured by over the visible spectrum (Fig. 22) as:

$$\Delta T = [(I_t - I_b)/I_b)] \tag{7}$$

Where I_t is the intensity of light transmitted through platelet thrombi, I_b is the intensity of light transmitted through whole blood, and λ indicates wavelength. Relative differences calculated using this method were used instead of absolute difference due to variations in I_b caused by differences in sample hematocrit. From these spectrometry experiments, we further verified the optimal wavelength by with quasi-monochromatic LED sources. From these values, the signal-to-noise ratio (SNR) was calculated as:

$$\text{SNR} = \frac{(I_t - I_b)}{\sigma_b} \tag{8}$$

Where σ_b represents the standard deviation of the intensity signal of whole blood.
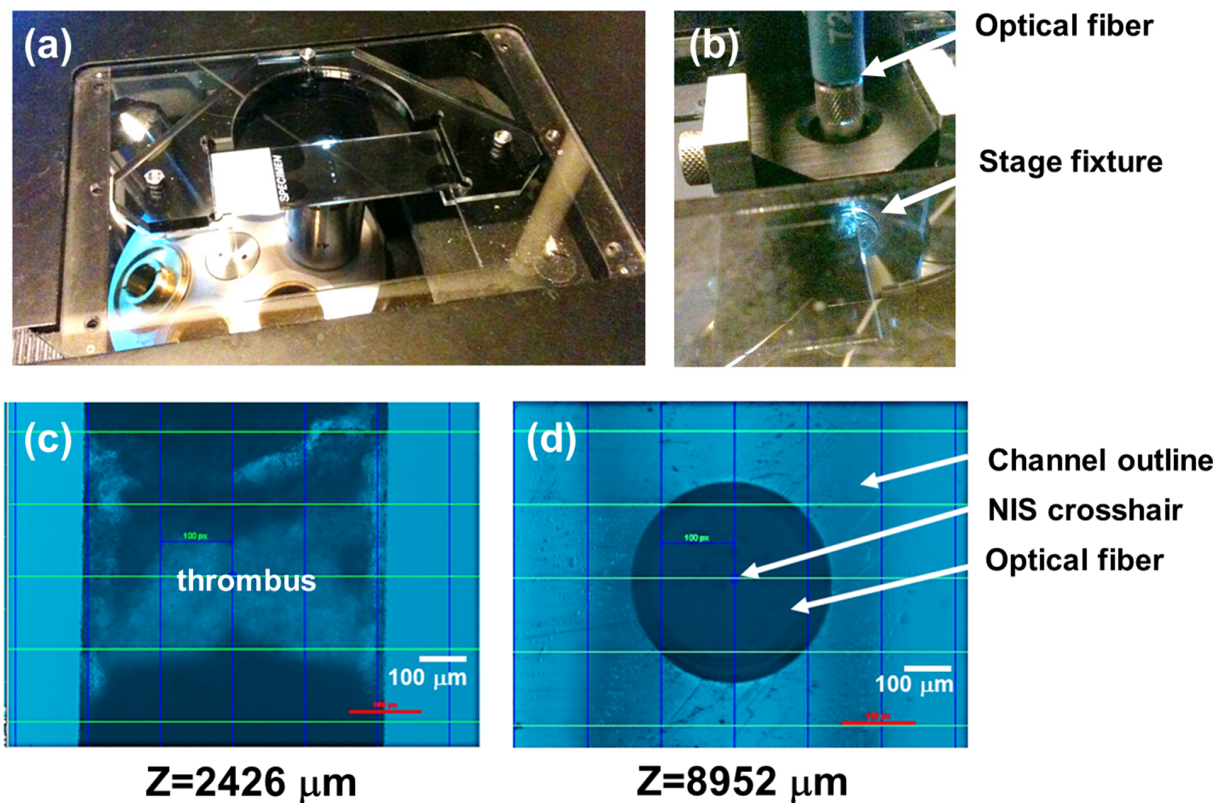
Figure 20: Precise alignment of the the optical fiber used for spectroscopy (300 μm in diameter), and the similarly sized thrombus required precisely aligned positioning in order to obtain accurate spectroscopy readings. To align the two, a custom-built base plate was made to fit onto a microscope stage, which holds the device with thrombus inside the stenoses. (b) Next a custom built stage fixture which holds the optical fiber upright was attached to the microscope base plate. (c) The microscope stage could be used to align the thrombus sample with the microscope objective. (d) Then the focus could be switched in the z-direction and the optical fiber positioned directly above the thrombus using a crosshair overlay avaiable through our Nikon Elements NIS software. Thus the optical fiber would be precisely aligned to take accurate spectroscopy images from samples with microscale dimensions.
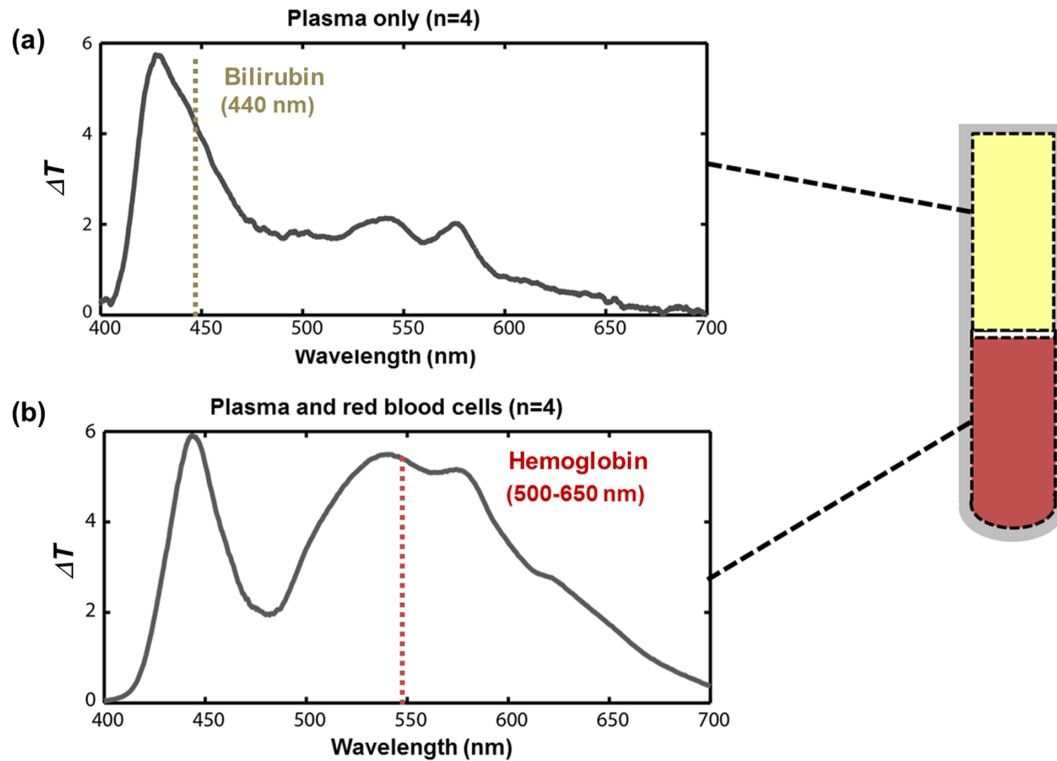
Figure 21: Control samples of plasma (a) and red blood cells (b) validated our spectroscopy readings by displaying, the 440 nm peak for the bilirubin chromophore and the 500-600 nm peak for hemoglobin, respectively.

For all tests, $\sigma_b = 2.4 \pm 1.5$.

To verify that our method could successfully determine the spectral output for blood's components, we first examined the spectral output of isolated components of the blood–a fraction of concentrated red blood cells, and another of plasma. In these control samples, we were able to observe the bilirubin chromophore peak at 440 nm in the plasma sample, as well as the 500-600 nm peak for hemoglobin in the red blood cell sample (Fig. 21). Thus our controls validated the spectroscopy method used.

Next we applied the validated spectroscopy method to evaluate the spectral properties of the concentrated platelet thrombus. To our knowledge, this is the first such characterization of this tissue, since as with the confocal measurements of the scattering coefficient, platelets are most often characterized as dilute cellular suspensions.

Results from spectrometry showed the maximum difference in ΔT to be near 590
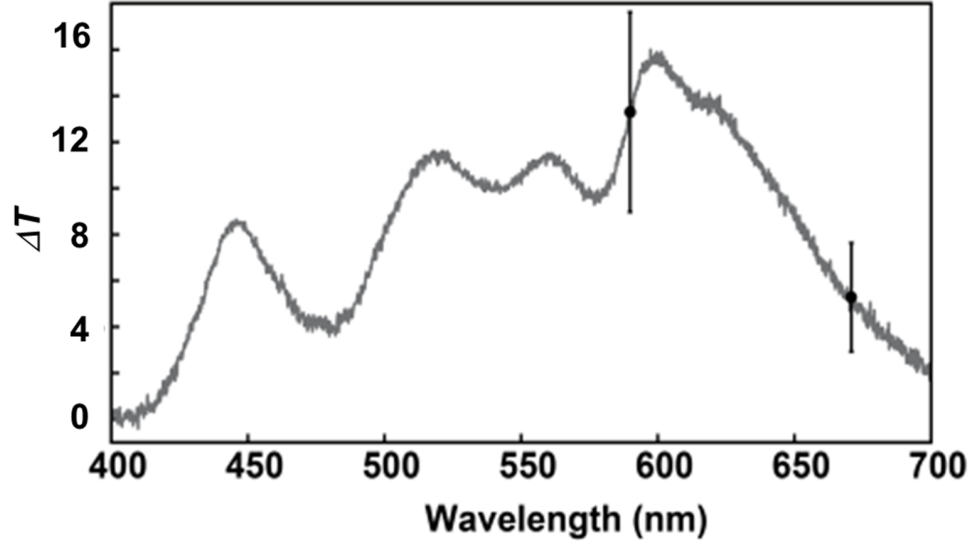
Figure 22: Relative difference in transmission (ΔT) between platelet thrombi and whole blood was measured by spectrometry over the visible spectrum using a high powered white light source over the 400-700 nm (Sutter Instruments, Novato, CA). Optimal ΔT occurs at wavelengths near 590 nm in contrast to those at wavelength of 671 nm. Results shown are averaged readings for N=18 occlusive thrombi samples vs. whole blood, with error bars indicating standard deviations

nm (13.2±4.04, N=18), with a lower magnitude ΔT at 671 nm at (5.06±2.02, N=18) (See Figure 1). Consistent with spectrometer predictions, the SNR of the monochromatic system at 590 nm (672.72, N=1) were much larger than those measured at 671 nm (87.4±146, N=68).

Standard deviations are largely attributable to natural variations in size and density of thrombi detected. Signal-to-noise ratio of thrombus detection by light transmission in the 400-700 nm range was optimal at 590 nm from experiments using

Table 5: Spectrometer readings showed a 2.6-fold increase in light transmission between the 671 nm and 590 nm wavelengths using a white-light source. Similarly, use of quasi-monochromatic light sources (e.g. light emitting diodes) in place of the broadband white-light source showed a similar fold increase in light transmission signal to noise ratio.

Wavelength (nm)	Spectrometer SNR	Monochromatic SNR
671	5.1 ± 2.02 (N=18)	87.4 ± 146 (N=68)
590	13.2 ± 4.0 (N=18)	227 ± 135 (N=24)

broadband spectrometry and two quasi-monochromatic optical systems. The optical detection described is applicable to current commercial and research methods.

3.4   Brightfield microscopy

In order to validate that our changes in light transmission could be used to measure platelet aggregation, we sought to create a system able to acquire simultaneous measurements of flow, CCD intensity at a monochromatic wavelength, and capture of microscopy images under white light. This was achieved through a custom built system which used a beamsplitter and two separate multiplexed light sources (Fig. 23). Hardware control and acquisition were sampled at 1 Hz with 20 ms integration time using Labview (National Instruments, Austin TX) and data was analyzed using Matlab (Mathworks, Natick, MA). Validations were run on both porcine blood samples using a 650 nm monochromatic light source (results shown in Chapter 5) as well as on human blood samples using the optimized 590 nm semi-monochromatic light source (results shown in Chapter 6).

Brightfield microscopy imaging relies on the interplay of a variety of properties including material scattering, absorption, and specular/diffuse reflectivity [99]. Thus brighter areas in microscopy images do not necessarily indicate increases in reflectivity (and thus decreases in transitivity through the sample), and such results do not run counter to predictions from our optical model. On the contrary, increases in brightfield contrast with increasing thrombus volume are expected due to thrombus related decreases in both scattering and absorption (see Table 4).

Flow rate measurements, $Q(t)$, shown in Fig. 24, also show the occlusion time. From this flow rate measurement, we were able to calibrate the intensity at which occlusion occurs in the laser optical system by setting a threshold as a percentage of maximum intensity. Flow rate is nearly constant while platelets accumulate in the stenosis because the stenosis is a small fraction of the overall resistance of the

73
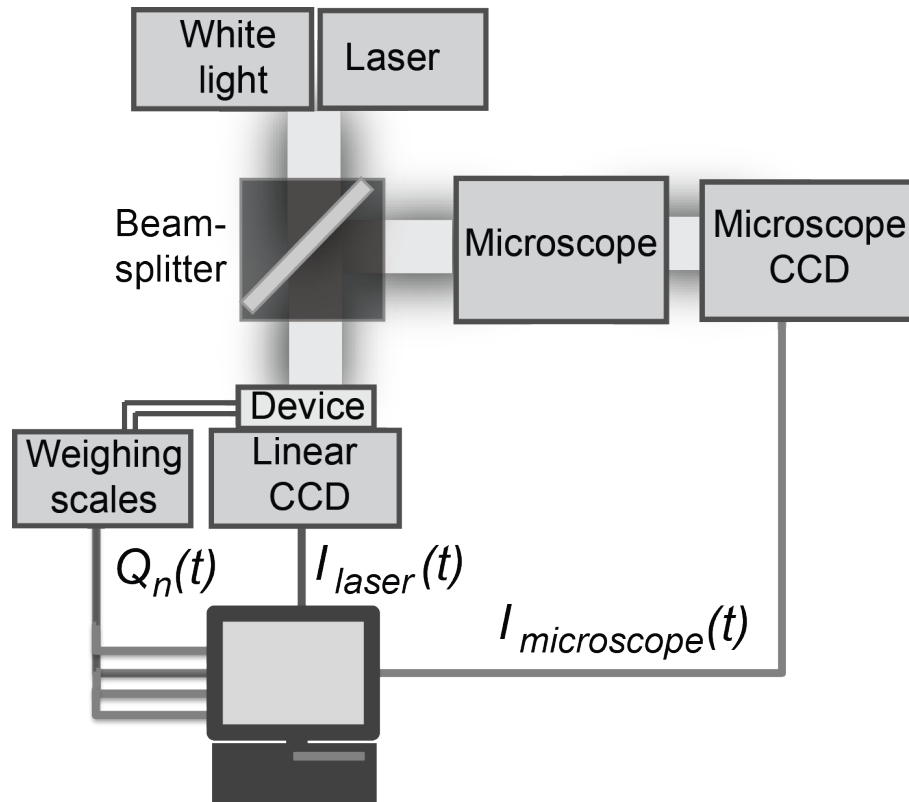
Figure 23: Schematic showing time multiplexed white-light microscopy and laser system optics. White-light microscopy images were acquired with a Zeiss Stemi 2000c microscope under 5.0X magnification and a Motic 2000 CCD camera. Laser light transmission measurements were obtained using a linear CCD and a laser (or LED) light source and detected with a linear CCD. Results were normalized as $[I(t) - I_{\mathrm{min}}]/I_{\mathrm{max}}$ and low-pass filtered to produce relative intensity measurements $I_{\mathrm{microscope}}(t)$ and $I_{\mathrm{laser}}(t)$. Timed switching between the white light and laser sources, in addition to the acquisition of flow rate data $Q(t)$ were controlled using Labview and results were post-processed in Matlab.

microfluidic channel and associated resistance tubing. From our fluid modeling, we estimate that the resistance of the stenosis reaches the same order of magnitude as the rest of the system at 28% occlusion, at which point ($\sim$400 s), the flow rate begins to decay logarithmically while shear rate increases, as confirmed by our fluid modeling efforts White-light microscopy images were acquired with a Zeiss Stemi 2000c microscope under 5.0X magnification and a Motic 2000 CCD camera in a detection method used by others [59]. Laser light transmission measurements were obtained using a linear CCD and a laser (or LED) light source and detected with a linear CCD. Results were normalized as $[I(t) - I_{\min}]/I_{\max}$ and low-pass filtered to produce relative intensity measurements $I_{\mathrm{microscope}}(t)$ and $I_{\mathrm{laser}}(t)$. Timed switching between the white light and laser sources, in addition to the acquisition of flow rate data $Q(t)$ were controlled using Labview and results were post-processed in Matlab.

We first used the microfludic system to form and detect platelet aggregation to full occlusion of flow at 10000 s^{-1} initial shear rate with simultaneous optical (microscope and laser optical system) and flow rate measurements. Results of a typical experiment are shown in Fig. 24.

From the time series of raw microscope images of platelets aggregating in the stenosis, normalized intensity, $I_{\mathrm{microscope}}(t)$, was computed for comparison with the laser optical system intensity transmitted, $I_{\mathrm{laser}}(t)$. Occlusion times between the methods differ by 3.97%$\pm$5.1% (N=6) with Pearson product-moment correlation coefficient, r=0.94, p<0.01, all measured from porcine blood samples.

Additionally, the system was also able to detect embolism events during which formed thrombi which had occluded flow would partially fragment or completely break away from the channel walls, creating a sudden decrease in measured $I_{\mathrm{laser}}(t)$ and $I_{\mathrm{microscope}}(t)$, and a sudden increase in flow rate $Q(t)$.

This build-up and detachment of thrombus is an important area of study due to its clinical relationship with stroke. In Chapter 5 of this work we discuss the relevance of
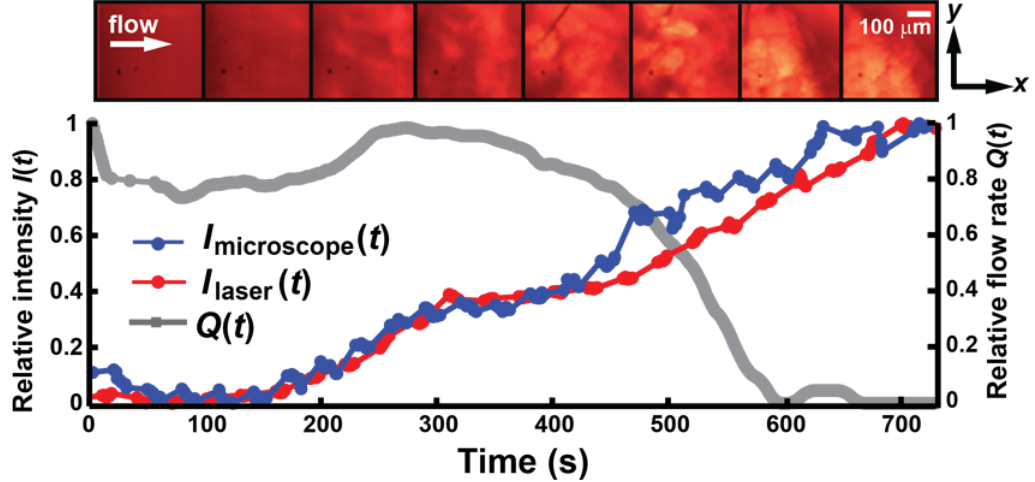
Figure 24: Formation and measurement of porcine platelet aggregation to full occlusion of flow in the microfluidic device using simultaneous measurements of microscope intensity, $I_{\mathrm{microscope}}(t)$; light transmission, $I_{\mathrm{laser}}(t)$; and flow rate, $Q(t)$, at 10000 s^{-1} initial shear rate. Microscope images (a) show aggregationbrighter areas of the images correspond to more platelet mass. The correlation between microscope intensity and light transmission measurements was calculated as Pearsons r=0.94. All data shown comes from a single trial.

this metric of thrombus fragmentation/embolism with anti-platelet drug treatment.

Next, we repeated these verifications on human blood samples using the optimized 590 nm quasi-monochromatic light source (Thorlabs, Newton NJ) in the multiplexed configuration previously shown (Fig. 23). Results showed similarly high Pearson's correlation values with microscopy (r=0.92, N=5) to porcine results.

Similar to the previously discussed porcine measurements, we also measured the use of semi-monochromatic transmitted light intensity with flow rate for human blood at 590 nm. Again, results showed significantly higher values for change in light transmission (Table 6).

Thus we have shown that light transmission is an effective endpoint detection for thrombosis using a variety of light sources and wavelengths.

So we next investigated whether this method could be used for more precise measurements of volumetric growth instead of simple binary detection. In order to assess the sensitivity of such measurements, we used the simultaneous measurements of
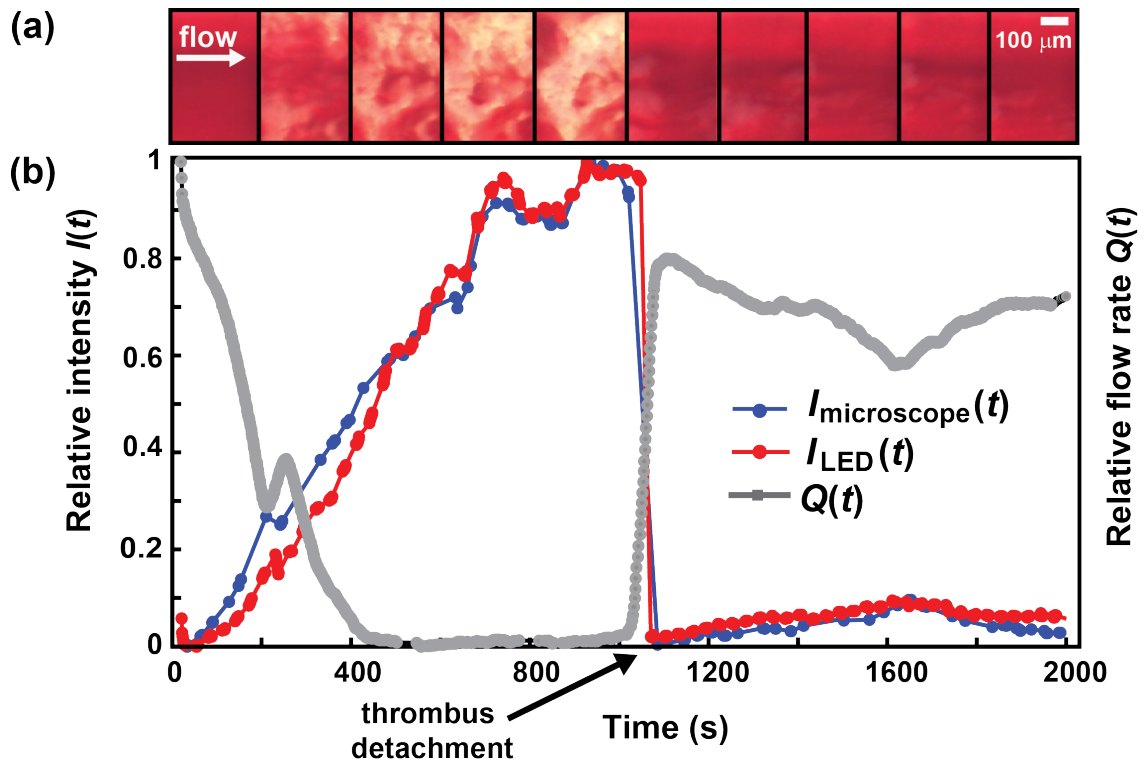
Figure 25: The microfluidic system detected thrombus detachment ("embolism") events, during which formed thrombi which had occluded flow would partially fragment or completely break away from the channel walls. Such events were observable both through microscopy images (a), as well as through Intensity measurements where they would cause a sudden decrease in measured $I_{LED}(t)$ and $I_{microscope}(t)$, and a sudden increase in flow rate $Q(t)$. As noted by the subscript, Intensity readings were acquired using microscopy and the 590 nm quasi-monochromatic LED light source. (b)

flow rate and intensity to plot the relationship between the two for each successful occlusion trial (Fig. 26)

As with previous experiments in this Chapter, intensity measurements are presented instead as CCD Signal-to-Noise Ratio (SNR), according to the Equation 8, (where the standard deviation of the noise due to blood flow was $\sigma_b = 2.4 \pm 1.5$). Volumetric flow rate $Q(t)$ vs. CCD Signal to Noise Ratio SNR measured $I(t)$ for N=10 trials at 10000 s^{-1}, N=10 trials at 4000 s^{-1}, N=4 trials at 1500 s^{-1}, and N=2 trials at 500 s^{-1}. When trials begin, values of $Q(t)$ are highest, and values of SNR are low due to the absence of thrombus. Next, there is a nearly linear regime during which decreases in flow rate are proportional to increases in SNR. Finally, after flow stops the thrombus continues to become more densely packed and SNR increases, especially in higher shear thrombi. Although the slopes of $Q(t)$ vs SNR were similar, their offsets prevent the use of a precise calibrations between these different trials.

While the previous Fig. 26 showed a relationship between $Q(t)$ and SNR as difficult to calibrate precisely, the relationship between the two can still have great value as a binary endpoint. To evaluate the utility of the SNR endpoint to detect occlusion, the distributions of SNR values for both non-occluded and occluded channels is shown in the box and whisker plot of Fig. 27. For each occluded channel, two SNR measurements, SNR$_{\text{occlusion}}$ and SNR$_{\text{final}}$. These are defined in Equations 9 and 10, respectively as:

$$\text{SNR}_{\text{occlusion}} = \frac{(I(t = t_{\text{occlusion}}) - I_b)}{\sigma_b} \tag{9}$$

$$\text{SNR}_{\text{final}} = \frac{(I(t = t_{\text{final}}) - I_b)}{\sigma_b} \tag{10}$$

Where $I(t = t_{\text{occlusion}})$ is the measured sensor intensity at the time when flow $Q(t) < 0.001$ mL/s, $I(t = t_{\text{final}})$ was the measured sensor intensity at the end of the testing duration (up to 3600 s), I_b) is the intensity at the beginning of the test due
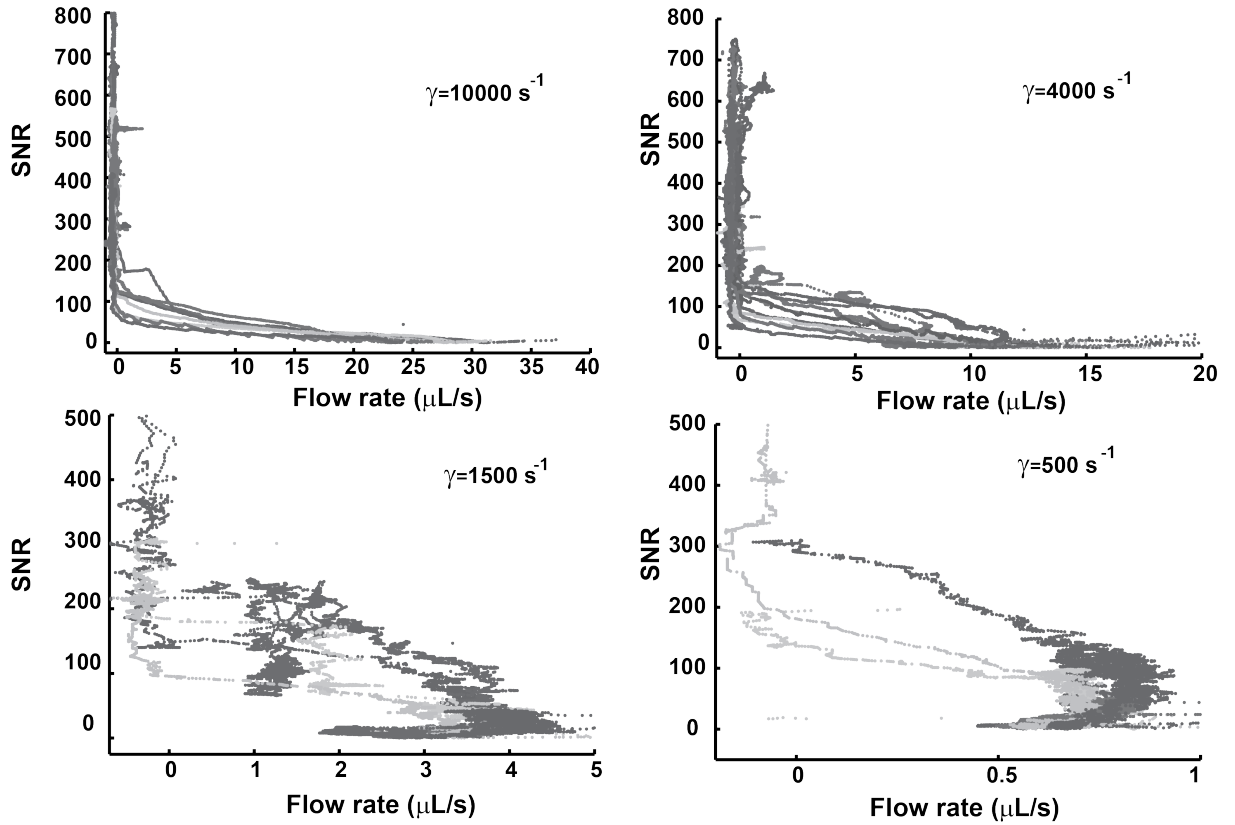
Figure 26: Volumetric flow rate $Q(t)$ vs. CCD Signal to Noise Ratio SNR measured according to Equation 8 for N=10 trials at 10000 s^{-1}, N=10 trials at 4000 s^{-1}, N=4 trials at 1500 s^{-1}, and N=2 trials at 500 s^{-1}. When trials begin, values of $Q(t)$ are highest, and values of SNR are low due to the absense of thrombus. Next, there is a nearly linear regime during which decreases in flow rate are proportional to increases in SNR. Finally, after flow stops the thrombus continues to become more densely packed and SNR increases, especially in higher shear thrombi. Although the slopes of $Q(t)$ vs SNR were similar, their offsets prevent the use of a precise calibrations between these different trials. Values of the standard deviation due to the whole blood sample, $\sigma_b = 2.4 \pm 1.5$

Table 6: Significance p values for Student's T-test comparisons between calculated CCD SNR values for channels which did not occlude (SNR_{NO}) vs. those which did occlude ($\text{SNR}_{occlusion}$ and SNR_{final}). The former is calculated by Equation 9 at the time when flow $Q(t) < 0.001$ mL/s, and the latter by Equation 10 at the end of the testing duration (up to 3600 s). Results show significant (p<0.05) differences between SNR values between channels of all tested shear rates with and without occlusions at both the time of flow occlusion and at the end of the testing period, although differences with the latter have much greater significance.

p-value	500 s^{-1}	1500 s^{-1}	4000 s^{-1}	10000 s^{-1}
SNR_{NO} vs. $\text{SNR}_{\text{occlusion}}$	0.023	0.007	$1.5e^{-6}$	$6.7e^{-6}$
SNR_{NO} vs. $\text{SNR}_{\text{final}}$	0.032	0.022	0.001	$9e^{-4}$

to intensity of the whole blood sample, and σ_b is the noise level at the beginning of the test due to the whole blood sample, which averaged 2.4 ± 1.5 over all tests. ($t = t_{\text{occlusion}}$) and , and the other calculated at the end of the testing duration (up to 3600 s). Average cutoff values for SNR at the time of [flow] occlusion fall between 50-200 for nearly all shear rates, reflected in the pooled value for SNR at occlusion time shown on the far right.

Next, significance p values for Student's T-test comparisons between calculated CCD SNR values for channels which did not occlude vs. those which did occlude were calculated. These results show significant ($p < 0.05$) differences between SNR values between channels of all tested shear rates with and without occlusions at both the time of flow occlusion and at the end of the testing period, although differences with the latter have much greater significance.

After determining that these values were significantly different, we next used the data to determine an optimal cutoff point for determining binary occlusion/non-occlusion. Optimal SNR cutoff value was that which maximized the difference in percentage of $\text{SNR}_{\text{occlusion}}$ vs. SNR_{NO}. Use of this cutoff would produce a "false positive" rate of 9.01% based on the number of non-occluded channels which still showed a rise in SNR above 90, and a positive detection rate of 96.7% and 74.2% at the final timepoint of the tests or at the time of occlusion, respectively. Numbers and
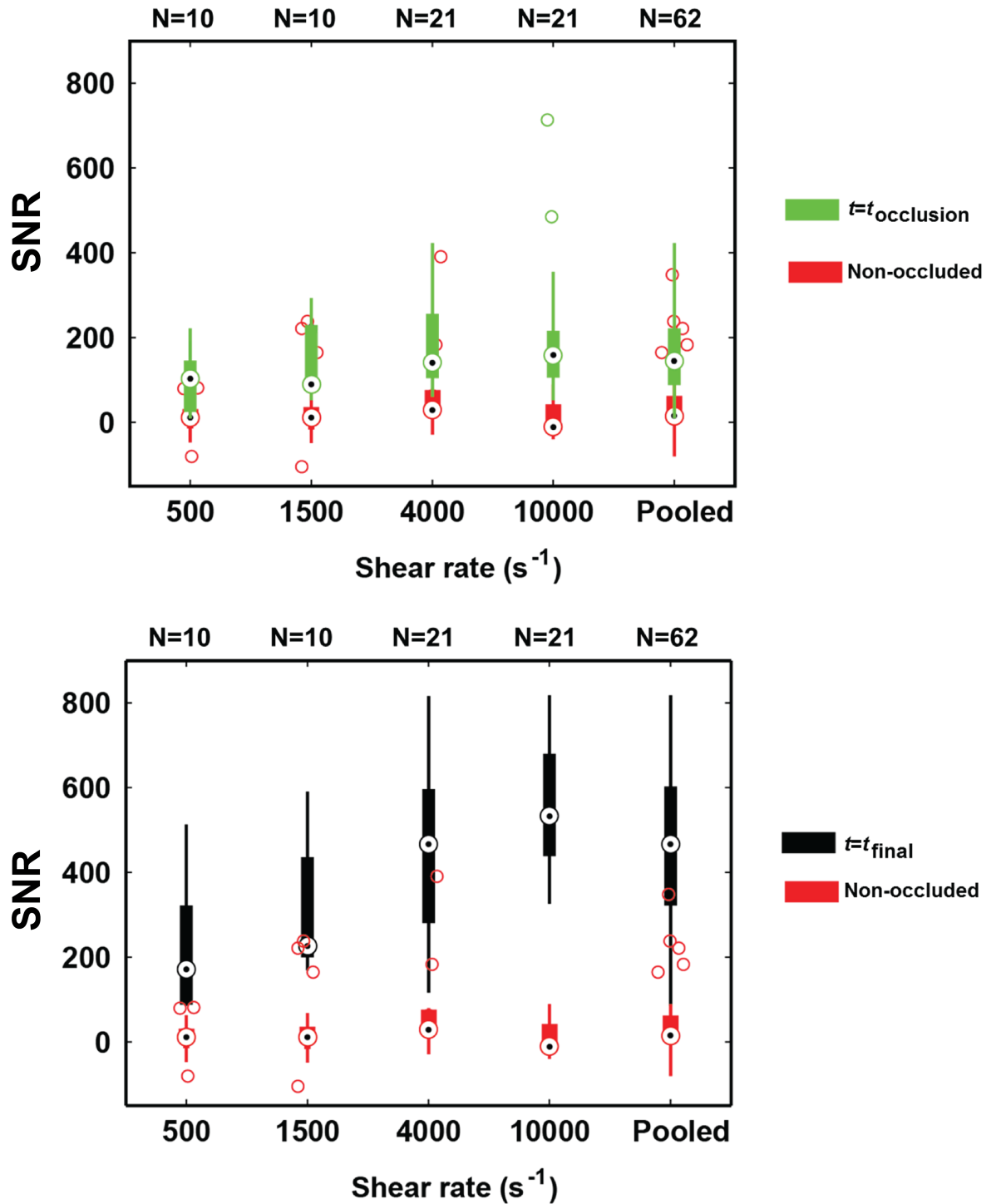
Figure 27: Box and whisker distributions of SNR values for both non-occluded (SNR_{NO}) and occluded channels ($SNR_{occlusion}$, SNR_{final}). $SNR_{occlusion}$ is calculated by Equation 9 at the time when flow $Q(t) < 0.001$ mL/s, and the SNR_{final} by Equation 10 at the end of the testing duration (up to 3600 s). Average cutoff values for SNR at the time of flow occlusion fall between 50-200 for nearly all shear rates, reflected in the pooled value for SNR at occlusion time shown on the far right

81

Table 7: Utility of the CCD SNR as an occlusion endpoint. Optimal SNR cutoff value was that which maximized the difference in percentage of $SNR_{occlusion}$ vs. SNR_{NO}. Use of this cutoff would produce a "false positive" rate of 9.01% based on the number of non-occluded channels which still showed a rise in SNR above 90, and a positive detection rate of 96.7% and 74.2% at the final timepoint of the tests or at the time of occlusion, respectively.

SNR cutoff = 90	$SNR_{occlusion}$	SNR_{final}	SNR_{NO}
> SNR cutoff (%)	96.7%	74.2%	9.01%
N Trials	124	124	111

percentages of trials exceeding this cutoff point are shown in Table 7.

3.5 Hematocrit

In addition to the goals of this work discussed at the beginning of this Chapter, we were also interested in the use of on-chip hematocrit measurement. Hematocrit is vital metric for thrombosis assays due to its considerable effect on the optical and biological characteristics of blood. Prior work has found that variation in hematocrit from 20% to 60% (clinical range) can affect the time to formation of an occlusive thrombus by 100% [20, 31].

Hematocrit can be measured by light transmittance through blood because other blood components (e.g., lymphocytes, plasma, and platelets) have comparatively much lower volumetric concentrations as well as much lower absorption and scattering indices [1] relative to red blood cells at visible wavelengths. This technique has been used by others in macro-scale cuvettes in spectrophotometers [100], and in this work we were able to show a nearly linear calibration relationship of hematocrit vs. transmitted intensity in whole blood samples using our microfluidic device as a stagnant cuvette. We did not pursue further use and characterization of this method since our future studies obtained Complete Blood Counts for each sample (a set of metrics that includes hematocrit, as quantified by a flow cytometer), however this technique would be valuable in future development as an integrated measurement for point-of-care applications where flow cytometry is not available. This measurement
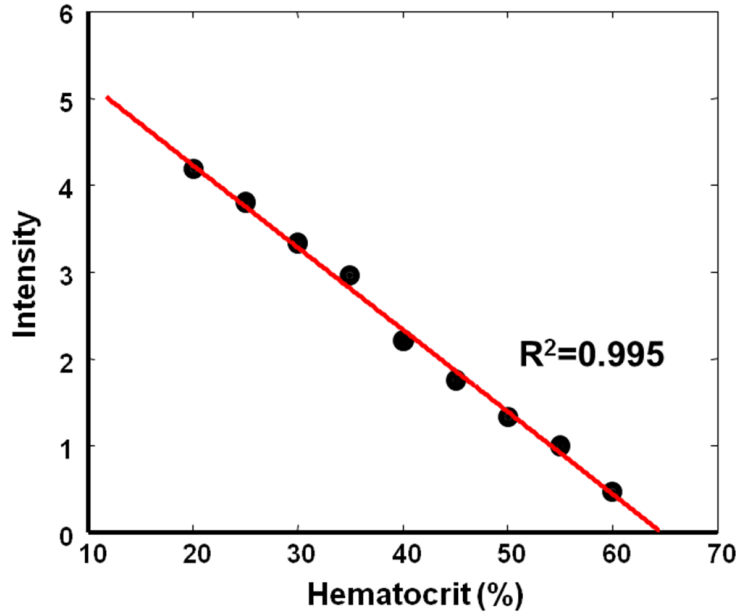
Figure 28: Intensity transmitted vs. hematocrit for unlabeled whole blood measured through the stenosis region in the microfludic system (N=3). This calibration was used to exclude samples outside of normal physiologic range (25-60% hematocrit) from analysis in subsequent platelet aggregation experiments

should be easy to integrate by allowing a small amount of blood to slowly fill the channels and then temporarily halting flow so that a hematocrit measurement can be taken and used to exclude patients with abnormal hematocrit or to adjust their results appropriately. Our calibration data is shown below in Fig. 28.

3.6   Conclusions

In the beginning of this Chapter, the stated goals for the optical sensing method were to detect thrombus kinetics in real time (including clinically relevant measurements of thrombus buildup, occlusion, and detachment events), scalable to detect thrombosis in many channels, and able to perform such tasks with capabilities similar to conventional microscopy techniques.

In this chapter we present the experimental characterization of the optical light scattering properties of platelet thrombus and describe the calculation of the 19 % increase in light intensity which should accompany the formation of an occlusive platelet

thrombus. We then demonstrate the construction and efficacy of a transmission measurement system using a variety of light sources (633 nm HeNe gas laser, a 650 nm diode laser, and a 590 nm LED array) and an 11 bit depth linear CCD. Additional experiments adding a multiplexed white light source and microscope camera showed that intensity measurements from microscopy image processing were nearly identical (Pearson's r=0.93) to measurements using our light transmission method. Characterizations of the relationship between flow rate and increases in light transmission showed that endpoint detection of flow occlusion could be reliably detected by light transmission measurements to detect 96.7% of fully occluded trials at a CCD SNR cutoff point of 90, although use of this method for finer measurements of thrombus volume will require further methodological improvements. The method is also able to detect thrombus detachment, verified by simultaneous flow rate measurements.

The system built and characterized in this work shows excellent correspondence with white light microscopy intensity readings. Thus the method provides a low cost, small-footprint alternative with similar potential capabilities. Due to methodological difficulties in measuring volume of thrombus during testing, it is currently difficult to use this method to precisely determine volume of thrombus formed. However, such capabilities may not be necessary for simple bedside tests for whom endpoints such as occlusion of SNR are easier and more clinically important. Thus this method shows great promise for future development for point-of-care devices.

Future work on optical thrombus detection might include the use of larger detectors which would avoid errors associated with thrombi migrating downstream of the stenosis. Another important aspect is the characterization of the thrombus prior to compaction–a better understanding of these changes might improve the precision of the transmission measurements to enable volume measurements of thrombi.

CHAPTER IV

EFFECTS OF SHEAR RATE ON PLATELET ACTIVITY IN PORCINE BLOOD

This chapter describes the application of the multi-shear microfluidic system in label-free, porcine whole blood samples. The data provides a survey on the effects of shear rate on untreated whole blood within a test population for an animal model and a proof-of-concept for the device and optics discussed in Chapters 2 and 3. These results form the foundation for the investigation of the simultaneous effects of shear rates and anti-platelet agents in this Chapter.

4.1 Methods

The purpose of these experiments was to first validate the ability of the system to form and measure the dynamic process of thrombosis and to establish an appropriate protocol for sample handling. Next, we desired to characterize the variability due to our experimental setup as well as in our samples. Finally, we applied the microfluidic system to whole porcine blood for shear rates spanning physiological to pathological flow conditions.

Porcine blood samples obtained fresh from a local abattoir (Holifield Farms, Covington, GA). Samples were gathered in quantities of 1 L from porcine carotids vessels and gently inverted in polystyrene bottles containing 3.5 Units/mL of unfractionated porcine heparin (Elkins-Sinn Inc., Cherry Hill, NJ). This concentration of heparin has been used by others to prevent clotting in storage reservoirs while allowing thrombus formation under flowing conditions [59, 101]. Although citrate is one of the most

often used anticoagulants by platelet researchers, it is a calcium chelator that requires the addition of ADP to re-activate platelets after its addition [89, 102]. In contrast, heparin does not require agonist addition to re-activate platelets, hence our preference. Early experiments examining the effects of altering added heparin concentrations showed no significant differences in platelet behavior after the addition of heparin within the window of concentrations from 2 to 10 Units/mL. However, at concentrations below 2 Units/mL, samples coagulated within ten minutes of collection, and at concentrations above 10 Units/mL, thrombosis was no longer observed in these porcine samples when exposed to acid-soluble collagen. In contrast, human samples retained platelet activity at higher concentrations of heparin (up to 40 Units/mL) when exposed to fibrillar collagen (see Chapter 5).

Samples were transported back immediately, but were not available for use until 1.5 to 2 hours after collection due to transit time. After transit, samples were placed on an orbital shaker at about 60 rpm.

Samples were used within five hours of collection, as longer times have been reported to reduce the efficacy of the low concentration of the added heparin. Samples older than five hours were noted to have larger deviations for occlusion times, and previous researchers have reported increased observations of emboli after this time. Due to the non-sterile conditions of sample acquisition, and/or large circulating lipid aggregates, artefact particles as long as 1 mm and as short as 20 μm were common. Thus, prior to experiments, the blood was filtered by flowing it slowly through a 200 μm pore polypropylene mesh (Smallparts, Seattle WA) to remove platelet or lipid aggregates that could cause embolic occlusion.

The collagen used to coat the interior surface of the device is a crucial initiator of platelet activity and adhesive substrate. Prior studies by others have shown that the choice of collagen type has a dramatic effect on subsequent thrombosis [85].

In initial studies of porcine blood, we used acid-soluble collagen I (Sigma Chemicals, St. Louis, MO) similar to others in the field [63]. While this collagen was suitable for initiation of occlusive thrombosis in porcine blood, it was not effective at initiating thrombus formation in human blood samples, a finding supported by investigations by Bernardo, *et al.*, who suggested that acid-soluble collagen was unlike the fibrillar collagen found physiologically due to its significantly reduced ability to bind the vWF adhesion protein [85]. Thus in human experiments, acid-insoluble collagen from equine tendon (Chronolog Corporation, Haverton, PA) recommended from the aforementioned group's publication was used (see Chapter 5).

For each porcine blood sample, four shear rates were run simultaneously in a single trial while platelet aggregation to occlusion was measured by the laser optical system only and flow rates were measured by the weighing scales. A trial is defined as a single experiment with one new microfluidic device comprising four channel runs. Up to three trials were run with each sample. An example of the output from one such multi-channel assay is shown in Fig. 30.

An example of the raw data from a trial (a single experiment with one new microfluidic device comprising four channel runs) is shown in Fig. 30, pictured next to the schematic of the system for context. Intensity measured by the CCD (top) is separated into four regions of interest according to the location of the stenoses and the intensity data is filtered to remove the high intensity white light time periods when microscopy images are being acquired (middle). Both microscopy images and CCD intensity information was acquired at 1Hz, and periods between white light and laser/LED source switching was 15 seconds. Flow rate data $Q(t)$ was simultaneously acquired through the weighing scales. Data was acquired in Labview and filtered and analyzed in Matlab.
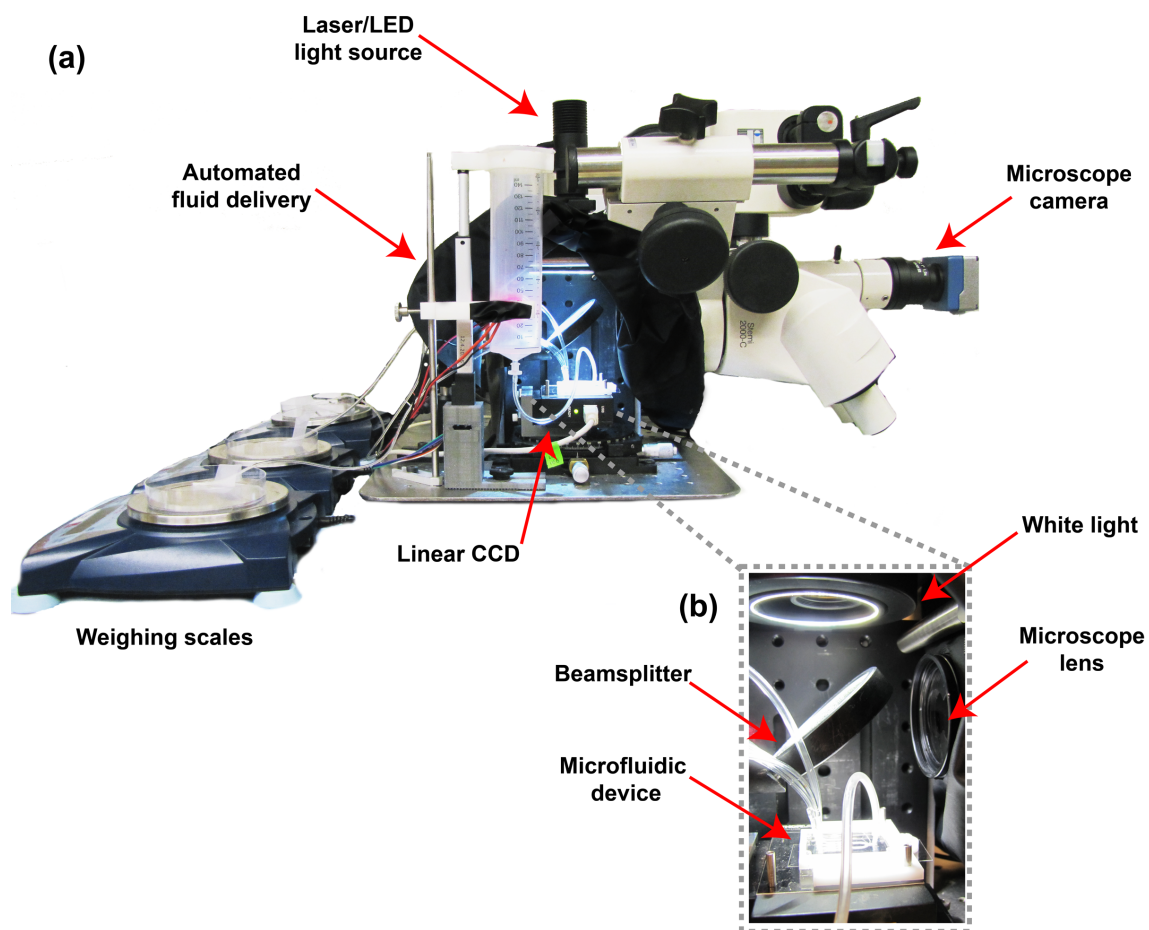
Figure 29: (a) The implementation of the experimental apparatus described previously by schematics in Fig. 19 and Fig. 23 which produces the output shown in Fig. 24. The system uses two light sources (white light and laser/LED), two sensors (CCD and microscope camera), and weighing scales in our assay measurements. Fluid delivery is achieved with an automated system which maintains gravity pressure head within 10-31 Pa of the target. Flow rate $Q(t)$ is measured using weighing scales. A beamsplitter positioned over the microfluidic device allows acquisition of images through the microscope lens to the microscope camera (b)
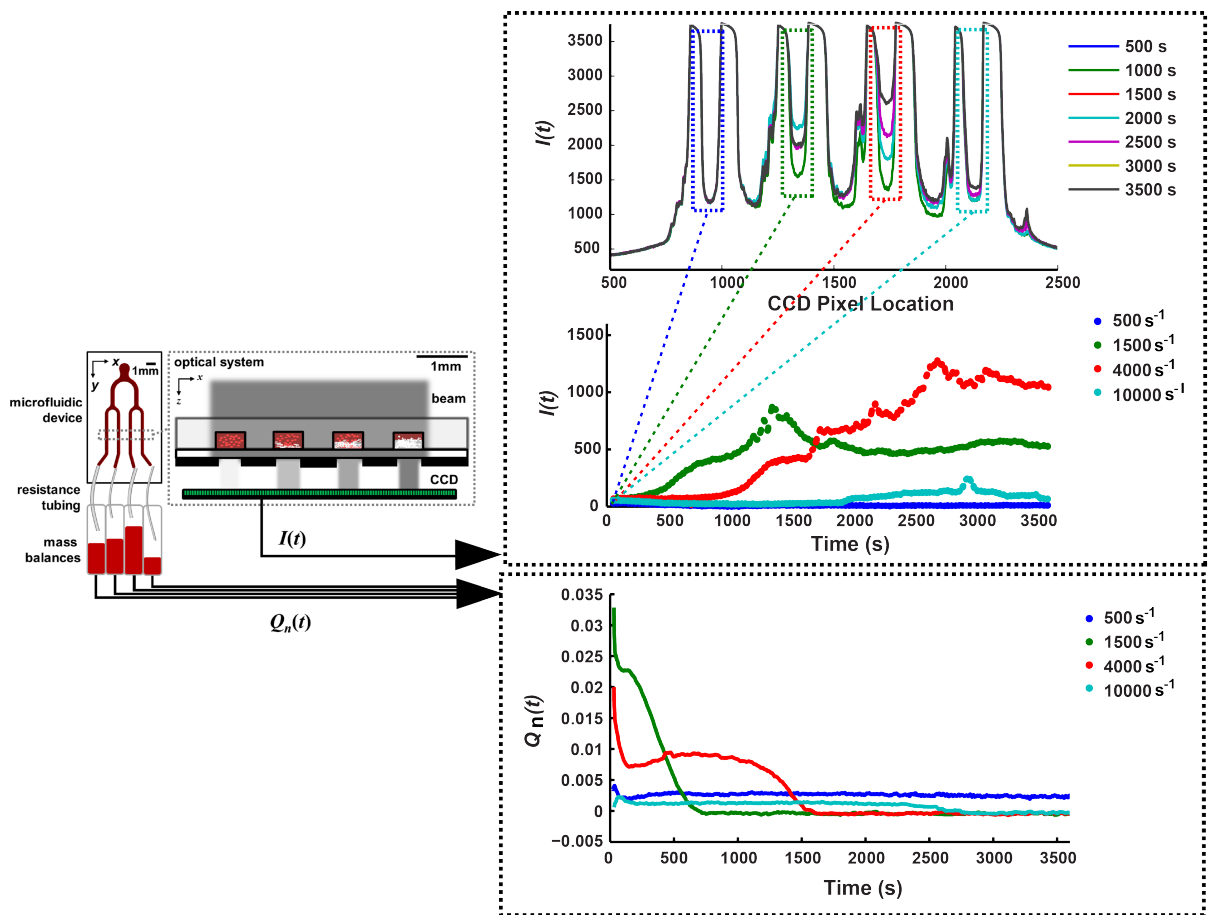
Figure 30: An example of the raw data from a trial (a single experiment with one new microfluidic device comprising four channel runs) is shown in Fig. 30, pictured next to the schematic of the system for context. Intensity measured by the CCD (a) is separated into four regions of interest according to the location of the stenoses and the intensity data is filtered to remove the high intensity white light time periods when microscopy images are being acquired (b). Flow rate data $Q(t)$ was simultaneously acquired through the weighing scales, and shown here in units of mL/s (c). Data was acquired using Labview and later filtered and analyzed in Matlab.

4.2 Results and discussion

In total, 14 porcine blood samples were run on a total of 27 trials resulting in N=4 channels/device $\times$ 27 trials=108 channel runs. Of these samples, 5/14 (36%) showed no occlusion at any shear rate or showed emboli at all shear rates, so these were excluded after a single trial. Embolus was defined as decrease in flow rate to less than 50% of initial within 30 s [59]. Of the remaining 9 samples run in 22 trials (N=88 channel runs), none of the channels with initial shear rate of 500 s^{-1} and 1500 s^{-1} formed occlusive thrombi over 2000 s (N=18). This finding is consistent with previous work which has shown that rapid platelet accumulation is absent with low shear rates (<2000 s^{-1}) [59].

The other N=70 channels were run at a variety of higher shear rates. Only two high-shear experiments did not clot (one at 4000 s^{-1}, one at 7000 s^{-1}), while in the other rest, occlusive thrombi formed at times less than 1200 s (N=68). This finding is consistent with reports from others that the platelet protein vWF begin to show significantly adhesive action at shear rates of 4000 s^{-1} [13]. The times to occlusion for the N=68 channel runs described are shown in Fig. 31, along with the corresponding standard deviations. The average difference between the optical and flow rate measurement of time to occlusion was 8.4%; the standard deviations of the time to occlusion measurements ranged from 50-212 s. For this range of pathological shear rates (4000-13000 s^{-1}), we did not observe a statistically significant (p<0.05) difference in the time to occlusion versus shear rate. Our findings with N=86 channel runs suggest that thrombosis is binary, present above 4000 s^{-1} and not present below 1500 s^{-1}. We have not studied this transition regime at higher resolution in this work.

Observable thrombus growth was only visible within the stenosis, although occasional aggregates were captured upstream of the stenosis entry. Thrombus growth typically began at the entrance of the stenosis, where previous fluid modeling (Fig. 4) has shown peak shear rates. These small ($\sim$50 μm in diameter), uniformly dispersed
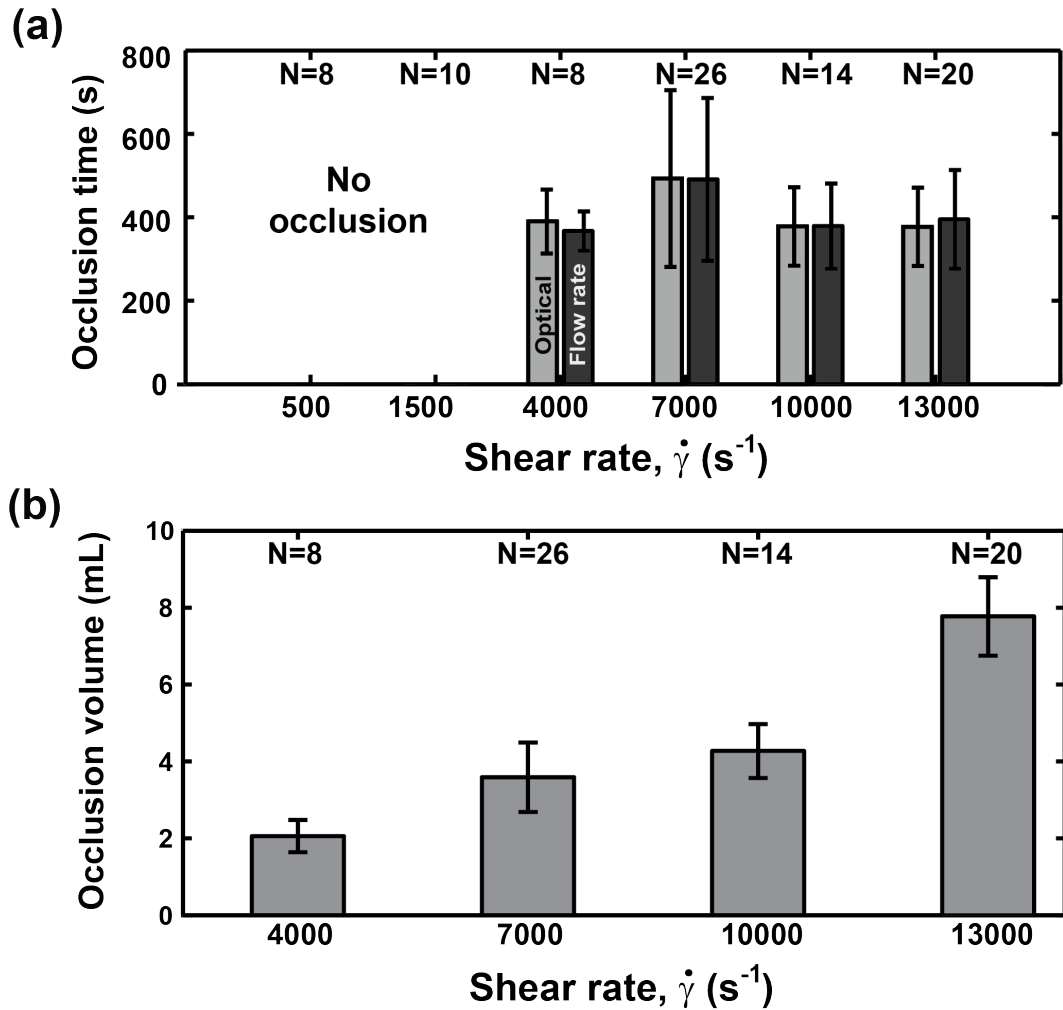
Figure 31: (a) Shear rates vs. occlusion times for six initial shear rates measured using the optical system and flow rate. Error bars indicate one standard deviation. For the range of pathologically relevant shear rates (4000-13000 s^{-1}), we did not observe a statistically significant (p<0.05) difference in the time to occlusion versus shear rate. (b) Shear rate vs. volume of blood (V) required to occlude flow. Error bars indicate one standard deviation. We observed statistically significant (p<0.05) differences in the volume to occlusion versus shear rate, save the 7000 s^{-1} to 10000 s^{-1} comparison.
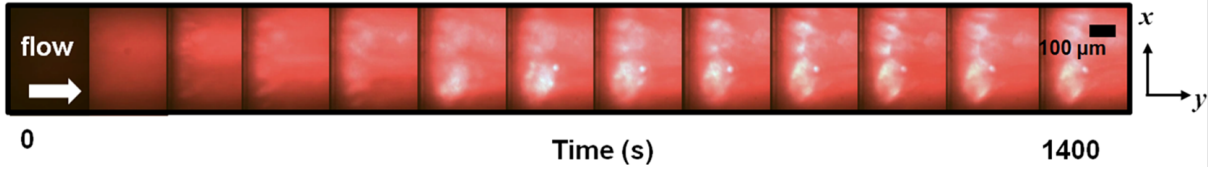
Figure 32: Observable thrombus formation typically begins after an initial lag time with small aggregates at the entrance of the stenosis. These aggregates rapidly grow in size and unite with later-forming downstream aggregates to create occlusive thrombi.

platelet aggregates would appear, enlarge, and unite with later-forming downstream aggregates to form larger aggregates (Fig. 32). The unified larger mass would often undergo significant remodeling, losing and gaining mass over time until the occlusion of flow. Despite the lack of flow, the thrombus often continued to develop by compacting into a dense, semi-transparent mass. This continued development was evident in measured intensity increases in both $I_{microscope}(t)$ and $I_{laser}(t)$. Occasionally the thrombus would shift downstream or embolize completely, resulting in decreases in $I_{microscope}(t)$ and $I_{laser}(t)$ although flow was still occluded.

To examine the intra-trial variability of blood clotting behavior, we measured how the blood clotting behavior varies between adjacent channels in the same trial with the same blood on the same device at the same shear rate. In 14 trials with duplicate shear rates channel runs (D=14 sets), we measured the average standard deviation of the clotting time, σ, for the sets. The average across all shear rates (D=14) was σ = 75 s. The average at specific shear rates was, for γ = 4000 s^{-1}, σ = 30 s (D=2); for γ = 7000 s^{-1}, σ = 99 s (D=9); and for γ = 10000 s^{-1}, σ = 34 s (D=3)).

To study the inter-trial variability, we measured how the blood clotting behavior varies between successive trials with the same blood at the same shear rate, we ran 9 triplicate channel runs (T=9 sets) and computed the average standard deviation of the clotting times for the sets. The average across all shear rates (T=9) was σ = 106 s. The average at specific shear rates was, for γ = 7000 s^{-1}, σ = 155 s (T=3); for γ = 10000 s^{-1}, σ = 61 s (T=2); and for γ = 13000 s^{-1}, σ = 91 s (T=4)). Since the

intra- and inter-trial variability measured were similar, occlusion time measurements across different trials and channels at common shear rates were comparable.

4.3   Conclusions

High shear rate platelet aggregation is central to the study of thrombosis. To study the effects of shear rate, we developed a multi-channel optical in-vitro method to simultaneously characterize changes in the times and volumes to platelet-based occlusive thrombus formation in whole, label-free blood samples across multiple shear rates over both the physiological to pathological range. The use of a laser to quantify thrombosis in whole, label-free blood is faster and simpler than fractionation and microscopy techniques[60, 64, 103]. For example, mepacrine staining requires low shear mixing and fluorescence imaging.

Our findings suggest that shear-dependent occlusion time from thrombosis is binary in untreated porcine blood samples, present above 4000 s^{-1} and not present below 1500 s^{-1}. We did not observe a statistically significant ($p<0.05$) difference in the time to occlusion versus shear rate. Intra- and inter-trial variability were similar, so occlusion time measurements across different trials and channels at common shear rates are comparable. In contrast, the blood volumes required for flow to full occlusion are significantly different ($p<0.05$), save the 7000 s^{-1} to 10000 s^{-1} comparison.

The laser optical system described should be scalable to tens to hundreds of channels whereas the conventional microscope and flow rate measurements, which yield similar occlusion times are typically limited to single channels. Measurements of occlusion from our optical system showed high correlation ($r=0.94$) compared with more expensive and bulky white light microscopy methods, and it is potentially more easily miniaturized.

Although the dimensions of the stenoses and channels used in the tests allowed for thrombus to form via rapid platelet-platelet accumulation (vs. smaller channels

which allow only small aggregates to form via a separate set of bonding events), there were some design tradeoffs. One issue with the system noted during this study was the large volume of blood required to occlude the channels (2-8 mL per channel, in contrast to the 0.8 mL used by alternative methods [20]). However, such expenditure of sample is specifically necessary for this set of studies, which requires not only sufficient channel heights to observe rapid platelet accumulation, but also high flow rates in order to obtain high shear rates.

Regarding a potential compliance mismatch between our PDMS flow channels and arteries, several groups have previously shown that vessel compliance has a minor effect on wall shear stress that would be dwarfed by the shear effect of thrombosis narrowing the lumen [10, 104, 105, 106, 107]. Further, reported Youngs Moduli are comparable (e.g., PDMS elasticity at pressures tested in this work = 0.38-0.75 MPa , human vessels elasticity at physiological blood pressure = 0.5-2 MPa [108, 109, 110]).

Endpoint detection of thrombosis using time to occlusion could be addressed using either optical or flow-rate based detection methods, and results of time to occlusion vs. shear rate were supported by previous research. Thus, it appears to be a useful metric well suited for these studies. However, the correlation of this method with microscopy data provides a fertile area for the addition of other metrics including thrombus detachment, mentioned in Chapter 1 as an important testing criteria for the ISTH, and is covered in experiments detailed in Chapter 5.

Future work will apply this microfluidic device and laser optical system to the clinical characterization of patient blood clotting with and without anti-platelet agents at varying shear rates, since these agents efficacy is suspected to be shear rate dependent. We have presented a proof of concept for applying clinically derived pathological flow conditions to whole blood samples in a microscope-free, high throughput, microscale system. In contrast to current clinical platelet diagnostics including parallel plate

assays and commercial devices [4], our system is able to examine platelet activity under multiple, well-defined shear flow conditions simultaneously at volumes consistent with typical clinical blood draws.

CHAPTER V

EFFECTS OF SHEAR RATE AND ANTI-PLATELET THERAPIES ON HUMAN BLOOD

This chapter describes the application of the multi-shear microfluidic system in label-free, human whole blood samples treated with varying dosages and types of anti-platelet agents. We first discuss the mechanism of anti-platelet agents and their applications. Next, a survey of the effect of shear rate on untreated human blood is presented and compared with the previously discussed porcine model. We then apply the system to examine the simultaneous effects of shear rate and anti-platelet dosing on human blood.

5.1   Experimental design

The pathology of myocardial infarction (heart attack) and cardiovascular accident (stroke) is thrombosis, the formation of platelet aggregates, in the coronary or cerebral vasculature. The mainstay of prevention for these events is the use of anti-platelet drugs to block the mechanisms underlying platelet aggregation. However, providing optimal drugs and dosages for patients therapy has been challenging, with estimates of 5-45% of patients misdiagnosed for the incorrect drug or dosage [20, 7]. Furthermore, the process of platelet aggregation is complex, involving multiple overlapping chemical mechanisms that are highly dependent upon blood flow conditions. Thus both local flow conditions and choice of anti-platelet therapy have inter-related effects which can dramatically affect patient outcomes, but has not been thoroughly characterized for clinically relevant conditions.

Specifically, previous work has described three specific shear flow regimes and their

associated mechanisms: "venous flow found in venules and veins (500-1000 s^{-1}), primarily governed by fibrinogen, coagulation factors, and the GPIIb/IIIa (also known as integrin $\alpha_{IIb}\beta_3$); "arterial flow found in healthy arteries (1000 - 4000 s^{-1}), primarily governed by GPIb, GPIIb/IIIa, and soluble agonists such as ADP; and "higher pathologic shear found in stenotic or obstructed arteries (4000 s^{-1} and above), primarily governed vWF and GPIb [4, 13, 12]. Anti-platelet drug therapies have been developed to disable specific targets of each of these aforementioned three mechanisms including: GPIIb/IIIa inhibitors (eptifibatide, abciximab), soluble agonist inhibitors (clopidogrel, acetylsalicylic acid), and anti-coagulants (heparin, citrate) [4]. A multi-shear approach to screening anti-platelet efficacy could thus provide salient information on shear-dependence to guide clinicians to choose appropriate drugs and dosages for patients with potential arterial pathologies, or to aid in the process of industrial drug candidate screenings [4].

Recent work by Hosokawa *et al.* [111] has examined changes in platelet accumulation due to both dosage and low shear rates (240, 600 s^{-1}) within non-stenotic channel geometries. While this work did examine changes in efficacy due to shear rate and drug dosage, the shear range and channel geometries used were not relevant to the intended therapeutic target of higher pathological shear rates in stenotic vascular geometries. Commercial systems for platelet evaluation have shown the ability to detect drug activity in-vitro. However, these systems operate at undefined shear rates and non-physiological flow conditions including closed-volume mixing using a stir bar or beads, flow through a membrane, or cone-and-plate mixing [20].

Thus most current methods for evaluating platelet thrombosis have not been addressed salient features including pathologically relevant stenotic flow [20, 112, 57], a wide range of shear rates from venous to pathological [60, 113], continuous monitoring of thrombus formation and detachment dynamics [4], and evaluation of advanced

stages of thrombus development. As a result, multi-shear, patient-specific characterization of drug efficacy has not yet been fully addressed. In previous work we characterized our microfluidic system and demonstrated its efficacy on thrombus detection in porcine blood samples [114]. In this work we report on the application of a microfluidic system to evaluate and quantify the influences of both clinically relevant drug dosage levels and a range of shear rates from venous to pathological levels on platelet aggregation within stenotic single-pass flow channels.

We began this study by validating the coating of the inner channel surfaces with fibrillar collagen to initiate thrombus formation. Next, we applied the system to evaluate the shear-induced effects of two different drug models, GPIIb/IIIa inhibitors and soluble agonists, in preventing advanced stages of platelet aggregation. Consistent with literature, effects of GPIIb/IIIa inhibitors were greatly reduced at pathologically high shear rates [115]. Experiments with acetyl-salicylic acid (ASA) show that therapy is most effective at inhibiting platelet function under physiological levels of shear 500 and 1500 s^{-1}. In contrast, at high shear rates there were no significant changes in occlusion times, in agreement with findings by clinicians and other researchers. Although thrombi grew as normal, the main effect of ASA appeared to be a destabilizing one since ASA-treated blood showed nearly 70 % more fragmenting or embolic effects at after treatment vs. untreated controls.

5.2   Methods

The design and construction of the microfluidic chips and associated hardware used to characterize thrombosis have been described previously [114]. Briefly, devices were designed and validated to simultaneously address shear rates of 500, 1500, 4000, and 10000 s^{-1} using finite volume fluid modelling and experimental flow rate testing. Device molds were fabricated from micromilled aluminum, and molded using poly-dimethylsiloxane (PDMS) and bonded to coverglass via surface plasma bonding

(Harrick Plasma) to form enclosed flow channels.

5.2.1 Collagen surface adsorption

The use of fibrillar equine collagen (in contrast to the acid-soluble collagen used in Chapter 4 on porcine blood) had a pronounced effect on promoting thrombotic occlusion. In initial tests using devices with acid-soluble collagen, 14% of trials at 1500 s^{-1}, 41% of trials at 4000 s^{-1}, and 48% of trials at 10000 s^{-1} reached occlusion with 60 mL of sample (N=55 trials runs for each shear rate). Channel runs which did occlude required volumes of 11, 17, and 19 mL (respectively), on average (Fig. 33). In order to initiate platelet adhesion, these enclosed channels were filled with fibrillar equine collagen (Chronolog Corp) at a concentration of approximately 100 μg/mL.

In contrast, using devices with fibrillar equine collagen yielded 68% of trials (N=20) at 500 s^{-1}, 71% of trials (N=29) at 1500 s^{-1}, 95% of trials (N=29) at 4000 s^{-1}, and 96% of trials (N=29) at 10000 s^{-1} reaching occlusion with the same 60 mL of sample. Requisite sample volume was also reduced, with occluded channel runs requiring 2.4, 4.4, 5.1, and 5.4 mL, respectively.

To determine whether this discrepancy in the percent of channel runs occluded under varying types of collagen was due to a deficiency in the adsorption of each collagen type (fibrillar or acid-soluble) to the device's surfaces, or whether it was due to the structure of the collagen itself, we examined the structure of each collagen type and its surface adsorption properties. Surfaces were characterized using both histological staining with Picrosirius Red and brightfield microscopy and collagen structures more closely examined using atomic force microscopy (AFM), both common methods for collagen characterization [116, 85, 63, 117, 118]. We characterized adsorption of both types of collagen onto coverglass by incubating glass slides with 30 μL of collagen solution in a humidified, covered petri dish overnight, after which they were gently rinsed with 1 mL of irrigated saline solution to remove excess collagen and to emulate
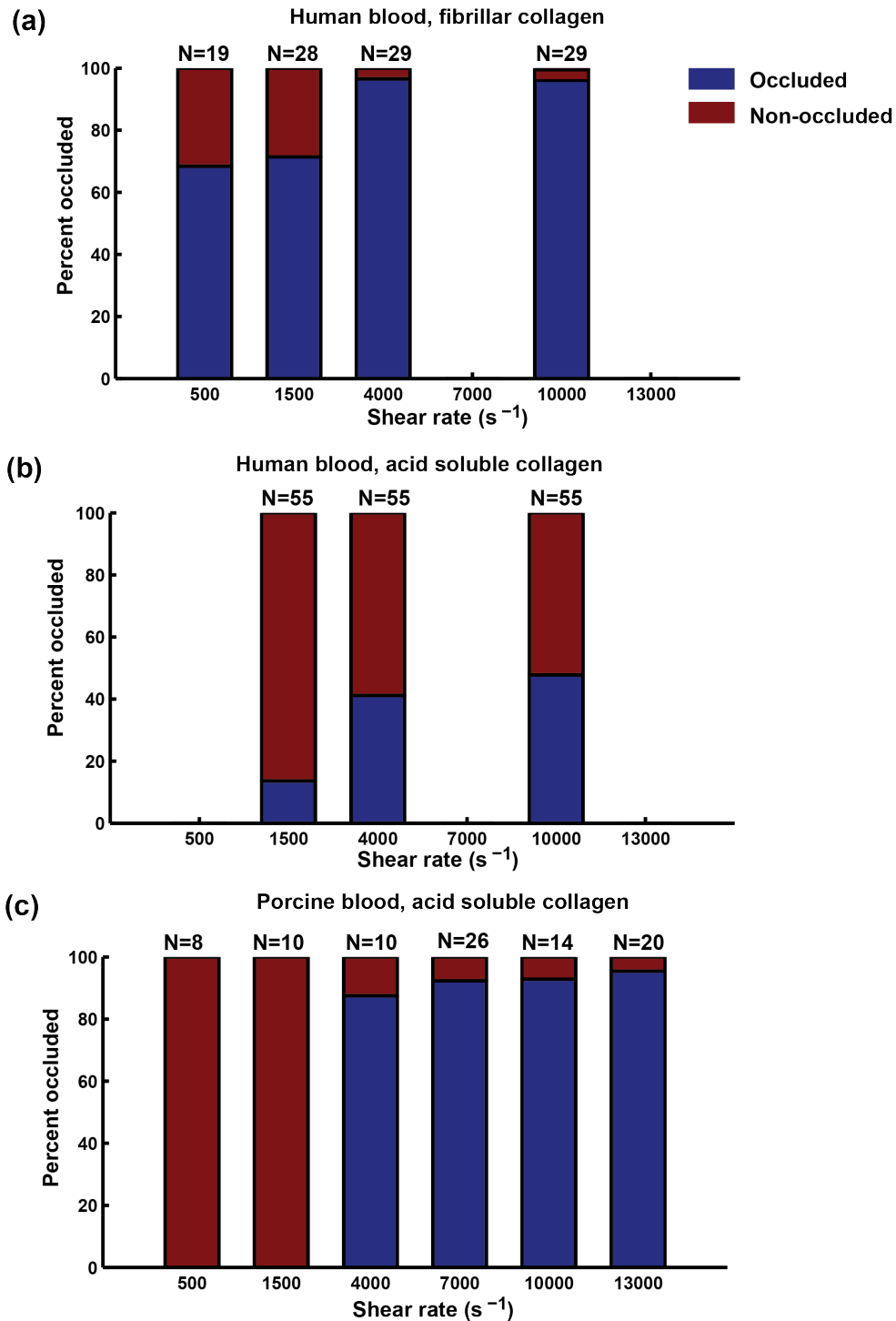
Figure 33: The use of fibrillar equine collagen (a) in contrast to the acid-soluble collagen (b) used in Chapter 4 showed a significantly higher percentage of occluded samples from human subjects at both high and low shear rates (57% increase at 1500 s^{-1}, 54% increase at 4000 s^{-1}, and 47% increase at 10000 s^{-1}). In contrast to human subjects' relative insensitivity to acid-soluble collagen, porcine blood (c) showed a high percentage of occlusion, suggesting comparatively enhanced sensitivity to shear induced platelet activity.

the priming process used in our devices.

We first characterized acid-soluble collagen. Staining and brightfield microscopy results showed that acid-soluble collagen had indeed adhered in a dense layer to the glass substrate of the device. Images and analysis from AFM data showed the structure of these collagen molecules were rounded globules of approximately 500 nm in diameter and 6-10 nm in height (Fig. 34).

Next, we characterized the fibrillar collagen, this time examining its adsorption onto two different types of substrates, glass and PDMS. Although collagen adsorption to glass has been well documented by other groups, adsorption to PDMS has not been well characterized. To examine the adsorption of collagen on each of these surfaces, slides were prepared by pipetting 30 μL of collagen solution onto a glass coated slide and a glass slide spin-coated in PDMS (200 μL of freshly mixed 1:10 PDMS spun at 1500 rpm for 60 seconds) and cured as normal. Afterwards, they were incubated overnight with collagen, after which they were rinsed with saline in the same process as the coverglass described previously.

Results from staining and brightfield microscopy revealed that fibrillar collagen did absorb to the surface of the coverglass, although the resultant layer was not as dense as that of the acid-soluble collagen (Fig. 35). We observed that while collagen did absorb in noticeable amounts to the inner PDMS surfaces of the device, the concentration was qualitatively much less than that of the glass surface (Fig. 35). The structure of the fibrillar collagen was also much different, with fibrils varying widely in length (20-50 μm), and diameter (0.025-1 μm).

In comparison to the surface imaging of the acid-soluble collagen shown in Fig. 34, it was clear that although the latter formed a denser layer of molecules on the surface, they were still unable to capture more platelets. Thus it appeared to be the structure and/or composition fundamental to the collagen type which made the fibrillar collagen a more adhesive molecule for platelets. Thus the order of surface

Acid-soluble collagen adsorption
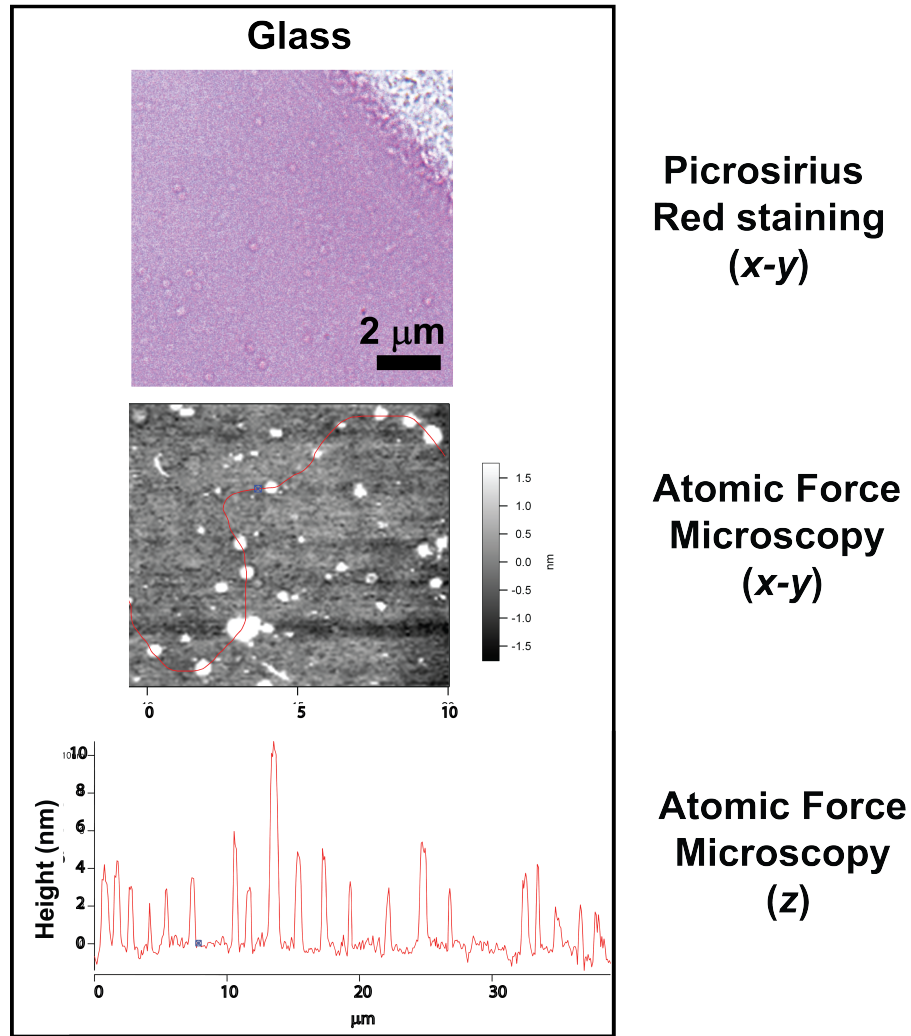
Figure 34: Surface adsorbed acid-soluble collagen onto glass surfaces. Brightfield microscopy of Picrosirius Red staining shows dense adsorption of acid-soluble collagen to coverglass. Individual acid soluble monomers are visible under Atomic Force Microscopy (AFM) in x-y place imaging, and surface traces along the red line in the middle image reveal rounded globular structures of approximately 500 nm in diameter and 6-10 nm in height (bottom). This step confirmed that our surfaces were coated with collagen, despite the lack of consistent platelet adhesion to these surfaces.
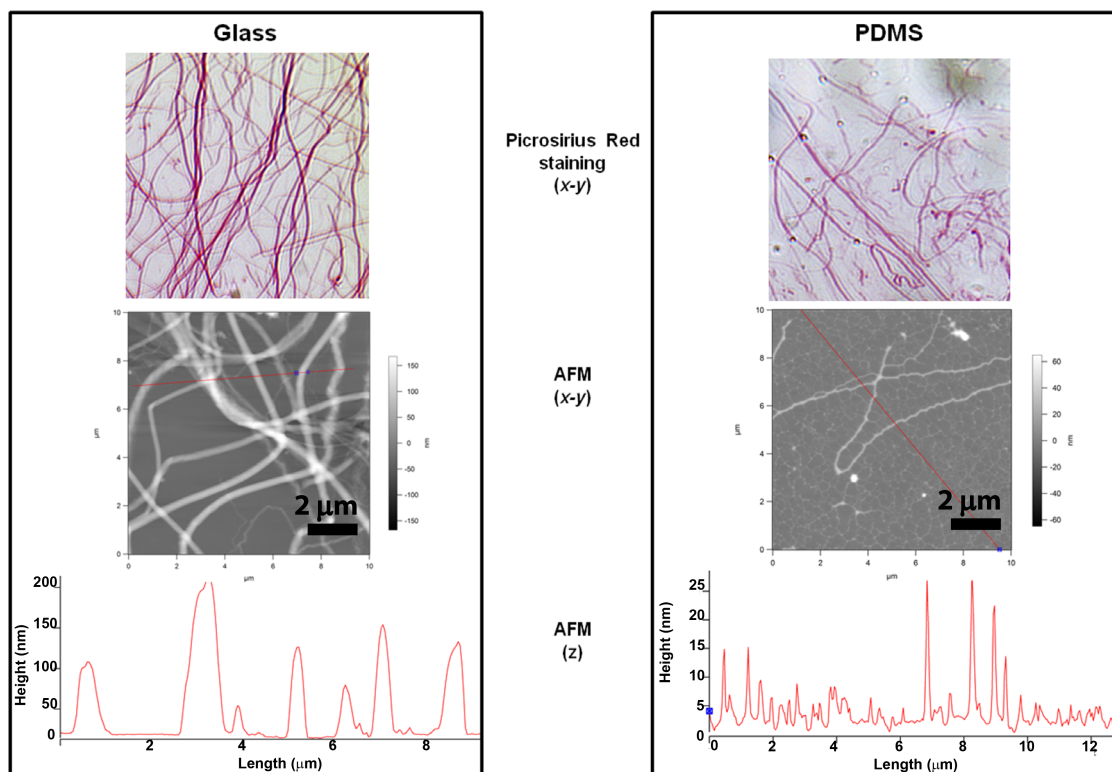
Figure 35: Surface adsorbed fibrillar collagen onto glass (a) and poly-dimethyl siloxane (PDMS) (b) surfaces. Brightfield microscopy of Picrosirius Red staining shows dense adhesion of collagen molecules on glass in comparison to PDMS surfaces. Images and analysis from AFM data shows Collagen fibrils visible in the x-y planes of both PDMS and glass surfaces under AFM and were probed along the red line of each sample to examine fibril heights. Height data show much shorter fibrils present on PDMS surfaces, as well as its surface imperfections. Glass shows superior collagen adhesion to PDMS, although an appreciable amount does appear on the latter.

adhesive properties from most adhesive to least adhesive for platelet binding can be ranked as: fibrillar collagen on glass, fibrillar collagen on PDMS, acid-soluble collagen on glass, acid-soluble collagen on PDMS.

This finding has been supported by recent work by Bernardo *et. al*, who provides evidence that this may be due to the presence of substantial amounts of vWF in the equine collagen, but not in acid soluble collagen [85]. Despite this report, it is notable that other recent research in this area has been conducting using microfluidic surfaces coated with the acid-soluble form of collagen used in Chapter 4 of this study after a similar AFM-based structural characterization [63].

Due to the increased efficiency of thrombosis and the wide commercial use of fibrillar collagen in contrast to acid-soluble collagen, the remainder of this work will show and discuss results using a fibrillar collagen model.

5.2.2 Device preparation and sample handling

Before use, each device was primed with a saline solution to prevent non-specific adsorption and to remove air bubbles. Blood samples were collected from N=9 healthy adults (6 males, 3 females; mean age 24 ± 5 years) who self-reported no anti-thrombotic or anti-coagulant drug use at the time of testing. Samples were collected in accordance with protocol H10090 approved by the Georgia institute of Technology Institutional Review Board. Blood was drawn through a 21 gauge needle into 60 mL syringes pre-filled with 3 Units/mL of un-fractionated heparin (Elkins-Sinn Inc, Cherry Hill, NJ) and used within five hours of collection. A small additional 2 mL aliquot was drawn to perform a cell count (Cell-Dyn Ruby, Abbott Diagnostics, Abbott Park, IL), which provided data on the number of platelets, platelet volume, hematocrit, white blood cell count, hemoglobin concentration, red blood cell count, and mean corpuscular volume. Samples with abnormally low platelet count ($<150 \times 10e^3/\mu L$) or hematocrit (< 30 %) were excluded from the study. In contrast
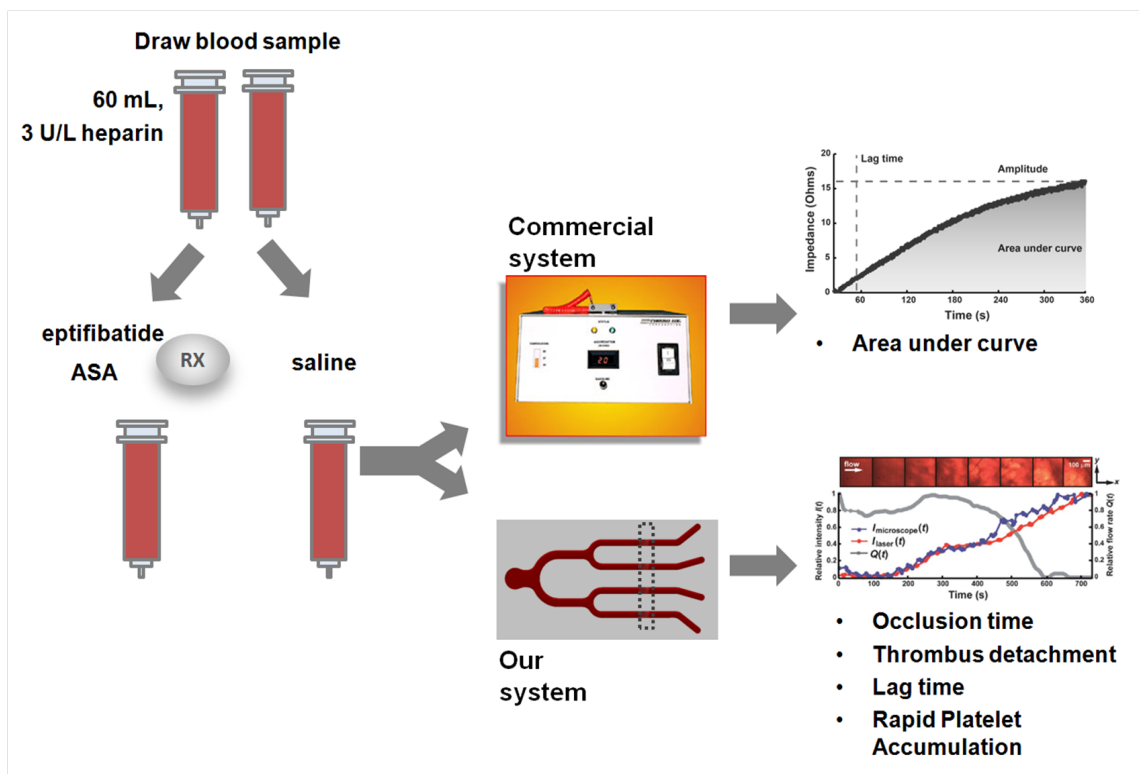
Figure 36: Flowchart for experimental method of anti-platelet agent testing on human blood. Blood samples were drawn into 60 mL aliquots and anti-coagulated with 3 Units/mL of heparin. An additional 2mL aliquot of blood was used for a complete blood count, and samples were checked for abnormal platelet count, platelet volume, or hematocrit. Experimental aliquots were treated with varying concentrations of anti-platelet agents (eptifibatide, ASA, or additional heparin), while control aliquots were treated with equal volumes of saline solution. Control and experimental samples were evaluated using a commercial platelet analyzer and our microfluidic system)

to citrate, the use of heparin does not require the addition of non-physiological adenosine diphosphate (ADP) to activate platelets in order to form white thrombus, both of which have been found by others to interfere with the function of eptifibatide.

Eptifibatide (Integrilin, Millennium Pharmaceuticals, South San Francisco, CA), unfractionated heparin, or ASA (MP Biomedical, Santa Ana, CA) were added within twenty minutes of sample collection into 60 mL sample aliquots. Eptifibatide was added in concentrations of 0, 0.24, 0.48, 0.72, and 2.4 μM. These concentrations were chosen such that the highest concentration corresponded to the clinically recommended dose for an adult human (a 250 μg/kg body mass bolus dose, assuming

average body mass of 70 kg and blood volume of 5 L), ASA (0.36, 1, 2mM), and heparin (3.5, 8, 20 Unit/mL). Due to the short life of ASA in solution, aliquots were prepared immediately before addition to the sample by dissolving 100 mg/mL into dimethyl-sulfoxide (DMSO) (Sigma Chemical, St. Louis, MO) and then diluted into saline to the appropriate concentrations before addition into blood samples, a technique employed by others [119]. Drug concentrations were chosen to reflect clinical recommendations and practice. Saline was added to control aliquots in equivalent volumes to drug dosages (0.526 mL). Each added dosage constituted less than 1% of the total aliquot volume to limit reductions in viscosity and hematocrit to 1.23% and 1.67%, respectively.

Flow was driven by pressure head of 1400 Pa and kept constant by a custom-built automated system consisting of a laser diode and photo-diode for detection of the fluid level and a linear actuator to keep the syringe at the correct height. For both eptifibatide and ASA, we applied our microfluidic system to evaluate thrombosis for shear rates from venous to pathological flow conditions. For each treated or untreated 60 mL sample aliquot, four shear rates were run simultaneously within a single trial while platelet aggregation to occlusion was measured by the four weighing scales at the outlet of each channel (Ohaus, Parsipanny, NJ) and acquired and processed using Labview (National Instruments, Austin, TX) and Matlab (Mathworks, Natick, MA), respectively.

A trial is defined as a single experiment with one new microfluidic device comprising four channel runs, each of a different shear rate. Our previous studies have shown good agreement on thrombosis detection between these flow rate measures and microscopy [114]. Occlusion times, $t_{occlusion}$, were measured as the time at which the flow rate as a function of time, Q(t), fell below 0.001 mL/s as measured over a 10 second time window. Tests were considered non-occluded if the 60 mL sample was exhausted during the course of the test or if occlusion did not occur in less than one

hour. Embolization events were defined by the occlusion of flow (Q<0.001 mL/s), followed by a resumption of flow (Q>0.001 mL/s) measured over a 10 second time window (see Fig.25).

Parallel measurements of platelet activity was measured using the commercially available Whole Blood Analyzer (Chronolog Corporation, Havertown, PA) according to manufacturer instructions. As described in Chapter 1, the machine is composed of a pair of electrodes, a stirring element, and a heating element. A 500 μL blood sample is added to an equal amount of saline, an electrode, and a small stir bar in a cuvette, and warmed for approximately five minutes at 37°C. The sample is then ready to be placed in the testing chamber, which has a rotating magnet that will spin the stir bar in the cuvette. The test will be able to begin when the electrode has been able to establish a consistent baseline. At that point, a chosen agonist is added to the cuvette, and the stir bar both distributes the agonist throughout the sample, and also provides a local shearing force on the blood. Activated platelets then adhere to the electrode, and the impedance will rise in accordance with the coverage of the electrode by platelets in the sample. The machine has three primary outputs used to describe its measurements of impedance due to platelet adhesion over time: lag time (the time period before impedance passes 2 Ohms), amplitude (the maximum change in impedance over the timecourse of the trial), and area under the curve (the integral of the impedance over time) also called the "AUC". In this work, sample activity was induced using 4 μL of collagen and/or Arachidonic Acid and a stirring rate of 1200 rpm, after which they were evaluated over six minutes.

5.2.3 Analysis

In order to depict both the frequency of occlusion and occlusion times, data is represented by $1/t_{\text{occlusion}}$. Thus as occlusion times are prolonged, $1/t_{\text{occlusion}}$ decreases until reaching zero, which represents a non-occlusion event. Error bars in this chapter
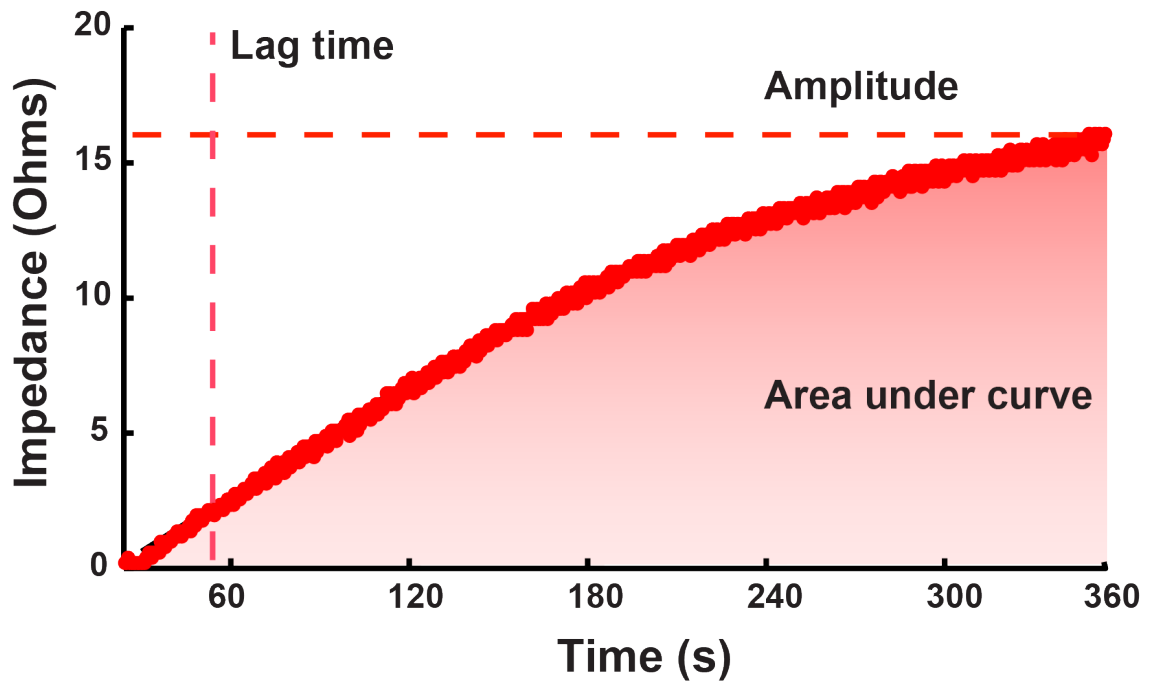
Figure 37: Experimental data obtained from the Whole Blood Analyzer (Chronolog Corporation). A 500 μL blood sample is added to an equal amount of saline, an electrode, and a small stir bar in a cuvette, and warmed for approximately five minutes at 37°C. Agonist activated platelets adhere to the electrode, and the impedance will rise in accordance with the coverage of the electrode by platelets in the sample. The machine has three primary outputs used to describe its measurements of impedance due to platelet adhesion over time: lag time (the time period before impedance passes 2 Ohms), amplitude (the maximum change in impedance over the timecourse of the trial), and area under the curve (the integral of the impedance over time) also called the "AUC". Here data is shown for a subject with untreated blood where the calculated lag time is 53 seconds, the amplitude is 16 Ohms, and the Area Under the Curve is 54.

is indicated as standard error of the mean since these measurements are intended to describe the variation of population values, not of individuals from each-other. Statistical analysis of results was performed using the SAS software package and Matlab. Matlab was used to calculate basic comparative statistics including student's t-test and standard error/standard deviation values.

SAS was used to construct and analyze a Cox proportional hazards model, which was performed for both drug models. This analysis format was chosen for its ability to analyze the weights of multiple, continuous variables (shear rate, dosage, donor) to predict the probability of an event (thrombotic occlusion) and its time to reach the event. The model is described by Equation 11, where β is the relative weight of each of the multiple variables, "$clot$" is the binary event describing whether occlusion occurs (1) or not (0), and $t_{\text{occlusion}}$ is a continuous numerical value. The format was also chosen due to its similarity to the Kaplan-Meier analysis method used in the GRAVITAS clinical study, which evaluated the VerifyNow Platelet Function Analyzer [38], and was the intended method in early phases of the study prior to its release [120]. Within the Cox survival model, independent variables were identified as significant by Chi-square statistics were used to calculate p-values under a predetermined alpha level of significance $\alpha = 0.05$, which was then used to calculate independent variable significance where p<0.05 was considered significant.

$$t_{\text{occlusion}} * clot = \beta_1 + \beta_2 * \text{shear} + \beta_3 * \text{dosage} \tag{11}$$

Lag time and Rapid Platelet Accumulation (RPA) growth were calculated using the following method. Flow rate data was used to estimate the thrombus volume, where 48% of the initial flow rate at each given shear rate as calculated in Chapter 2 was used as the point at which the thrombus reached 48% the volume of the stenosis region, for comparison and consistency with Para et. al. [73]. Lag time was measured as the time at which thrombus reached this same 48% (Equations 13, 12). While this

109

calculated lag time occurs later than the 19% shown in the same work by Para, it was consistent and easily detectable for these experiments, although such post-analysis would be possible with more attention to data filtering algorithms.

$$0.48 * Q(t = 0) = Q(t = t_{\text{lag time}}) \tag{12}$$

$$\text{RPA growth} = 0.48 * (V_{\text{stenosis}})/(t_{\text{final}} - t_{\text{lag time}}) \tag{13}$$

Lower shear rates 500 and 1500 s^{-1} were difficult to study due to the resolution limit (0.3 μL/s) of the scales at such low flow rates (0.5 to 5 μL/s). Further studies might be able to approximate thrombus growth rates similar to previous findings in units of volume/surface*time using more advanced image processing including surface area and edge detection methods which could be applied to microscopy images or intensity readings.

5.3 Results and discussion

To study the effects of these anti-platelet agents on platelet activity at varying shear rates, we first examined the effects of shear rate on untreated human blood on intra-subject and inter-subject occlusion times and volumes in our microfluidic system. These results were compared with porcine results previously discussed in Chapter 4. Next, we examined the dose-response of anti-platelet agents on clotting times and volumes at varying shear rates. Our results with varying shear rates were then compared with results from a commercial platelet function analyzer.

5.3.1 Effects of shear rate on untreated human blood

We first characterized the variations in our assay by examining intra-sample variation in human samples. Intra-patient $1/t_{\text{occlusion}}$ (mean $\pm$ SEM) were $(5.1 \pm 1.2) \times 10^{-4}$ at 500 s^{-1}, $(4.1 \pm 1.4) \times 10^{-4}$ at 1500 s^{-1}, $(16 \pm 0.1) \times 10^{-4}$ at 4000 s^{-1}, and $(24 \pm 2.1) \times 10^{-4}$
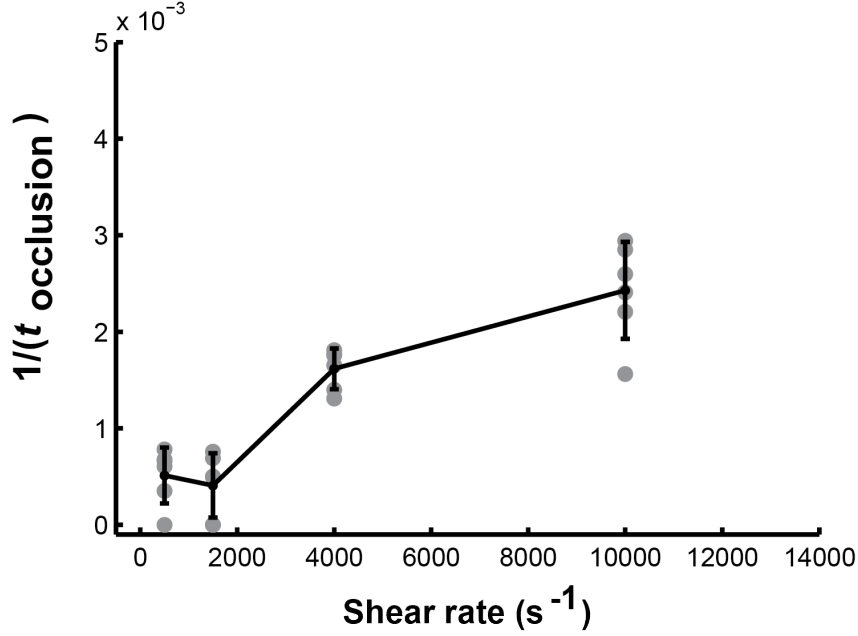
Figure 38: Intra-subject variation in $1/t_{\text{occlusion}}$ responses were evaluated in N=5 trials of a single subject over different days and blood draws in control trials. $1/t_{\text{occlusion}}$ varied from 0.9 to 2.1 $\times 10^{-4}$ for the tested shear rates of 500, 1500, 4000, and 10000 s^{-1}.

at 10000 s^{-1} (N=5 for all shear rates). The average SEM for all tested shear rates was 1.36×10^{-4}. Due to the nature of previous porcine sample acquisition data for intra-sample variation was not available for comparison.

Next, we examined shear-induced variations in $1/t_{\text{occlusion}}$ within samples from multiple subjects (N=9) tested at varying shear rates. Results pooled from this subject group showed $1/t_{\text{occlusion}}$ (mean $\pm$ SEM) of $(4.8 \pm 1.6) \times 10^{-4}$ at 500 s^{-1}, $(3.9 \pm 0.1) \times 10^{-4}$ at 1500 s^{-1}, $(16 \pm 2.4) \times 10^{-4}$ at 4000 s^{-1}, and $(24 \pm 1.9) \times 10^{-4}$ at 10000 s^{-1} (N=9 for all shear rates). The average SEM for all tested shear rates was 1.7×10^{-4}, 25% greater than the measured intra-patient variation.

Similar to results from the porcine model, occlusion times at physiological shear rates tested (500, 1500 s^{-1}) did not differ significantly from eachother (p>0.1). Results from the previous porcine data (Chapter 4) quantified using $1/t_{\text{occlusion}}$ (mean $\pm$ SEM) showed $(25 \pm 3.0) \times 10^{-4}$ at 4000 s^{-1} (N=8), $(24 \pm 2.5) \times 10^{-4}$ at 7000 s^{-1}
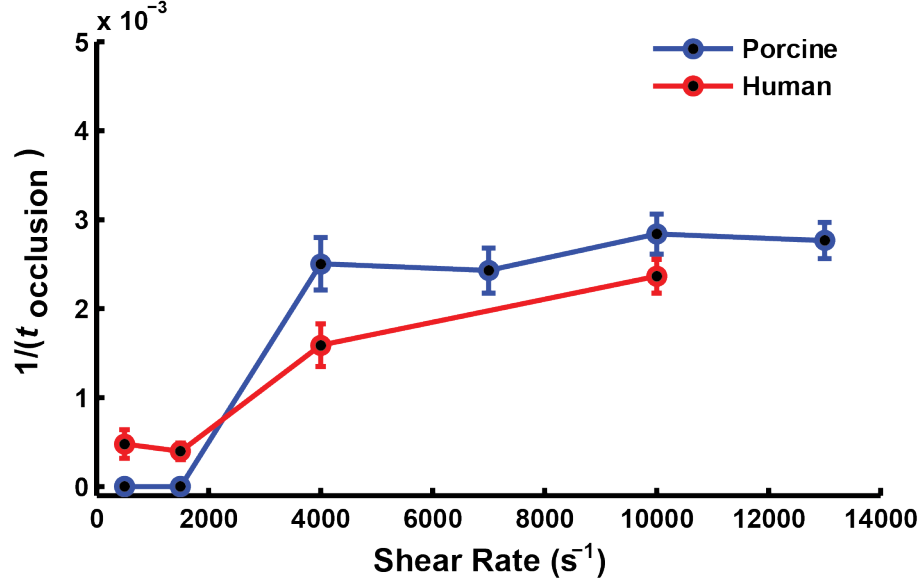
Figure 39: Comparison of $1/t_{\mathrm{occlusion}}$ in human vs. porcine blood samples. For both sample types, occlusion times at physiological shear rates tested (500, 1500 s^{-1}) did not differ significantly from eachother (p>0.1). In contrast to the porcine model, higher shear rates did show significantly different

(N=26), (28$\pm$2.2)$\times 10^{-4}$ at 10000 s^{-1} (N=14), (28$\pm$2.0)$\times 10^{-4}$ at 13000 s^{-1} (N=20). The average SEM for all tested shear rates in porcine samples was 2.5 $\times 10^{-4}$.

While porcine samples showed no significant differences between its high and low shear occlusion times, higher shear rates did show significantly faster occlusion times (p>0.05) in human samples. Values for ratio of occluded channels (Fig. 33) were nearly identical at 0.95 for 4000 and 10000 s^{-1}. However, platelet activity was higher in porcine samples at high shear rates (4000 and 10000 s^{-1}) than in human samples, reflected elevated $1/t_{\mathrm{occlusion}}$ values. Additionally, values for SEM in $1/t_{\mathrm{occlusion}}$ values were 1.5 fold higher in porcine blood than human, showing greater variation in occlusion for porcine samples than human samples.

We next examined RPA growth and lag time. This work estimates rapid platelet accumulation (RPA) growth from 0.47 to 50 ($cm^3 * 10^{-6}/s$), mean value of 14$\pm$1.1 ($cm^3 * 10^{-6}/s$) for N=72 samples over all tested initial wall shear rates 500, 1500, 4000, 10000 s^{-1}. These values are similar to the range of RPA growth values determined in
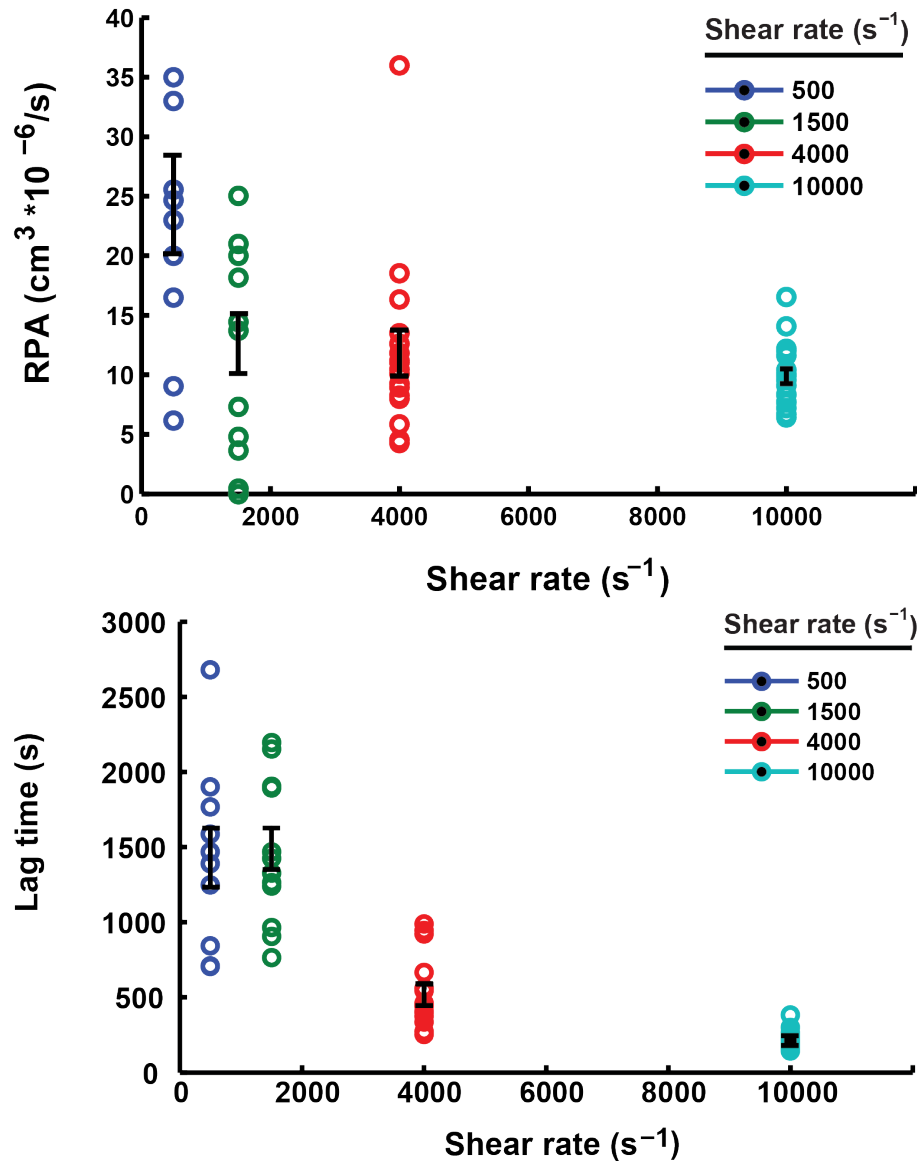
Figure 40: RPA growth and lag time measurements for untreated human blood samples. This work estimates rapid platelet accumulation (RPA) growth from 0.47 to 50 $(cm^3 * 10^{-6}/s)$, mean value of 14 ± 1.1 $(cm^3 * 10^{-6}/s)$ for N=72 samples over all tested initial wall shear rates 500, 1500, 4000, 10000 s^{-1}. These values are similar to the range of RPA growth values determined in previous work by Para and Bark as 20 ± 4.5. Lag times ranged from 144 to 2668 seconds, mean value of 803 ± 77 for N=72. Higher shear rates (4000, 10000 s^{-1}) were 365 ± 37 s (N=36).

previous work by Para and Bark as 20 ± 4.5 $(cm^3 * 10^{-6}/s)$ within stenoses of 70-83 % and initial wall shear rate values near 5000 s^{-1} [73, 59, 5]. Lower shear rates 500 and 1500 s^{-1} showed larger standard deviations in lag time and RPA growth results due to the resolution limit (0.3 μL/s) of the scales at such low flow rates (0.5 to 5 μL/s).

Lag time values determined at the higher shear rates (4000, 10000 s^{-1}) were 365 ± 37 s (N=36), similar to the activation time of near 100 s determined by Hellums, and the 100-200 s range determined by Bark and Para [5]. Since these lag times are calculated in a different method than both authors, such levels of error are expected. Also, our lag time measured growth until 48% volumetric growth, which may be considered beyond initial lag by some definitions which define it as 20% [73].

Also similar to the results of Bark and Para, this work notes lag times inversely proportional to shear rate, shown in Fig 40 measurements of shear vs. lag time. Statistical analysis showed significant (p<0.001) differences between lag times at all shear rates except for the lowest shear rates (500, 1500 s^{-1}).

After characterizing intra-patient and inter-patient variation of untreated human samples, and comparing our results with previous porcine data, we next examined the effects of treating human samples with anti-platelet agents.

5.3.2 Effects of eptifibatide and shear rate on human blood

We first characterized the effects of the anti-platelet injectable drug eptifibatide (Integrilin). The drug was added in-vitro at concentrations of 0.24, 0.48, 0.72, and 2.4 μM to construct dose-response curves for N=5 different subjects' blood samples, shown in Fig. 41.

Dose-response behavior varied throughout patients, with maximum response values for $1/t_{\text{occlusion}}$ at the highest shear rate (10000 s^{-1}) ranging from 0.0013 to 0.0032 s^{-1}. Drug sensitivity varied as well with subjects showing non-occlusion at a dosage

range of 0.72 to 1.2μM, half the manufacturer recommended clinical dosage of 180 μg/kg per patient (or 2.4 μM in whole blood).

Notably, each of these tested subjects show reduced drug sensitivity at the highest shear rate of 10000 s^{-1} in comparison to lower shear rates 500, 1500, and 4000 s^{-1}, although their individual thresholds for loss of activity vary.

Results from dose-response curves pooled from all N=5 subjects showed decreases in platelet activity with increasing doses of eptifibatide, reflected in the decreasing values of $1/t_{\text{occlusion}}$ and increasing error values due to differences in inter-subject drug sensitivity shown in Fig. 41.

While samples subjected to physiological shear rates of 500 and 1500 s^{-1} ceased to show platelet activity at drug dosages of 0.48 and 0.72 μM , respectively, higher shear rates of 4000 and 10000 s^{-1} required dosages of 1.2 μM or higher to completely inhibit platelet activity. As with the results from untreated human subjects, all shear rates were shown to be statistically different (p<0.001) from each other using Cox survival analysis, save for 500 s^{-1} and 1500 s^{-1}.

In addition to dose-response curves of constant shear rate, the data can also be visualized by shear-response curves of constant dosage (Fig. 43). Here we can see that shear-response decreases proportionally with increasing dosages until the application of dosages above 0.72 μM.

We next examined RPA growth and lag times vs. eptifibatide dosage. Lag times at mid range shear 4000 s^{-1} increased significantly (p<0.01) in lag time by 4.15X, although this result is confounded by non-occluded trials. In contrast, high shear 10000 s^{-1} lag times were not significantly different (p>0.1) with increasing dosages in trials which did occlude, until occlusion was lost in all trials at 1.2 μM. A possible explanation for sudden transition is that the initial binding of platelets at high shear is mediated primarily by vWF-GPIb, not the GPIIb/IIIa platelet cohesion mechanism affected by eptifibatide [17], which could slow or inhibit occlusion but not delay the
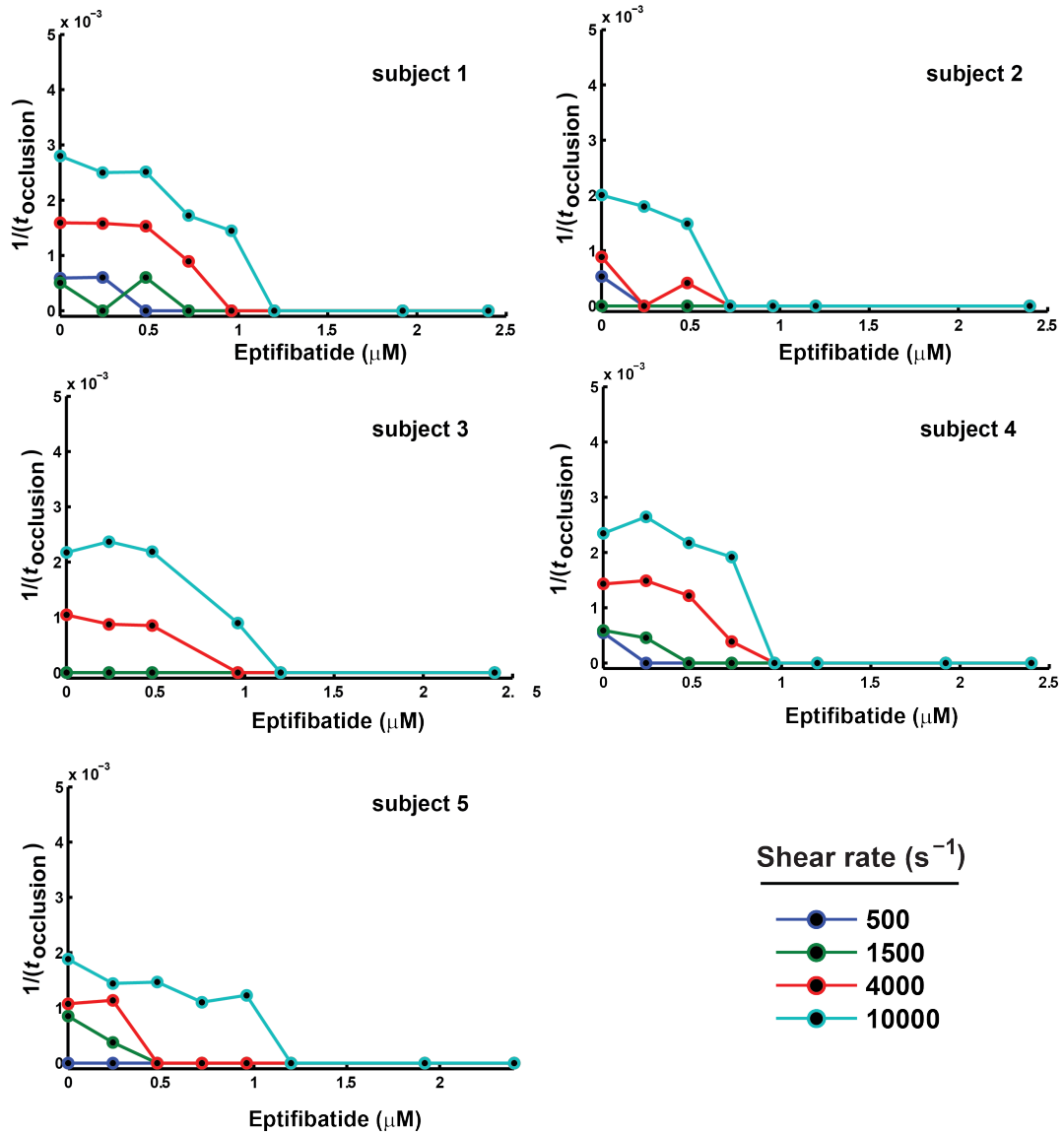
Figure 41: Eptifibatide dose-response curves of varying shear rates in N=5 human subjects. Platelet response is defined by $1/t_{\text{occlusion}}$, where $t_{\text{occlusion}}$ is the time at which platelet thrombus occludes the stenosis. All subjects show reduced drug sensitivity at the highest shear rate of 10000 s^{-1} in comparison to lower shear rates 500, 1500, and 4000 s^{-1}
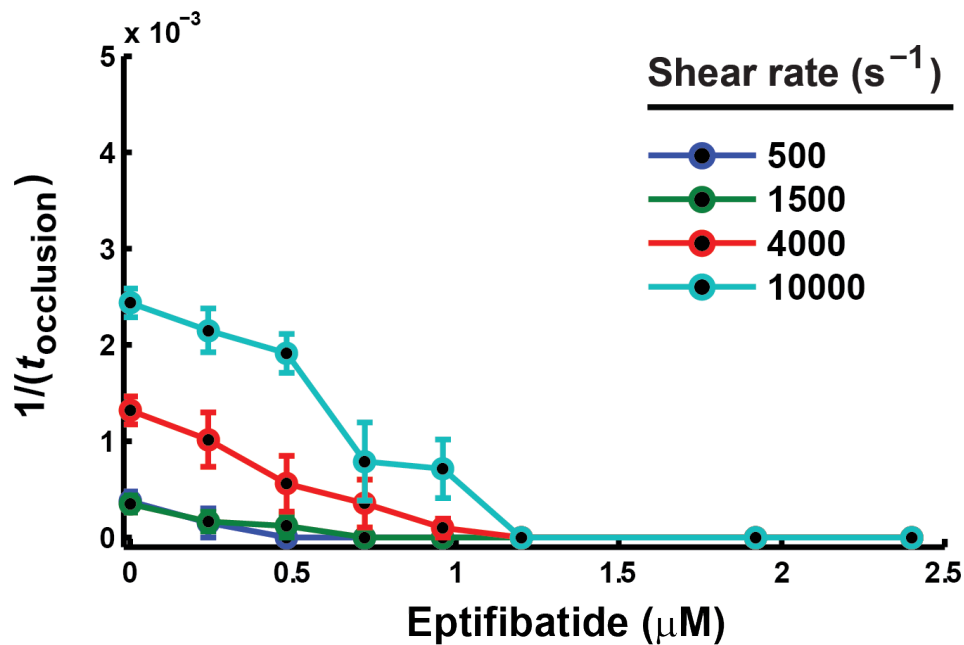
Figure 42: Eptifibatide dose-response curves of varying shear rates pooled from N=5 human subjects. Platelet response is defined by $1/t_{occlusion}$, where $t_{occlusion}$ is the time at which platelet thrombus occludes the stenosis. At physiological shear rates of 500 and 1500 s^{-1}, occlusion is eliminated at dosages of 0.48 and 0.72, respectively, while dosages of 1.2 μM or higher are required to eliminate occlusion at high shear rates of 4000 and 10000 s^{-1}. As with the results from untreated human subjects, all shear rates were shown to be statistically different (p<0.001) from each other using Cox survival analysis, save for 500s^{-1} and 1500 s^{-1}.
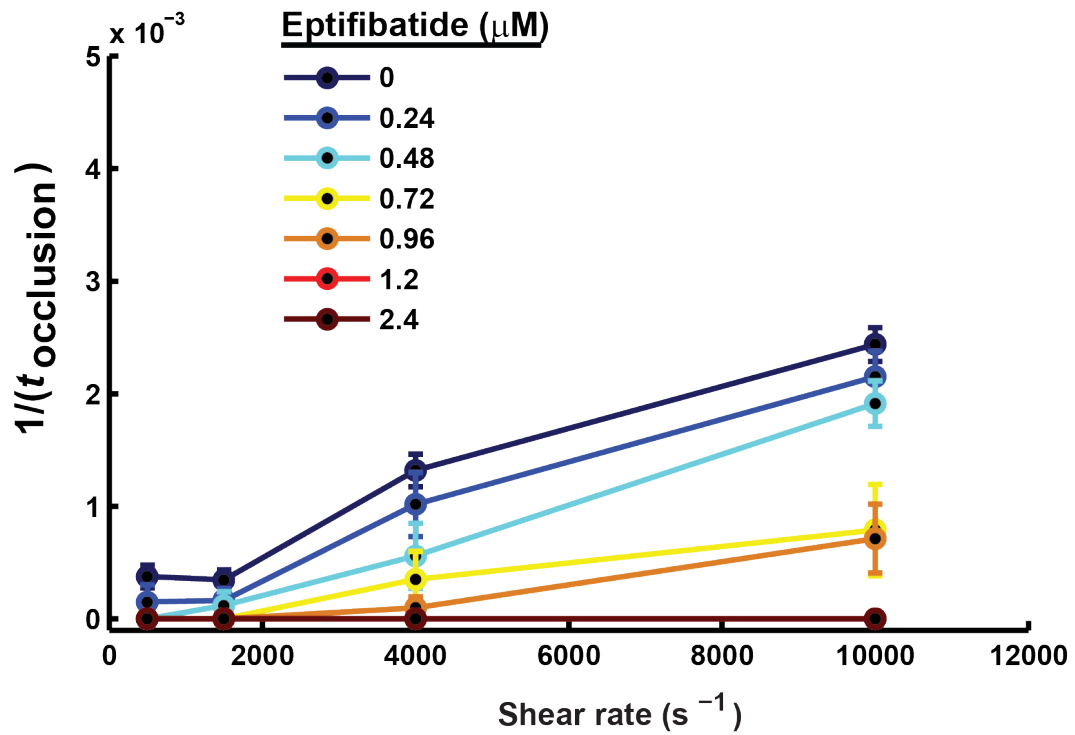
Figure 43: Eptifibatide shear-response curves for varying dosage concentrations pooled from N=5 human subjects. Increasing dosages appears to reduce the $1/t_{\text{occlusion}}$ by similar proportional amounts at all tested shear rates until approaching the effective concentration range of 0.96 to 1.2 μM.
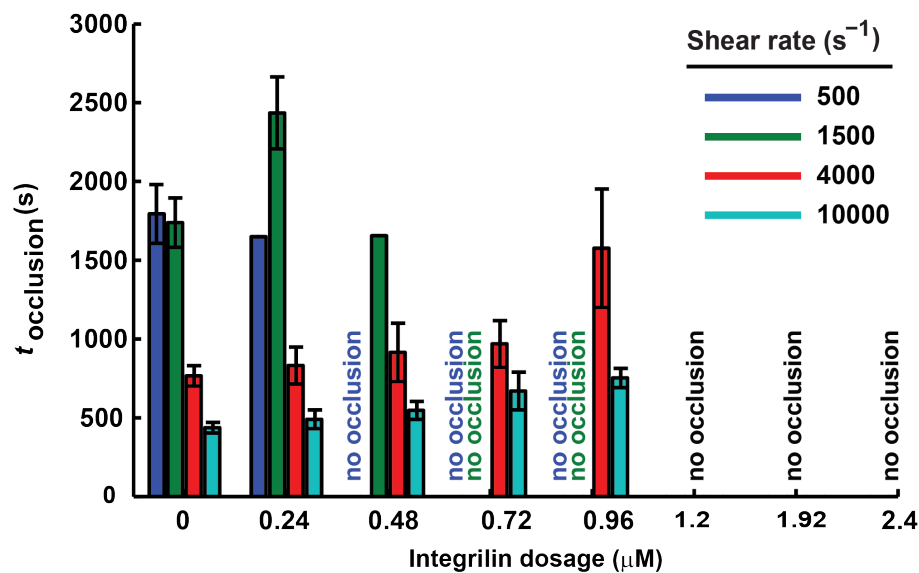
Figure 44: Raw occlusion times, $t_{\text{occlusion}}$, for varying shear rates and concentrations of eptifibatide. Unlike the $1/t_{\text{occlusion}}$ metric used in the previous Fig 50, this metric is more intuitively understandable for the reader. However, it does not account for non-occlusion events and thus shows very small sampling N for some points, in contrast to the previous figure which is able to provide means and standard error amounts for five samples per point. No occlusion times are available at dosages greater than 1.2 μM, since channels did not occlude.

onset of thrombosis. RPA growth decreased consistently over increasing dosages in channels which did occlude for all shear rates.

We next determined the volume of sample required to produce occlusion. Unlike occlusion times, occlusion volumes $V_{occlusion}$ were not significantly different at higher shear rates of 4000 and 10000 s^{-1}, although higher eptifibatide dosages required progressively higher sample volumes at all tested shear rates. These results contrast with our previous findings on porcine blood, whose occlusion times did not vary significantly at high shear rates, but did show increasing occlusion volumes with increasing shear rates (Fig. 31). Occlusion times for samples which did occlude are shown in Fig. 44, although it should be noted that this method does not account for non-occluded samples.

Thrombus detachment events provide a measure for the stability of platelet aggregates formed. Under increasing dosages of eptifibatide, thrombi formed at high shear rates did embolize by more than 20 % when compared with controls, indicating that the thrombi which were able to form were weakened by the inactivation of the GPIIb/IIIa receptor.

Thus we characterized platelet activity in our microfluidic system using metrics of $1/t_{occlusion}$, $1/V_{occlusion}$, and the ratio of thrombus detachment events. Next, we compared these performance metrics with a commercial system, the Chronolog Whole Blood Analyzer (WBA).

The WBA measures platelet activity by the changes in electrical impedance induced by platelets adhering to the surface of an electrode. The electrode is submerged in a sample of constantly stirred whole blood and measures changes of impedance over time after the addition of agonist. Thus, resulting metrics of platelet activity during a standard (6 minute duration) test are the amplitude (the maximum change in impedance), area under the curve (integral of area under the change in impedance curve), and the lag time (time until impedance begins to rise above the initial zero
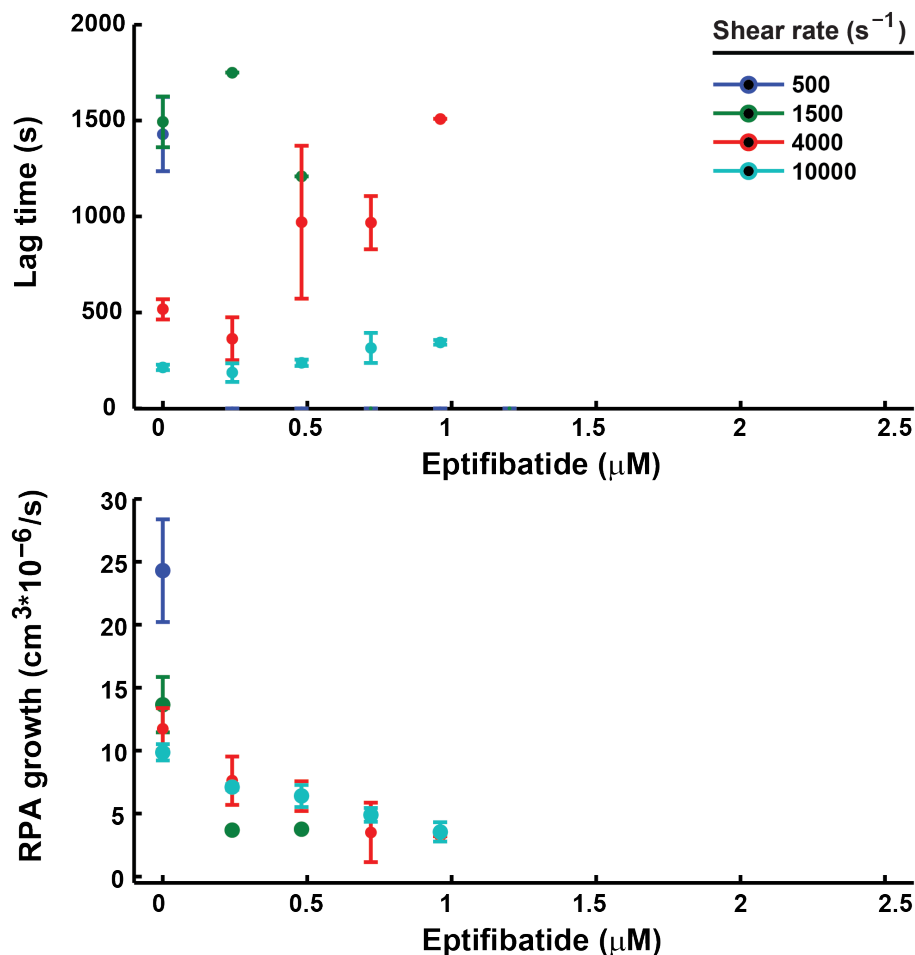
Figure 45: Lag times and RPA growth vs. eptifibatide dosage in human blood. Lag times at mid range shear 4000 s was significantly (p<0.01) affected by increases in eptifibatide dosage, until occlusion ceased at 1.2 μM. In contrast, high shear 10000 s^{-1} lag times were not significantly different (p>0.1) with increasing dosages in trials which did occlude, until occlusion was lost in all trials at 1.2 μM. RPA growth decreased consistently over increasing dosages in channels which did occlude for all shear rates.
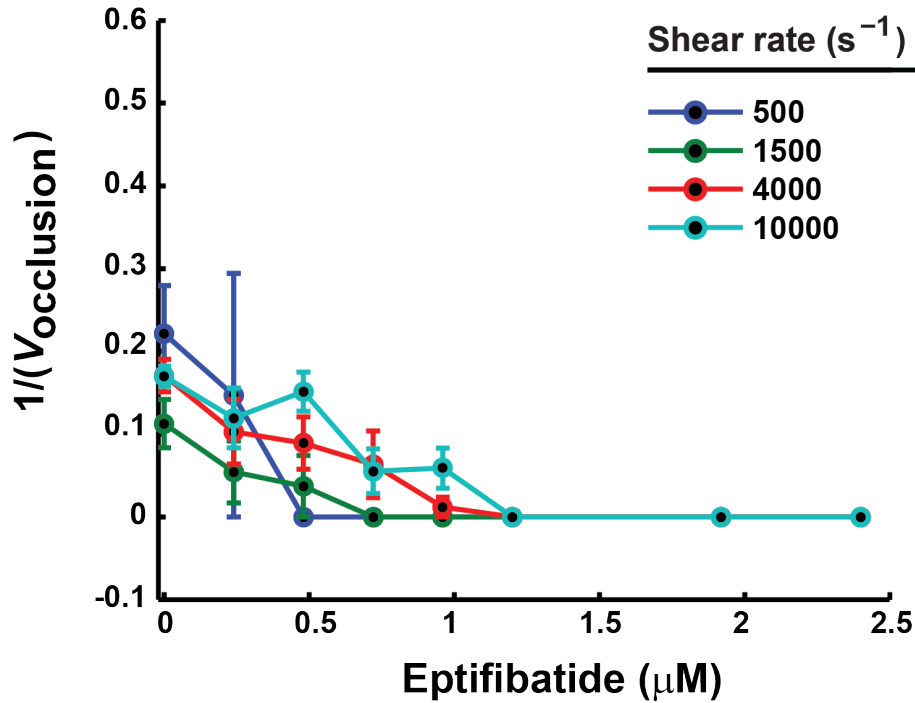
Figure 46: Eptifibatide dose-response curves for varying dosage concentrations pooled from N=5 human subjects. Unlike occlusion times, occlusion volumes $V_{occlusion}$ were not significantly different at higher shear rates of 4000 and 10000 s^{-1}, although higher eptifibatide dosages required progressively higher sample volumes at all tested shear rates.
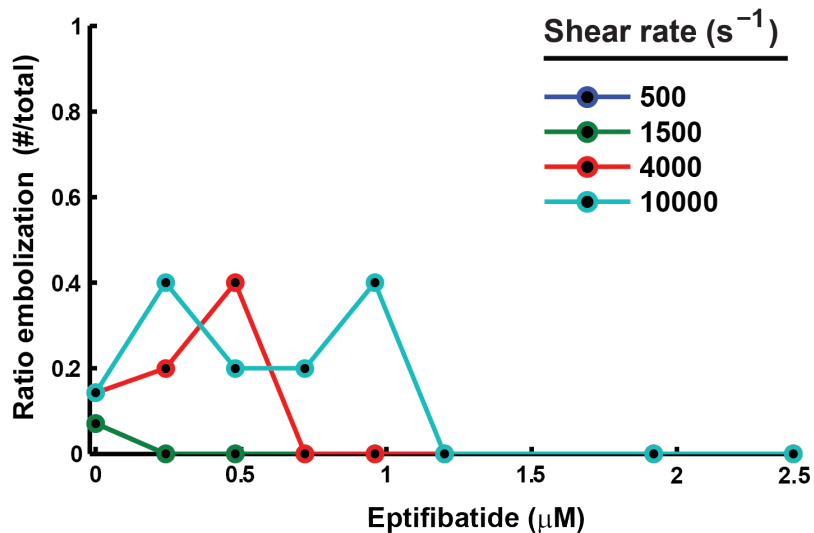
Figure 47: Effects of eptifibatide on the stability of occlusive thrombi. Under increasing dosages of eptifibatide, occlusive thrombi which were able to form at high shear rates did detach (embolize) by more than 20 % when compared with controls
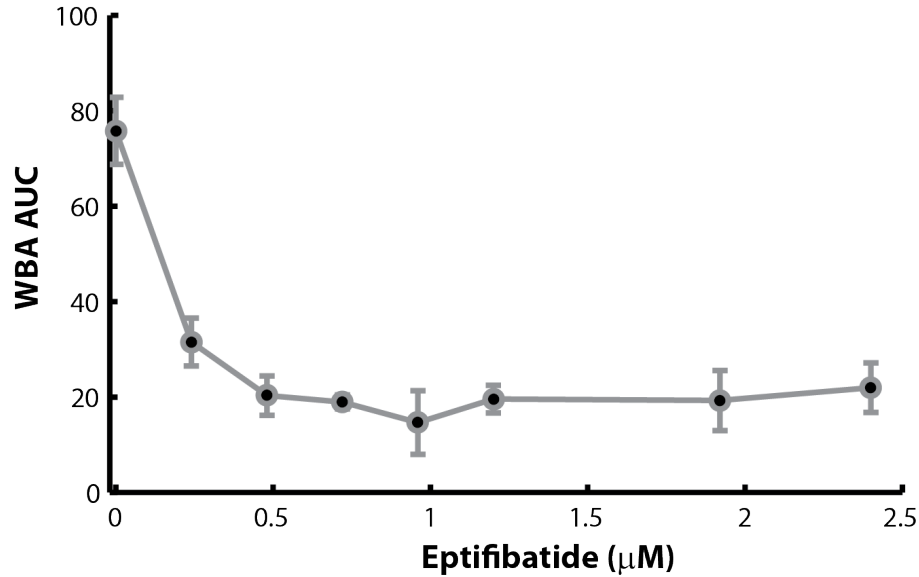
Figure 48: Dose-response measurements using the Chronolog Whole Blood Analyzer showed detectable differences in Amplitude, Area Under the Curve (AUC), and lag time until reaching a concentration of 0.5 μM, after which response did not change significantly for increased dosages. Both methods showed significant differences in respective thrombosis metrics ($1/V$ occlusion and Area Under the Curve) at the clinical dosage of 0.24 μM.

baseline). Results showed similar dose-response capabilities between these three metrics which detected eptifibatide concentrations up to 0.5 μM until responses did not change significantly.

Comparison of the WBA performance with the shear curves produced in our system showed significant (p<0.05) reductions in platelet function metrics after the addition of eptifibatide, although the thresholds for dosage sensitivity were different.

The commercial WBA did not show significant differences in successive readings following 0.5 μM, thus this was determined as its sensitivity threshold. In contrast, our microfluidic method ceased to show significant differences after 1.2 μM at the higher shear rates (4000, 10000 s^{-1}), and 0.72 μM at the lower shear rates (500, 1500 s^{-1}). Both methods showed significant differences in respective thrombosis metrics ($1/V_{\text{occlusion}}$ and Area Under the Curve) at the clinical dosage of 0.24 μM, a capability which has been validated in clinical trials of the WBA [20]. While we did

not anticipate identical results to the WBA, this procedure confirmed that we were able to show significant differences due to the application of the drug within a similar order of magnitude for dosage. Since the clinical utility of the WBA for determining dosage efficacy has not yet been determined, we cannot yet assess the importance of this difference in threshold [20, 25].

Clinical implications: Results from this study showed statistically significant differences ($p < 0.001$) between all shear rates (save the lower shear rates 500, 1500 s^{-1}), as well as between eptifibatide dosages. Our system also provides clinical implications that higher dosages of this therapeutic may be necessary in patients with existing cardiovascular pathologies such as atherosclerosis, which induce high local shear rates similar to the 10000 s^{-1} condition shown in this work. These findings that both dosage and shear have significant effects on our occlusive thrombosis are important because dosage is usually thought of as the main determinant of efficacy, while this model shows that both have significant effects for a large range of values. The system thus shows potential for creating more precise models for dosing patients with eptifibatide and other GPIIb/IIIa inhibitors. Such a prospect is particularly compelling due to the serious bleeding complications inherent in overdosing with this class of platelet therapies.

Comparison with the WBA show that our device performs at least to the standard of current commercial devices, as our device has shown both detection of clinically recommended dosages, and a similar sensitivity limit. The latter is expected, since clinically relevant sensitivity limits and their implications for treatment have not yet been defined.

5.3.3   Effects of acetylsalicylic acid and shear rate on human blood

After characterizing the direct GPIIb/IIIa receptor inhibitor anti-platelet agent, eptifibatide, we next examined a the effects of acetylsalicylic Acid (ASA) a class of drugs

which prevents the release of soluble factors.

We characterized the effects of in-vitro addition of ASA at concentrations of 0, 0.36, 1.0, and 2.0 μM to construct dose-response curves for N=5 different subjects' blood samples (Fig. 49). The pool of human subjects in this study used 3/5 of the same subjects from the previous eptifibatide trials, while 2/5 subjects were different.

Dose-response behavior varied throughout subjects, with maximum response values for $1/t_{\text{occlusion}}$ at the highest shear rate (10000 s^{-1}) ranging from 48×10^{-4} in Subject 4 to 28×10^{-4} in Subject 1, representing an overall difference of 16×10^{-4}, more than one standard deviation above other subjects. Drug sensitivity varied slightly with subjects showing loss of occlusive thrombus formation only at lower shear rates (500 and 1500 s^{-1}) for dosage concentrations of 0.36 to 1 mM. Unlike eptifibatide experiments, no dosage tested was able to completely eliminate occlusion at high shear rates, despite the use of much higher ASA concentrations than clinically prescribed (1 and 2 mM concentrations are 10-20X the recommended daily dosage of aspirin, respectively).

Results from dose-response curves pooled from these N=5 subjects showed similar SEM values in subjects' responses at all tested concentrations of ASA, in contrast to increasing SEM values with increasing dosages of eptifibatide shown in the previous subsection (Fig. 42). High shear rates 4000 and 10000 s^{-1} showed non-significant ($p>0.05$) decreases in $1/t_{\text{occlusion}}$ responses with increasing doses of eptifibatide using a student's t-test.

Similar to untreated human tests and eptifibatide tests, there was no significant difference in response values between the two lower shear rates at all measured dosages, although all other combinations of shear rates were significant ($p<0.001$) according to Cox survival analysis.

We next examined RPA growth and lag times vs. ASA dosage. Measurements of both Lag time and RPA growth at mid-to-high shear rates 4000 and 10000 s^{-1}
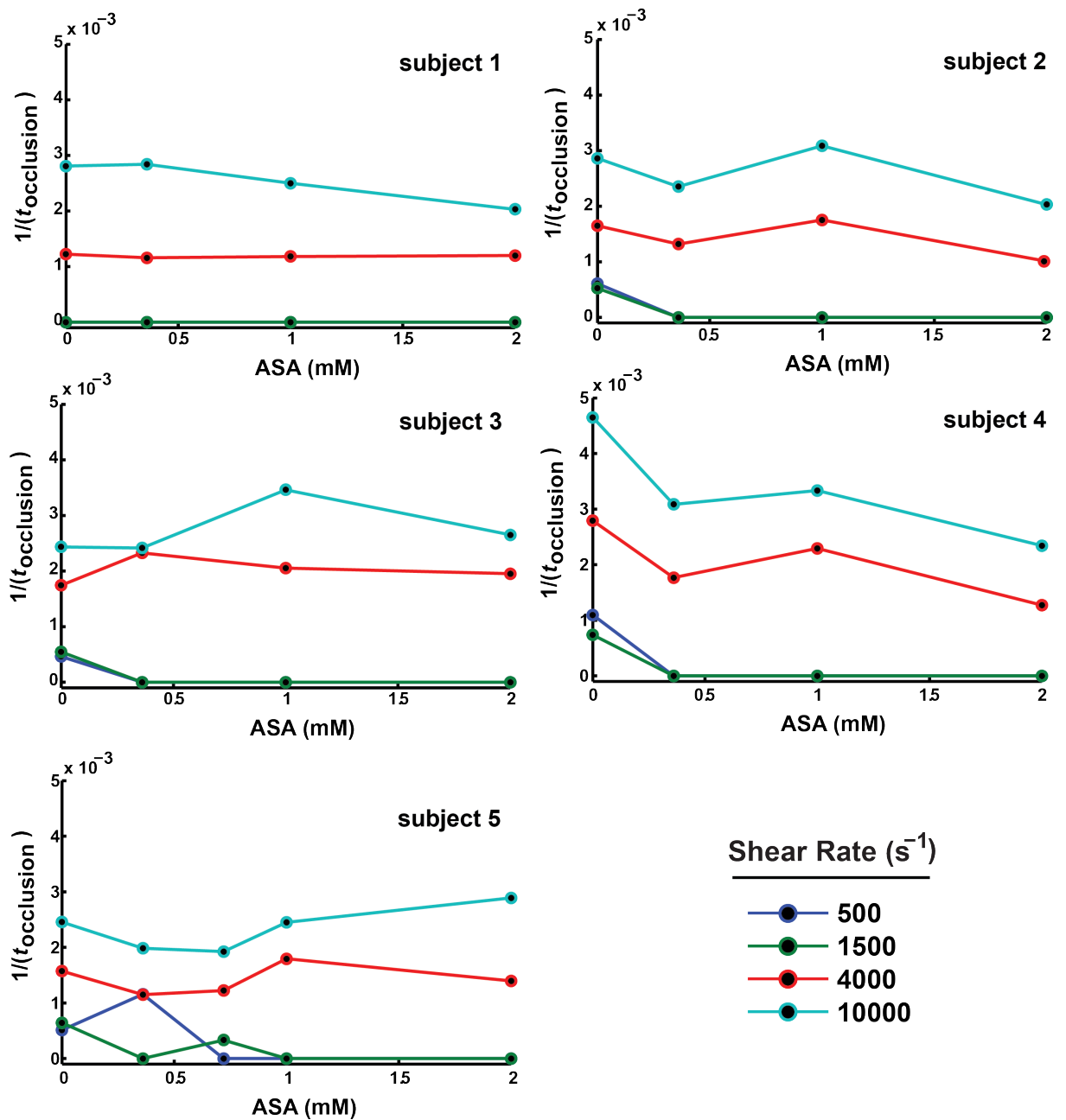
Figure 49: ASA dose-response curves of varying shear rates in N=5 human subjects. Platelet response is defined by $1/t_{occlusion}$, where $t_{occlusion}$ is the time at which platelet thrombus occludes the stenosis. Addition of ASA appeared to eliminate occlusive thrombosis only at physiological shear rates of 500 and 1500 s^{-1}, but was unable to prevent occlusion at high shear rates of 4000 and 10000 s^{-1} despite the use of high concentrations of up to 20X recommended daily values.
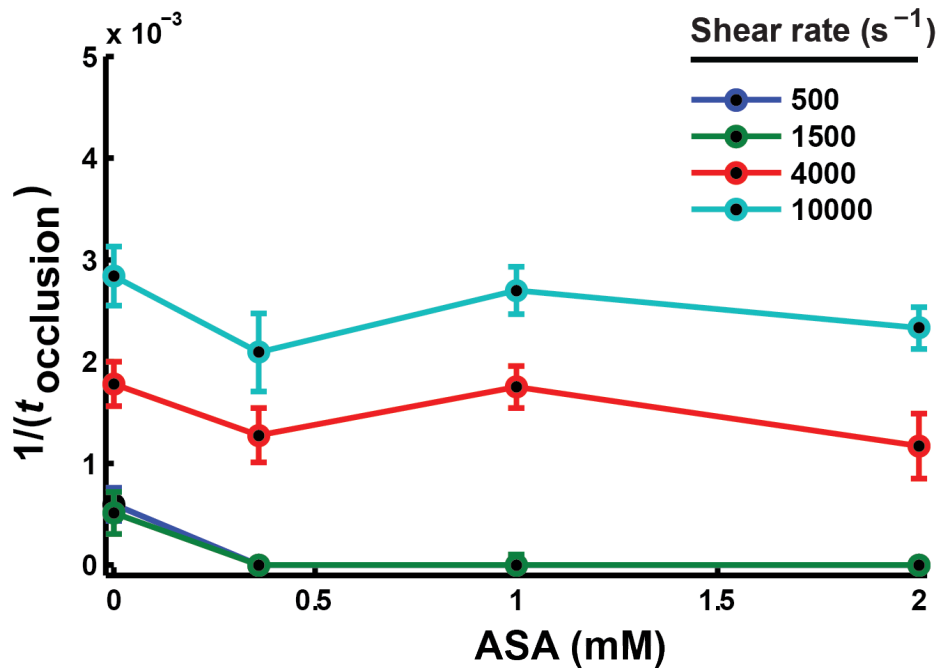
Figure 50: ASA dose-response curves of varying shear rates pooled from N=5 human subjects. Platelet response is defined by $1/t_{occlusion}$, where $t_{occlusion}$ is the time at which platelet thrombus occludes the stenosis. At physiological shear rates of 500 and 1500 s^{-1}, occlusion is eliminated at dosages between 0.36 and 1 mM. In contrast, none of the tested dosages were able to prevent or even significantly (p>0.05) affect $1/t_{occlusion}$ at high shear rates of 4000 and 10000 s^{-1}. Similar to eptifibatide results, Cox survival analysis showed all shear rate curves were significantly (p<0.001) different from one-another, save for the 500 to 1500 s^{-1} comparison.
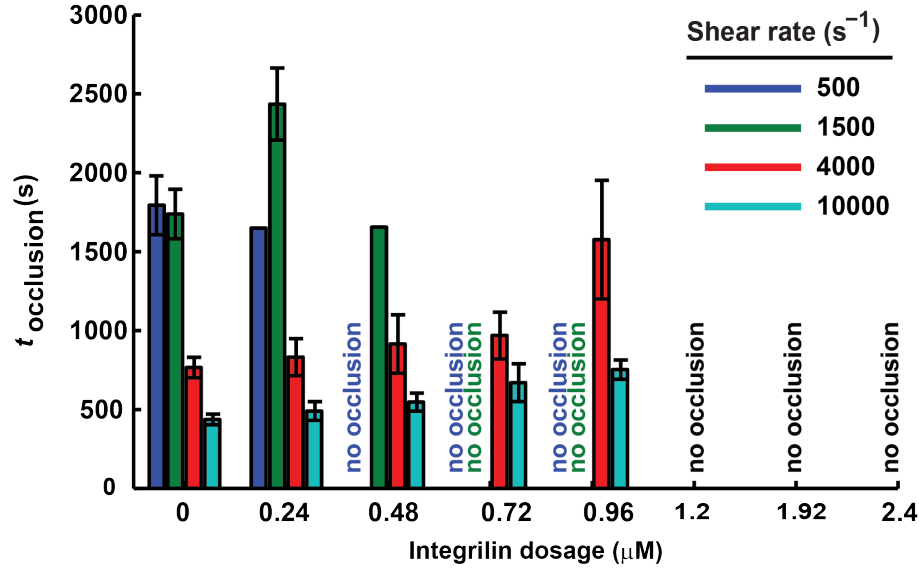
Figure 51: Raw occlusion times, $t_{\text{occlusion}}$, for varying shear rates and concentrations of ASA. Unlike the $1/t_{\text{occlusion}}$ metric used in the previous Fig 50, this metric is more intuitively understandable for the reader. However, it does not account for non-occlusion events and thus shows very small sampling N for some points, in contrast to the previous figure which is able to provide means and standard error amounts for five samples per point.

were not significantly ($p>0.1$) different in either lag time or in RPA growth. Again, apparent changes in RPA growth and Lag time were confounded by reduced numbers of occluded trials, and thus fewer data points. Although the timescale of activation is similar to lag times found in this work (as with Hellums and Bark) [121, 5], the addition of ASA, an anti-platelet agent which should block platelet activation, did not appear to significantly affect lag times at high shear rates 4000 and 10000 s^{-1}, indicating that platelet activation might not be the operative mechanism as such high shear levels. This finding is in agreement with theories on high shear platelet binding from others [17].

As with eptifibatide, we also measured platelet response by $1/V_{\text{occlusion}}$, where $V_{\text{occlusion}}$ is the sample blood volume required to occlude flow (Fig. 53). Unlike eptifibatide results, occlusion volumes, $1/V_{\text{occlusion}}$ at higher shear rates of 4000 and 10000 s^{-1} were not significantly different ($p>0.05$), nor did their values change over
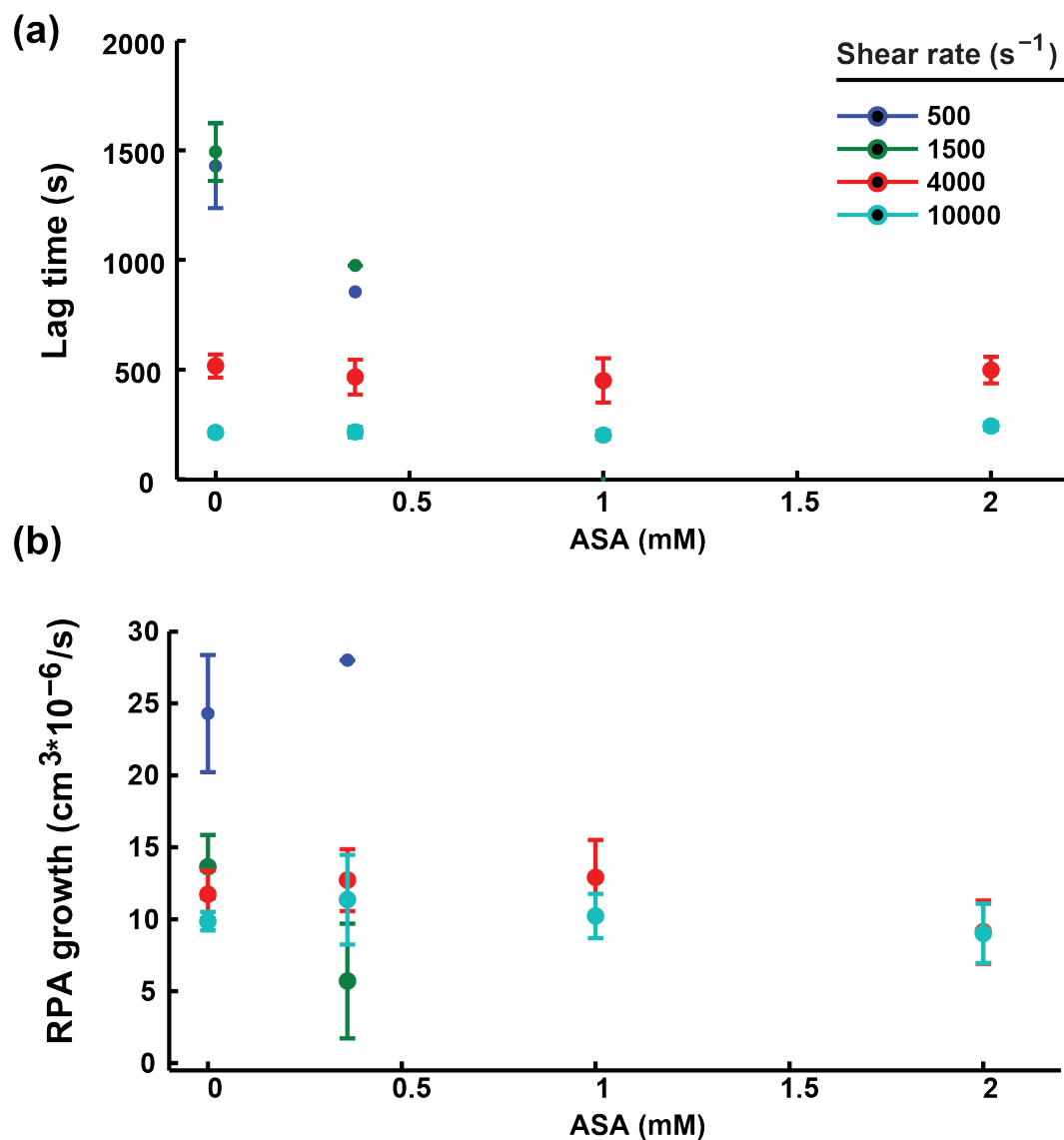
Figure 52: We next examined RPA growth and lag times vs. ASA dosage. Measurements of both Lag time (a) and RPA growth (b) at mid-to-high shear rates 4000 and 10000 s^{-1} were not significantly (p>0.1) different in either lag time or in RPA growth. Again, apparent changes in RPA growth and lag time were confounded by reduced numbers of occluded trials, and thus fewer data points.
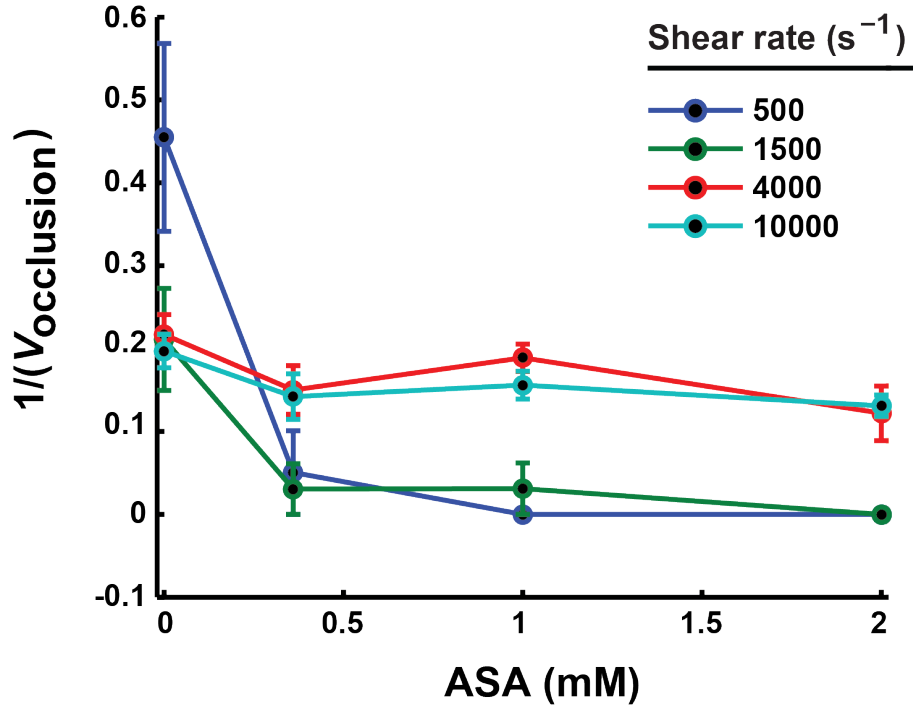
Figure 53: ASA dose-response curves for varying dosage concentrations pooled from N=5 human subjects. Platelet response here is measured by $1/V_{occlusion}$, where $V_{occlusion}$ is the sample blood volume required to occlude flow. At high shear rates of 4000 and 10000 s^{-1}, $1/V_{occlusion}$ values did not differ from eachother nor change in value significantly for all tested ASA concentrations of 0 to 2 mM

all concentrations. Similar to eptifibatide, the lowest tested venous shear rate of 500^{-1} showed the largest variation in $1/V_{occlusion}$ values. Also similar to eptifibatide results, Cox survival analysis showed all shear rate curves were significantly (p<0.001) different from one-another, save the 500 to 1500 s^{-1} comparison.

Thus ASA did not appear to affect the formation of occlusive thrombi. However, did it affect the formed occlusive thrombus? To answer this question, we again examined the Ratio of Embolization, defined as (# trials with thrombus detachment)/(# total trials). (Fig. 54).

Controls in both the previous eptifibatide study and this ASA study showed embolization of 13% and 14%, respectively. However, as ASA concentrations increased, embolization increased dramatically and nearly all samples embolized. Furthermore,
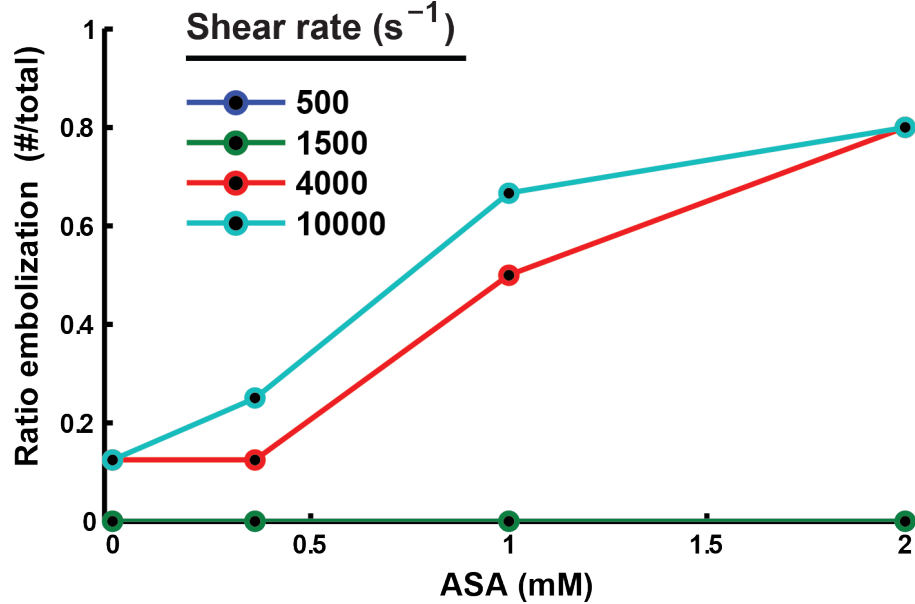
Figure 54: Ratio of Embolization, defined by (# trials with at least one thrombus detachment)/(# total trials). Controls in both the previous eptifibatide study and this ASA study showed embolization of 13% and 14%, respectively. However, as ASA concentrations increased, embolization increased dramatically and nearly all samples embolized.

all of the 3/5 subjects from the previous eptifibatide study showed the same or increased numbers of emboli formed in this study (0-5 additional embolic events over all trials with added concentrations of added ASA or eptifibatide).

Thus from our microfluidic system, we found non-significant (p>0.05) decreases in platelet activity at high shear rates 4000 and 10000 s^{-1}, and a significant (p>0.05) loss of activity between 0.36 and 1 mM for lower shear rates 500 and 1500 s^{-1}. Unlike with eptifibatide, we were not able to detect a drug concentration threshold at which platelet activity ceased for all shear rates.

Comparison of the WBA performance with the shear curves produced in our system provided a similar sensitivity limit to our findings at low shear rates 500 and 1500 s^{-1} of 0.36 mM ASA. (Fig. 55). As with eptifibatide, this limit was defined by the dosage concentration at which the $1/t_{\text{occlusion}}$ values did not change significantly for increasing concentrations.
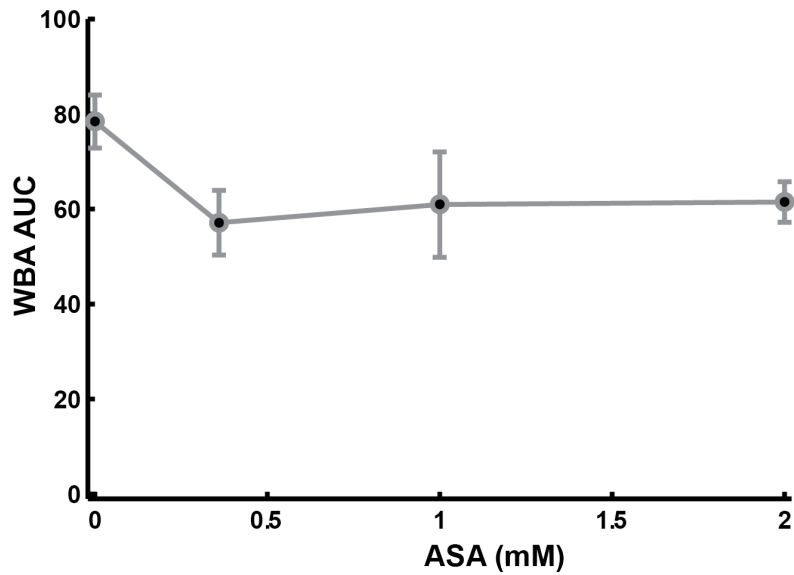
Figure 55: Dose-response measurements using the Chronolog Whole Blood Analyzer with 4 μL collagen agonist shows detectable differences in Amplitude, Area Under the Curve (AUC), and lag time until reaching a concentration of 0.72 μM, after which responses did not change significantly for increased dosages.

To exclude the possibility the ASA used was properly prepared and affecting platelet function, we used an agonist called arachidonic acid. ASA affects platelets through inhibition of the enzymes cyclo-oxygenase-1 and -2 (COX-1, COX-2), which use Arachidonic acid to form the pro-aggregation soluble factor TXA2 [122], and is employed in commercial platelet function tests including the VerifyNow, Light Transmission Aggregometry, the PFA-100, and impedance aggregometry [25]. Thus adding Arachidonic acid to platelets and observing loss of platelet aggregation indicates that ASA is properly affecting platelet function.

Use of Arachidonic acid as an agonist in the WBA did indeed showed a complete loss of platelet response at all of the ASA concentrations tested in this work (Fig. 56). Thus we verified that these tested concentrations were properly able to inhibit the production of the soluble factors which promote platelet aggregation.

Clinical implications: Results in this section are supported by both clinical trials and by previous research groups.

132
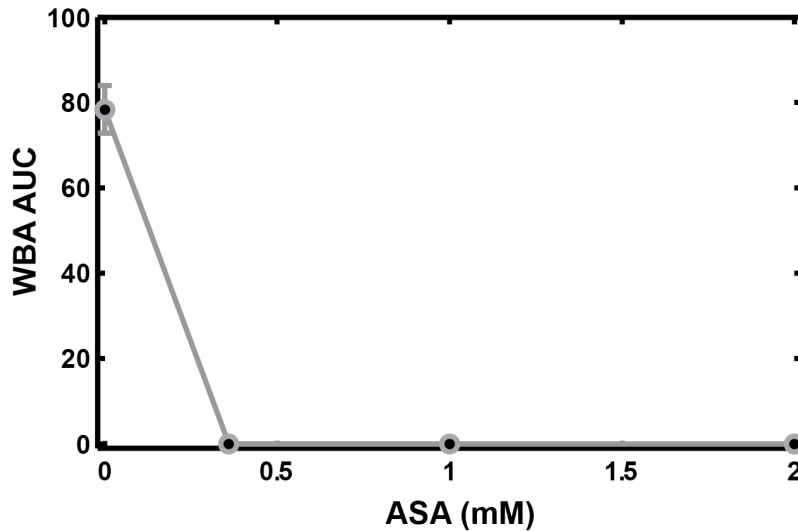
Figure 56: Dose-response measurements using the Chronolog Whole Blood Analyzer with 10 μL of Arachidonic Acid showed complete inhibition of platelet activity at all tested concentrations of ASA.

Clinical trials have reported "no antithrombotic benefit...in patients with severe atherosclerosis and stenoses...however anti-thrombotic protection...in patients with less severe lesions is reported", and that high dosage ASA therapy is ineffective at preventing re-occlusion in high shear stenosis (i.e. greater than 90%) in angiographic studies [123]. Such reports are supported by our results, which showed elimination of low shear platelet activity at 500 and 1500 s^{-1}, and insensitivity to platelet activity to aspirin at 4000 and 10000 s^{-1}.

Researchers have reported similar results using ex-vivo flow models. One group testing ASA efficacy when ingested and metabolized *in-vivo* reported that ASA sensitivity is lost in eccentric stenoses of shear rates at 10500 s^{-1} [124]. In contrast, at low shear rates of 2600 s^{-1}, platelet binding is more dependent on shape change, fibrin deposition, and fibrinogen bonds [15]. It is notable that these results are controversial, with other researchers have reporting that both in-vivo and in-vitro (as in this study) models of ASA had no significant effect at 800-3000 s^{-1} [125]. Such studies may be reconciled with findings in this study if there is a distinct change in platelet

bonding in the 3000-4000 s^{-1} range, as predicted by some [13].

Multiple justifications are available to describe this phenomenon. First, ASA loses efficacy when shear-enhances transport of soluble factors such as TXA2 (one of the main targets of ASA) away from the growing platelet thrombus [126, 115]. Additionally, platelet shape changes induced by soluble factors is not necessary to form thrombi at high shear [12].

The primary clinical applications of our findings are twofold. First, that high dosages of aspirin does affect thrombus embolization and stability provides evidence that a system such as our may be useful in detection of stroke risk in patients. Currently, ASA is a commonly used prevention measure for ischemic stroke, but resistance to such treatment is common and effectiveness has been found to vary over time [127]. Thus the high shear thrombus formation and embolization seen in this study may be one possible mechanism for the observed resistance to treatment.

Second, it provides strong evidence that the poorly characterized phenomenon of "aspirin resistance" may in fact be primarily mechanically related. Thus, this work advises that future clinical tests for characterizing causes for aspirin resistance consider angiographic data in addition to previously considered genetic testing and dose-response data.

While the microfluidic system in its current state may not be directly applicable to determining patient dosages, it does provide valuable information on potential improvements in preventing or predicting bleeding and stroke. For example, future work may create a system which is able to calculate thrombosis risks based on shear rate and dosage using the Cox survival method employed in our analysis methods. Patients angiograms would be assessed for percent stenosis, which could then be used to correlate with a shear rate range. Using the relative risk table, physicians could then use this shear rate to "look up" the closest dosage corresponding to a low risk of thrombosis to reduce the risk of overdose/bleeding.

The system may also be used for predicting bleeding or thrombosis tendency in a similar way to current commercial methods by using a "cut-off value" for untreated samples [20, 25], with pre-determined low values hitting a cut-off for "likely to undergo thrombosis" and pre-determined high values hitting a cutoff for "likely to bleed/low baseline platelet activity". However, as with current commercial tests, such results will require significant clinical validation to determine suitable cut-off points.

5.4   Conclusions

This Chapter has shown the application of the multi-shear microfluidic system in label-free, human whole blood samples treated with dosages of eptifibatide (0 to 2.4 μM) and acetyl-salicylic acid (0 to 2 mM), representatives of two popular types of anti-platelet therapies.

Both porcine and human samples showed significant elevations in platelet thrombosis prior to the administration of therapy, with the former showing nearly binary shear-dependent occlusion time (present above 4000 s^{-1} and not present below 1500 s^{-1}), and the latter showing a more graded response with increasing shear rate. Administration of increasing dosages of eptifibatide in human samples showed that the drug was effective at all shear rates, with increasing dosages showing significantly (p<0.01) different $1/t_{occlusion}$ dose-response curves for all shear rates save the lowest physiological shear rates 500 and 1500 s^{-1}. At all shear rates, increased dosages of eptifibatide decreased response until thrombosis was not detectable. Notably, increasing shear rates required similarly increasing concentrations of eptifibatide to eliminate thrombosis, indicating that optimized patient dosages are indeed shear dependent.

Similar to eptifibatide, all dosages of ASA showed significantly (p<0.001) different $1/t_{occlusion}$ dose-response curves for all shear rates save the lowest physiological shear rates 500 and 1500 s^{-1}. In contrast to eptifibatide, addition of increasing dosages of ASA did not show significant alterations in platelet thrombosis at high shear, but

was eliminated at clinically relevant dosages at physiological shear rates 500 and 1500 s^{-1}. Findings from both drug models agree well with published clinical observations and research studies. Thus the microfluidic system and its applied studies show the effects of pathologically high shear rates on increasing platelet thrombosis and demonstrate the widely varied shear-dependent efficacy of two types of therapies. This study lays the foundation for the future development of a medical diagnostic for optimizing the type and dosage of patient platelet therapy and to better understand their mechanisms of action.

Thus we have shown that ASA therapy is most effective at inhibiting platelet function under physiological levels of shear 500 and 1500 s^{-1}. In contrast, at high shear rates only moderate reductions in platelet activity can be measured, in agreement with findings by clinicians and other researchers. Although thrombi grew as normal, the main effect of ASA appeared to be a destabilizing one since ASA-treated blood showed nearly 70% more fragmenting or embolic effects after treatment vs. untreated controls. We theorize that this may be due to the enhanced transport of soluble factors away from the site of thrombus growth at high shear regions, a concept well supported in current literature [57, 63, 115, 125, 124].

Findings of this Chapter can be generally stated as follows:

Shear rate is a significant determinant of occlusion time

- In eptifibatide, both dosage and shear create significant differences in occlusion times

- In ASA, dosage is significant for low shear only. Shear rate has significant effects at all dosages

- Results supported by previous clinical and research finding

Commercial comparison

- Our device is able to measure changes in thrombus embolization, commercial device cannot.

- Commercial device has similar results to single shear curve from our multi-shear system

- Our device is able to measure changes in thrombus embolization, commercial device cannot.

5.4.1 Endpoint Recommendations

This study examined a variety of different endpoints to characterize thrombosis under varying drug dosages and shear rates, including $1/t_{\text{occlusion}}$, $t_{\text{occlusion}}$, occlusion volume, thrombus detachment, RPA growth, and lag time. The ability to extract data from all of these methods presents a significant advancement in the field and great potential for enhanced point of care readouts (although the clinical correlates of such metrics still need to be confirmed through clinical studies). The preferred metrics from this list were $1/t_{\text{occlusion}}$ or $t_{\text{occlusion}}$, and thrombus detachment. $1/t_{\text{occlusion}}$ data was an excellent method for visualizing data due to its ability to display non-occlusion events as zero. However, such estimates can provide small distortions in data, since the assumption that the channel would "never occlude" may be an exaggeration.

Metrics of $t_{\text{occlusion}}$ were useful in Cox survival analysis, which does not require processing of all trials into $1/t_{\text{occlusion}}$ format. $t_{\text{occlusion}}$ is also more intuitive to understand, although it is can be misleading in data plots due to changing N which compose its average and standard deviation at each shear/dosage point.

The thrombus detachment endpoint provided relevant information for future clinical recommendations in the case of ASA, and consistent with the recommendations of the ISTH, would be an excellent addition to current devices which do not include it.

Control values for RPA growth and lag time measurements provided valuable

points of comparison with previous work, despite their methodological flaws mentioned in the Methods: Analysis subsection [5, 121, 59]. In this study we found control lag times and RPA values similar to theirs, and a similar trend of decreased lag times for increased shear rates. Although the timescale of activation is similar to lag times found in this work (as with Hellums and Bark), the addition of ASA, an anti-platelet agent which should block platelet activation, did not appear to significantly affect lag times at high shear rates 4000 and 10000 s^{-1}, indicating that platelet activation might not be the operative mechanism as such high shear levels. This finding is in agreement with theories on high shear platelet binding from others [17]. Thus these measurements provided interesting insights into dose-response behavior in eptifibatide, showing significantly (p<0.05) reduced RPA growth and increased lag times over the same shear rates, and between different shear rates.

However, one major difference between this work and the previously cited authors is the use of a constant flow system and extensive work on edge detection in order to make predictions of shear rate, since these metrics were extracted in a post-analysis fashion and not explicitly planned for. This study employed the use of initial wall shear rates only. Thus the measurement of the shear rate at which lag time and RPA occur and how these varies with shear rate is presently unknown for this study. Furthermore, results for RPA growth should be approached with caution since non-optimal, low resolution flow-rate measurements were poorly suited to measuring RPA growth at low shear rates. Finally, measurements of RPA growth and lag time were difficult to extract meaning from since subjects who did not form occlusive thrombus had none of these metrics, and thus the N of trial data varied widely across conditions. Further studies might be able to approximate thrombus growth rates similar to previous findings in units of volume/surface*time using more advanced image processing from microscopy or intensity readings.

Lag time and RPA growth are potentially interesting areas of study for thrombosis

studies. Future recommendations for those who would like to use this system to study these metrics would be first to develop a method for more thoroughly characterizing changes in shear rate over time within these trials, especially for changing flow rate values. Next, studies should be repeated with higher N subjects to allow a sufficient number of readings to be made at each shear rate and dosage point to verify the findings described in the previous paragraph. Intensity measurements using our existing optical sensing method could also provide improved metrics for RPA growth and lag time, and would have been used in this study if it had been part of the beginning testing criteria.

CHAPTER VI

CONCLUSIONS AND FUTURE DEVELOPMENT

6.1   Conclusions

Thrombosis is the pathological formation of platelet aggregates which occlude blood flow causing stroke and heart attack—the leading causes of death in developed nations and the largest domestic healthcare expenditure. The mainstay for prevention and post-operative treatment of these events is the use of platelet therapies. Determining dosage for platelet therapies (e.g. aspirin, Integrilin, and Plavix) is a persistent medical challenge, and studies estimate up to 45% of patients exhibit insufficient responses to them. Recent studies have shown that this loss in anti-platelet therapy efficacy may be dependent on local flow conditions including high shear rates and stenosis morphology. In Chapter 1 of this thesis, current thrombosis evaluation methods were reviewed and demonstrated to be limited by one or more of the following parameters: non-pathologically relevant flow conditions, need for external cell labeling and/or centrifugation, low throughput, high costs, channel sizes insufficient to observe later stages of occlusive thrombosis, and the need for large volumes of blood. There is presently no instrumentation able to simultaneously examine therapeutic efficacy for a wide range of fluid shear rates from physiological to pathological levels. Thus the creation and application of such high throughput instruments could enable essential, large scale, comprehensive studies which would inform research on cardiovascular pathologies and their appropriate anti-platelet therapies.

In this work, a microfluidic device and associated optical system were designed and fabricated for simultaneous measurement of platelet aggregation at multiple initial wall shear rates within multiple stenotic channels in label-free whole blood and used

to characterize thrombosis under varying dosages of platelet therapies. In Chapter 2, we demonstrate a device for inducing platelet aggregation to full thrombotic occlusion within four microfluidic stenotic channels in label-free whole blood at initial wall shear rates from 500 to 13000 s^{-1}, as confirmed by finite volume modelling and by flow rate experiments. Next, in Chapter 3, we discussed the development of an optical system that allows label-free microscope-free, multi-channel, real-time, non-contact, high temporal resolution measurements of platelet-based thrombosis and showed excellent agreement with results from traditional brightfield microscopy, flow rate, and histology measurements.

In Chapters 4 and 5, the microfluidic system was applied to characterize thrombosis at multiple initial wall shear rates and at varying dosages of two platelet therapies: acetyl-salicylic acid (aspirin) and eptifibatide (Integrilin). Both porcine and human samples showed significant elevations in platelet thrombosis prior to the administration of therapy, with the former showing nearly binary shear-dependent occlusion time (present above 4000 s^{-1} and not present below 1500 s^{-1}), and the latter showing a more graded response with increasing shear rate. Administration of increasing dosages of eptifibatide in human samples showed that the drug was effective at all shear rates, with increasing dosages showing significantly (p<0.01) different $1/t_{\text{occlusion}}$ dose-response curves for all shear rates save the lowest physiological shear rates 500 and 1500 s^{-1}. At all shear rates, increased dosages of eptifibatide decreased response until thrombosis was not detectable. Notably, increasing shear rates required similarly increasing concentrations of eptifibatide to eliminate thrombosis, indicating that optimized patient dosages are indeed shear dependent.

Similar to eptifibatide, all dosages of ASA showed significantly (p<0.01) different $1/t_{\text{occlusion}}$ dose-response curves for all shear rates save the lowest physiological shear rates 500 and 1500 s^{-1}. In contrast to eptifibatide, addition of increasing dosages of ASA did not show significant alterations in platelet thrombosis at high shear, but

was eliminated at clinically relevant dosages at physiological shear rates 500 and 1500 s^{-1}. Findings from both drug models agree well with published clinical observations and research studies. Thus the microfluidic system and its applied studies show the effects of pathologically high shear rates on increasing platelet thrombosis and demonstrate the widely varied shear-dependent efficacy of two types of therapies. This study lays the foundation for the future development of a medical diagnostic for optimizing the type and dosage of patient platelet therapy and to better understand their mechanisms of action.

Thus we have shown that ASA therapy is most effective at inhibiting platelet function under physiological levels of shear 500 and 1500 s^{-1}. In contrast, at high shear rates only moderate reductions in platelet activity can be measured, in agreement with findings by clinicians and other researchers. Although thrombi grew as normal, the main effect of ASA appeared to be a destabilizing one since ASA-treated blood showed nearly 70% more fragmenting or embolic effects after treatment vs. untreated controls. We theorize that this may be due to the enhanced transport of soluble factors away from the site of thrombus growth at high shear regions, a concept well supported in current literature [57, 63, 115, 125, 124].

6.2   Original contributions

In summary, this system presents the first systematic, in-vitro characterization of the effects of a spectrum of physiological to pathological shear rates and platelet therapy doses on occlusive platelet thrombosis and embolus. The system, developed according to best practices recommendations of ISTH, simultaneously measures thrombosis by changes in flow rate, transmitted light intensity, and microscopy in an in-vitro diagnostic. Results from studies using this instrument lay the groundwork for more accurate platelet therapy treatment models by identifying shear rate as a significant factor in thrombosis. The work showed that pathological vs. physiological shear

rates have significant effects on thrombosis dose-response curves. For eptifibatide (Integrilin), both dosage and shear create significant differences in occlusion times while ASA (Aspirin) dosage is significant for low shear only. Finally, the system also presents the first characterization of the bulk optical properties of platelet thrombus, useful for future instrument development.

We have shown that the system can indicate decreased platelet thrombosis after addition of drugs in an *in-vitro* model and verified them through a commercial method (which has shown efficacy in predicting MACE events in clinical trials) although the $in - vivo$ correlate effects (e.g. induction/cessation of MACE events, excessive bleeding) of such treatments in our studies must still be assessed.

6.3   Future Development

Currently the primary deficiency of platelet analysis systems is their questionable clinical relevance. We hope to have eliminated some of these concerns through the developments discussed in the previous section. However, the focus of this work is a scientific quantification of how shear rate changes anti-platelet efficacy, not as a commercial platelet function diagnostic. Development of this work as a clinical diagnostic will require a new set of criteria, including reduced testing volumes, extended clinical validations, and simplified design.

6.3.1   Instrumentation development

The dimensions of the current microfluidic device were chosen to ensure the observation of platelet-platelet cohesion present in late stage thrombosis, in contrast to many prior microfluidic studies which focused on platelet adhesion. Furthermore, the dimensions were also chosen to prevent early occlusion by the emboli present in many porcine blood samples. However, recent geometric analysis (Casa, unpublished), have theorized that platelet-platelet bonding dominates platelet-substrate binding by an order of magnitude at dimensions as small as 100 μm in diameter, in contrast to

the smallest dimension in our device, 250 μm. In addition, studies described in this work have found that human blood lacks the large emboli present in human blood. Furthermore, the same study estimates that the reduced size of each assay channel should require significantly reduced trial times and sample volumes. Reduced sample volumes would greatly benefit future clinical studies by decreasing the time between sample blood draws (due to volumetric limits), time required to draw blood (approximately 15 minutes per 60 mL aliquot), and reduce safety risks. Our very limited study on the shape effects of channels implies that circular channels show significantly different occlusion time results in some porcine samples, but further tests of this principle using human blood should be examined before further action is taken on the significant task of repeatably and easily creating circular cross section devices.

Although flow was used in Chapter 5 as the primary metric for occlusion, optical metrics have much greater potential for future development due to lower complexity and greater scalability and affordability. This work thus recommends future development of optical metrics to replace flow. Efficacy of the optical measurement of occlusion endpoint in Chapter 3, and this can potentially be improved upon with some of the instrumentation recommendations listed in the following part of this Chapter as well as in Chapter 3.

Recent collaborative work with the Capstone undergraduate Mechanical Engineering class has seen the development of a point-of-care benchtop prototype able to replicate the salient features of our detection and data acquisition methods in a compact and user-friendly format. The prototype measures 30 cm x 16 cm x 15 cm (11.8"×6.3"× 5.9") in size including fluidic handling and optics that takes an average of 30 minutes per test. The system takes advantage of the optical methods described in this work to rapidly and inexpensively screen platelet activity without the use of added fluorophores, labelled beads, or microscopy involved with alternative methods. The reader unit shown in Fig. 57 uses the same disposable microfluidic

chip developed in Chapter 2 of this project to form thrombus. Similar to the method described in Chapter 2, blood is flowed into the device using automated gravity pressure head control from a syringe on a motorized actuator. Blood is delivered to the stenoses from the syringe, and collected in disposable blood bags downstream in this prototpe. Hardware control, data acquisition, data processing, and even the printing of results is made possible by two onboard Arduino micro-controllers and a small receipt printer. The light source in the device is a set of four green laser diodes which deliver light through fiberoptic cables incident on the surface of the chip, which is then collected by four independent photodiodes situation underneath the stenoses of the microfluidic device opposite the fiberoptic cables. The device was able to detect thrombus formation in porcine blood samples. The system's small footprint, low cost components, and relative ease of use are promising for future development.

6.3.2 Clinical applications

Future clinical studies are required to determine the relationship of these results to clinical MACE endpoints, similar to those described in Chapter 1. If provided with unlimited resources, an ideal study would examine $t_{occlusion}$ (or predicted risk for occlusion calculated by Cox-analysis), RPA/lag time, thrombus detachment, vWF titers, known genetic fingerprints of drug non-responders, platelet count, and mean platelet volume in a population of patients with varying degrees of stenosis being treated with aspirin and/or a GPIIb/IIIa inhibitor. Angiographic data from patients would provide information on internal shear rates of 500-1500, 2000-4000, and 10000 s^{-1} and higher. Initial patient number targets would be N=40 per shear rate for a total of N=120 subjects. Numbers are estimates for achieving statistical significance in RPA and lag time, which required more subjects than the present results shown in this work. Blood samples would be run with no, low, and high and dosages of the given drug and corresponding $t_{occlusion}$ and thrombus detachment metrics recorded.
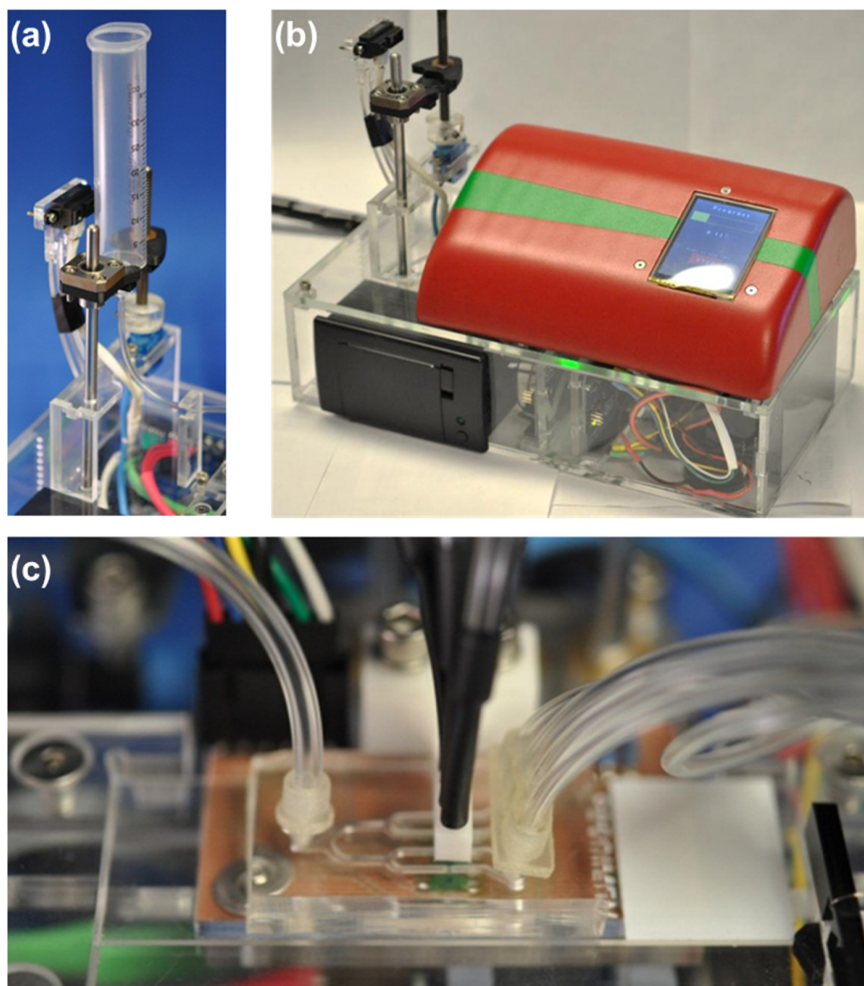
Figure 57: Collaboration with a team of students in Georgia Tech's Mechanical Engineering Capstone program saw the creation of a promising point-of-care benchtop prototype able to replicate the salient features of our detection and data acquisition methods in a compact and user-friendly format. The prototype measures 30 cm × 16 cm × 15 cm (11.8"×6.3"× 5.9"). Similar to the method described in Chapter 2, blood is added to the system using automated gravity pressure head control from a syringe on a motorized actuator (a). A touchscreen interface on the cover of the reader unit (b) allows the user to begin the test. When testing has begun, blood will flow from the syringe to the to the microfluidic device, which sits beneath the hinged touchscreen cover (c). Hardware control, data acquisition, data processing, and even the printing of results is made possible by two onboard Arduino microcontrollers and a small receipt printer housed inside the device's acrylic body. The light source in the device is a set of four green laser diodes which deliver light through fiberoptic cables incident on the surface of the chip (c).

Half of each patient/shear population would be treated with the high dosage, and the other with the low dosage, and patient outcomes tracked for 10 years, with any MACE events recorded.

Obvious challenges with reaching this clinical goal are the aforementioned instrumentation challenges, and the financial challenges of such a large, long-term test. However, it may be able to "piggy-back" off the many pre-existing angiographic cohort studies which appear to be common in cardiovascular research.

The technology also prompts additional interesting future clinical investigations. While the studies presented in Chapter 5 presented an interesting proof of concept *in-vitro* characterization of thrombosis in healthy individuals, additional studies will be required to define the utility of this instrument for diagnosing more diverse patient populations with pre-existing pathologies. There are to could also be used to probe a number of interesting hematological pathologies including von Willebrand's disease, thrombocytopenia, sickle-cell anemia, and coronary artery disease. Successful detection of von Willebrand's disease has been shown by other high shear platelet function tests such as Siemens' PFA-100, a system with similar capabilities to the system described in this work. Sickle-cell anemia presents specific scientific interest due to the large number of children with the condition affected by strokes. The application of this model system to studies of that pathology might reveal novel pro-thrombotic interactions between red blood cells and platelets.

Additional future clinical studies should also examine other popular drug models, especially clopidogrel, which remains one of the most popular anti-platelet drugs on the market. Other popular drug models of interest include abciximab, prausgrel, and ticlopidine. With the need for platelet therapeutics only increasing, we anticipate applications of this system to experimental drug screenings. In fact, recent work has shown pharmaceutical firms such as Portola (the developer of Integrilin) publishing on the use of a traditional parallel plate flow chamber to screen known drugs [54],

147

proving that there is an immediate need and application for a flow system such as ours with significantly improved throughput and scientific relevance.

It is also notable that the study presented in Chapter 5 examines the effects of anti-platelet agents added *in-vitro*. While this model may recapitulate the initial behavior of injectable drug bolus (relevant for heparin and Integrilin), it may not accurately describe the long-term effects, nor the behavior of orally administered drugs such as aspirin and Plavix due to metabolic or otherwise genetically linked efficacy factors [22]. Thus it is recommended that future studies examine blood from two separate blood draws before and after patient use to determine how this system may be used to optimize anti-platelet therapy. Additional long term studies of patient outcomes will be necessary to determine the long term benefits of such therapies and their efficacy at preventing re-stenosis, stroke, or heart attack.

6.3.3 Translational development

In order to achieve significant clinical impact, this system will also need to transition to a more streamlined and user-friendly design. While current devices on the market such as the VerifyNow have not achieved strong clinical results, they have demonstrated the commercial potential of a platelet function analyzer in the point-of-care market. Over the course of this project, we have made some progress towards this goal. Collaboration with a team of students in Georgia Tech's Mechanical Engineering Capstone program saw the creation of a promising point-of-care benchtop prototype 30 cm × 16 cm × 15 cm (11.8"× 6.3"× 5.9") in size including fluidic handling and optics that takes an average of 30 minutes per test.

Translational development of this project will require steps towards FDA clearance. This path begins with the FDAs 510(k), which requires that our device show equivalency to another category of device currently on the market, such as the 21CFR864.5700 "automated platelet aggregation system". However, while 510(k)

approval would allow the legal marketing of such a product, we anticipate that it would require significant clinical validation, certification from Clinical Laboratory Improvement Amendments (CLIA), and/or a Current Procedural Terminology (CPT) code from the American Medical Association before it is well-received in the medical community.

This thesis has described the motivations for platelet research as well as current methods for measurement and analysis, and set forth goals for advancing our methods and knowledge in the field. Specifically, it has developed a microfluidic device and associated light transmission optical measurement method for studying the simultaneous effects of shear rate and platelet therapy dosage on platelet thrombosis. Finally it has demonstrated the utility of this method using two different drug models at a range of shear rates from physiological to pathological, to determine two different activity profiles. It is my hope that the findings of this work will be of use in future clinical, research, and/or translational efforts in thrombosis detection and prevention.

APPENDIX A

THROMBOSIS METRICS

This section summarizes the primary thrombosis metrics used in this work, and summarizes their advantages, disadvantages, and relationships to one-another.

A.1 Measurements using flow

- *Flow rate*: $Q(t)$

  Advantages: Flow rate measurements provide direct feedback on channel occlusion with little data processing in comparison to optical methods. Flow rate can also be used to detect thrombus detachment events.

  Disadvantage: Cannot directly measure number of platelets or thrombus morphology, unlike optical methods.

  Related metrics: $t_{occlusion}$, $V_{occlusion}$

- *Occlusion time*: $t_{occlusion}$

  Advantages: Flow occlusion also provides a clinical analog to cerebral or myocardial infarct. Also, measurements of flow cessation are comparable to those of the commercial platelet function analyzer, the PFA-100 [20]. In the PFA-100, the equivalent metric for $t_{occlusion}$, found in this work, is known as the closure time, (CT), which occurs when a collagen-coated cellulose membrane hole is filled with platelets during pressure driven flow of whole blood at 4000 s^{-1}. For rough comparison, $t_{occlusion}$ of whole, human blood at 4000 s^{-1} in our device with a minimum cross-sectional area of 9.3∗10-2 mm^2 (cross sectional area) occurs at 521 ± 128 seconds, vs. the PFA-100s closure times of 137-300 s^{-1} in a 2.25∗10-2 mm^2 (cross sectional area) orifice.

Disadvantages: Requires significant extra instrumentation bulk for measurements in comparison to non-contact optical methods such as LED and laser light transmission. Additionally, this method is hindered by high costs and limited resolution at low flow rates (<1 μL/s). As a final metric, use of raw $t_{\text{occlusion}}$ values do not reflect non-occluded trials, a problem which can be circumvented through the use of $1/t_{\text{occlusion}}$ (see below).

- *Inverse occlusion time*: $1/t_{\text{occlusion}}$

  Advantages: This metric is valuable for statistical analysis including parametric and pairwise comparison analysis (e.g. logistic and MANOVA models, corresponding Tukey post-hoc methods) due to its ability to assign endpoint values to both occluded and non-occluded channel runs.

  Disadvantages: The estimate of non-occluded events as 0 assumes infinite occlusion time, which adds distortion to data.

  Related metrics: $t_{\text{occlusion}}, V_{\text{occlusion}}$

- *Occlusion volume*: $V_{\text{occlusion}}$ Total volume of blood required to occlude the channel.

  Advantages: This value is useful for determining required sample volumes during testing, and can provide an estimate of the total number of platelets that would have passed through the stenosis in order to cause occlusion.

  Disadvantages: This metric has large variations in data and not often used by other commercial methods.

  Related metrics: $t_{\text{occlusion}}, Q(t)$

- *Rate of Platelet Accumulation growth*: *RPA growth*

  Advantages: *RPA growth* provides an estimate of platelet behavior during its accumulation phase, which prior research has indicated as a defining event

distinct from adhesion and early aggregation. RPA values were 14 ± 1.1 (cm^3 $*$ $10^{-6}/s$) for N=72 samples, similar overall to the average value determined by Para, 20(cm$^3 * 10^{-6}/s$). However, unlike that study we did not observe increases in *RPA growth* for increasing initial shear rate, perhaps due to the pressure-controlled (vs. flow rate controlled) flow.

Disadvantages: *RPA growth* is difficult to study for low shear rates due to the low resolution of weighing scales. Results were also confounded by changing experimental N due to non-occluded trials, which did not have a measurable t_{final}.

- *Lag time*: $t_{lagtime}$

  Advantages: $t_{lagtime}$ gives an indication of the time required for platelets to complete the adhesion phase, nominally dependent on the GPIb-vWF high shear bond, a separate measurement from overall occlusion time. As expected, we observed decreasing lag times with increasing shear rates, a result reported by many others [59, 17, 128].

  Disadvantages: Like *RPA growth*, $t_{lagtime}$ is also not easy to measure for low flow rates (shear rates). This is reflected in decreasing SEM values with increasing shear rates.

  Related metrics: *RPA growth, Q(t)*

A.2 Optical measurements

- *Intensity of microscopy imaging*: $I_{\mathrm{microscope}}(t)$ Changes in total intensity values at each CCD element corresponding to the stenosis ROI. Values were normalized by subtracting baseline noise due to changes in ambient light and/or changes in the angle of the light source.

  Advantages: Excellent for determining thrombus morphology and relative

platelet (vs. fibrin/RBC) content. Although this method is difficult to correlate to volumes without the use of confocal methods or thin adhesion layers, it remains a standard method for many researchers [128, 3, 59, 129], and can be used for rough estimates of numbers/concentrations of platelets, unlike flow-based methods. Like $Q(t)$, also able to detect thrombus detachment.

Disadvantages: This method determines overall intensity of the entire image, thus morphology data is lost. Due to small observation areas, requires the use of an expensive automated stage to observe multiple channels, which can slow the acquisition times.

Related metrics:$I_{\text{laser}}(t)$, $I_{\text{LED}}(t)$

- *Intensity of laser transmission*: :$I_{\text{laser}}(t)$, $I_{\text{LED}}(t)$ Both raw values are on a 0 to 211 (2048) scale due to the sensitivity of the CCD sensor. Values are captured and averaged over the width of the stenosis, for an approximate ROI size of 200 × 700 μm region of interest.

  Advantages: Large sensor area negates the need for automated stage (allows faster acquisition times and is more suitable to point-of-care applications), while retaining the advantages of optical measurements similar to above (standard method, non-contact). Threshold values can be related to Q(t). Dynamic measurements are similar to more expensive and less convenient microscopy methods (R correlation value of 0.94 with Imicroscope(t)). Similar to microscopy, can be used for rough estimates of numbers/concentrations of platelets.Like Q(t) andImicroscope(t), also able to detect thrombus detachment.

  Disadvantages: Cannot determine thrombus morphology or relative platelet (vs. fibrin/RBC) content.

  Related metrics:$I_{\text{microscope}}(t)$

Signal to Noise Ratio: $\text{SNR}_{\text{occlusion}}$,$\text{SNR}_{\text{NO}}$, $\text{SNR}_{\text{final}}$

Advantages: Takes into account small variations in baseline noise due to differences in sample hematocrit, and can be used for a cut-off value for when channels occlude within 8.4% accuracy.

Disadvantages: Use of SNR to determine occlusion resulted in some false positives (non-occluded channels whose intensity rose but did not fully occlude) of 9%

Related metrics:$I_{\text{laser}}(t)$, $I_{\text{LED}}(t)$

A.0.4 Summary and opinions

The preferred metrics in this study are $t_{\text{occlusion}}$ and $1/t_{\text{occlusion}}$ (based on flow rate $Q(t)$) for their ability to be compared with current commercial platelet function tests (i.e. the PFA-100) and use in statistical analysis methods, respectively.

In this study, $t_{\text{lag time}}$ and *RPA growth* were difficult to study due to low resolution data from flow rate measurements, and thus were not preferable metrics. Optical methods based on $I_{\text{laser}}(t)$, $I_{\text{LED}}(t)$ are promising for measurements of overall platelet concentrations within the stenosis, but are less accurate than flow rate $Q(t)$ based measurements for $t_{\text{occlusion}}$ and $1/t_{\text{occlusion}}$. Thus, although these methods and metrics show promise for future use, they were not used in the majority of Aim 3 of this thesis work. Recommendations for improvements of optical methods can be found in the Conclusions chapter.

REFERENCES

[1] Martina Meinke, Gerhard Muller, Jurgen Helfmann, and Moritz Friebel. Optical properties of platelets and blood plasma and their influence on the optical behavior of whole blood in the visible to near infrared wavelength range. *Journal of Biomedical Optics*, 12(1):014024–9, January 2007.

[2] Nicoline J. Breet, Jochem W. van Werkum, Heleen J. Bouman, Johannes C. Kelder, Henk J. T. Ruven, Egbert T. Bal, Vera H. Deneer, Ankie M. Harmsze, Jan A. S. van der Heyden, Benno J. W. M. Rensing, Maarten J. Suttorp, Christian M. Hackeng, and Jurrien M. ten Berg. Comparison of platelet function tests in predicting clinical outcome in patients undergoing coronary stent implantation. *JAMA*, 303(8):754–762, February 2010.

[3] Carolyn G. Conant, Michael A. Schwartz, Tanner Nevill, and Cristian Ionescu-Zanetti. Platelet adhesion and aggregation under flow using microfluidic flow cells. *Journal of Visualized Experiments : JoVE*, (32), October 2009. PMID: 19859055 PMCID: 3164058.

[4] J. J. Zwaginga, K. S. Sakariassen, G. Nash, K. R. King, J. W. M. Heemskerk, M. Frojmovic, and M. F. Hoylaerts. Flow-based assays for global assessment of hemostasis. part 2: current methods and considerations for the future. *Journal of Thrombosis & Haemostasis*, 4(12):2716–2717, 2006.

[5] David L. Bark, Andrea N. Para, and David N. Ku. Correlation of thrombosis growth rate to pathological wall shear rate during platelet accumulation. *Biotechnology and Bioengineering*, 2012.

[6] D.K. Sardar and L.B. Levy. Optical properties of whole blood. *Lasers in Medical Science*, 13(2):106–111, June 1998.

[7] Vronique L. Roger, Alan S. Go, Donald M. Lloyd-Jones, Robert J. Adams, Jarett D. Berry, Todd M. Brown, Mercedes R. Carnethon, Shifan Dai, Giovanni de Simone, Earl S. Ford, Caroline S. Fox, Heather J. Fullerton, Cathleen Gillespie, Kurt J. Greenlund, Susan M. Hailpern, John A. Heit, P. Michael Ho, Virginia J. Howard, Brett M. Kissela, Steven J. Kittner, Daniel T. Lackland, Judith H. Lichtman, Lynda D. Lisabeth, Diane M. Makuc, Gregory M. Marcus, Ariane Marelli, David B. Matchar, Mary M. McDermott, James B. Meigs, Claudia S. Moy, Dariush Mozaffarian, Michael E. Mussolino, Graham Nichol, Nina P. Paynter, Wayne D. Rosamond, Paul D. Sorlie, Randall S. Stafford, Tanya N. Turan, Melanie B. Turner, Nathan D. Wong, and Judith Wylie-Rosett. Heart disease and stroke statistics 2011 update. *Circulation*, 123(4):e18–e209, February 2011.

[8] M. J. Maxwell. Shear induces a unique series of morphological changes in translocating platelets: Effects of morphology on translocation dynamics. *Arteriosclerosis, Thrombosis, and Vascular Biology*, 26(3):663–669, December 2005.

[9] Zaverio M. Ruggeri. Platelets in atherothrombosis. *Nat Med*, 8(11):1227–1234, November 2002.

[10] David M. Wootton and David N. Ku. Fluid mechanics of vascular systems, diseases, and thrombosis. *Annual Review of Biomedical Engineering*, 1(1):299–329, August 1999.

[11] J. J. Zwaginga, G. Nash, M. R. King, J. W. M. Heemskerk, M. Frojmovic, M. F. Hoylaerts, and K. S. Sakariassen. Flow-based assays for global assessment of

hemostasis. part 1: biorheologic considerations. *Journal of Thrombosis and Haemostasis*, 4(11):2486–2487, 2006.

[12] S. P. Jackson. The growing complexity of platelet aggregation. *Blood*, 109(12):5087–5095, 2007.

[13] Brian Savage, Jan J. Sixma, and Zaverio M. Ruggeri. Functional self-association of von willebrand factor during platelet adhesion under flow. *Proceedings of the National Academy of Sciences*, 99(1):425 –430, January 2002.

[14] Zaverio M. Ruggeri, Jennifer N. Orje, Rolf Habermann, Augusto B. Federici, and Armin J. Reininger. Activation-independent platelet adhesion and aggregation under elevated shear stress. *Blood*, 108(6):1903–1910, 2006.

[15] M. J. Maxwell, E. Westein, W. S. Nesbitt, S. Giuliano, S. M. Dopheide, and S. P. Jackson. Identification of a 2-stage platelet aggregation process mediating shear-dependent thrombus formation. *Blood*, 109(2):566–576, 2007.

[16] V. T. Turitto and C. L. Hall. Mechanical factors affecting hemostasis and thrombosis. *Thromb Res*, 92(6 Suppl 2):S25–31, 1998.

[17] S. P. Jackson, W. S. Nesbitt, and E. Westein. Dynamics of platelet thrombus formation. *Journal of Thrombosis and Haemostasis*, 7:17–20, 2009.

[18] Kjell S. Sakariassen, Stephen R. Hanson, and Yves Cadroy. Methods and models to evaluate shear-dependent and surface reactivity-dependent antithrombotic efficacy. *Thrombosis Research*, 104(3):149–174, November 2001.

[19] BR Alevriadou, JL Moake, NA Turner, ZM Ruggeri, BJ Folie, MD Phillips, AB Schreiber, ME Hrinda, and LV McIntire. Real-time analysis of shear-dependent thrombus formation and its blockade by inhibitors of von willebrand factor binding to platelets. *Blood*, 81(5):1263–1276, March 1993.

[20] Christoph K Hofer, Andreas Zollinger, and Michael T Ganter. Perioperative assessment of platelet function in patients under antiplatelet therapy. *Expert Review of Medical Devices*, 7(5):625–637, September 2010.

[21] P. A. Gum, K. Kottke-Marchant, E. C. Poggio, H. Gurm, P. A. Welsh, L. Brooks, S. K. Sapp, and E. J. Topol. Profile and prevalence of aspirin resistance in patients with cardiovascular disease. *American Journal of Cardiology*, 88(3):230–235, 2001.

[22] Center for Drug Evaluation and Research. Postmarket drug safety information for patients and providers - FDA drug safety communication: Reduced effectiveness of plavix (clopidogrel) in patients who are poor metabolizers of the drug. 2010.

[23] Shara Rosen. The worldwide market for in vitro diagnostic (IVD) tests: 2008. Technical report, Kalorama Information, 2012.

[24] Alan D. Michelson. *Platelets*. Academic Press, 2007.

[25] A. R. Rechner. Platelet function testing in clinical diagnostics. *H\mostaseologie*, 2011:31, 2010.

[26] Thomas Cuisset, Corinne Frere, Raphael Poyet, Jacques Quilici, Bndicte Gaborit, Laurent Bali, Olivier Brissy, Marc Lambert, Pierre-Emmanuel Morange, Marie-Christine Alessi, and Jean-Louis Bonnet. Clopidogrel response: Head-to-head comparison of different platelet assays to identify clopidogrel non responder patients after coronary stenting. *Archives of Cardiovascular Diseases*, 103(1):39–45, January 2010.

[27] Anne De Paepe and Fransiska Malfait. Bleeding and bruising in patients with EhlersDanlos syndrome and other collagen vascular disorders. *British Journal of Haematology*, 127(5):491500, 2004.

[28] Hayes TE Peterson P. The preoperative bleeding time test lacks clinical benefit: College of american pathologists' and american society of clinical pathologists' position article. *Archives of Surgery*, 133(2):134–139, February 1998.

[29] S. E. Lind. The bleeding time does not predict surgical bleeding. *Blood*, 77(12):2547–2552, June 1991.

[30] Patricia A Gum, Kandice Kottke-Marchant, Patricia A Welsh, Jennifer White, and Eric J Topol. A prospective, blinded determination of the natural history of aspirin resistance among stable patients with cardiovascular disease. *Journal of the American College of Cardiology*, 41(6):961–965, March 2003.

[31] C. P. M. Hayward, M. Pai, Y. Liu, K. A. Moffat, J. Seecharan, K. E. Webert, R. J. Cook, and N. M. Heddle. Diagnostic utility of light transmission platelet aggregometry: results from a prospective study of individuals referred for bleeding disorder assessments. *Journal of Thrombosis and Haemostasis*, 7(4):676–684, April 2009.

[32] H K Breddin. Can platelet aggregometry be standardized? *Platelets*, 16(3-4):151–158, June 2005.

[33] S. Harder, U. Klinkhardt, J. Graff, D. Westrup, CM Kirchmaier, E. Glusa, MA Mascelli, SJ Marciniak, A. Just, W. Lsche, et al. In vitro dose response to different GPIIb/IIIa-antagonists: inter-laboratory comparison of various platelet function tests. *Thrombosis research*, 102(1):3948, 2001.

[34] Axel C. Matzdorff, Gitta Khnel, Bettina Kemkes-Matthes, and Reinhard Voss. Comparison of GP IIB/IIIA inhibitors and their activity as measured by aggregometry, flow cytometry, single platelet counting, and the rapid platelet function analyzer. *Journal of Thrombosis and Thrombolysis*, 12(2):129–139, October 2001.

[35] Steven R Steinhubl, J. David Talley, Gregory A Braden, James E Tcheng, Peter J Casterella, David J Moliterno, Frank I Navetta, Peter B Berger, Jeffrey J Popma, George Dangas, Richard Gallo, David C Sane, Jorge F Saucedo, Gang Jia, A. Michael Lincoff, Pierre Theroux, David R Holmes, Paul S Teirstein, and Dean J Kereiakes. Point-of-care measured platelet inhibition correlates with a reduced risk of an adverse cardiac event after percutaneous coronary intervention : Results of the GOLD (AU-Assessing ultegra) multicenter study. *Circulation*, 103(21):2572–2578, May 2001.

[36] Helle L. Nielsen, Steen D. Kristensen, Sofie S. Thygesen, Jette Mortensen, Susanne B. Pedersen, Erik L. Grove, and Anne-Mette Hvas. Aspirin response evaluated by the VerifyNow aspirin system and light transmission aggregometry. *Thrombosis Research*, 123(2):267–273, December 2008.

[37] Wai-Hong Chen, Pui-Yin Lee, William Ng, Jeanette Yat-Yin Kwok, Xi Cheng, Stephen Wai-Luen Lee, Hung-Fat Tse, and Chu-Pak Lau. Relation of aspirin resistance to coronary flow reserve in patients undergoing elective percutaneous coronary intervention. *The American Journal of Cardiology*, 96(6):760–763, September 2005.

[38] Matthew J. Price, Peter B. Berger, Paul S. Teirstein, Jean-Franois Tanguay, Dominick J. Angiolillo, Douglas Spriggs, Sanjeev Puri, Mark Robbins, Kirk N. Garratt, Olivier F. Bertrand, Michael E. Stillabower, Joseph R. Aragon, David E. Kandzari, Curtiss T. Stinis, Michael S. Lee, Steven V. Manoukian, Christopher P. Cannon, Nicholas J. Schork, and Eric J. Topol. Standard- vs high-dose clopidogrel based on platelet function testing after percutaneous coronary intervention. *JAMA: The Journal of the American Medical Association*, 305(11):1097 –1105, March 2011.

[39] Rossella Marcucci, Anna Maria Gori, Rita Paniccia, Betti Giusti, Serafina Valente, Cristina Giglioli, Piergiovanni Buonamici, David Antoniucci, Rosanna Abbate, and Gian Franco Gensini. Cardiovascular death and nonfatal myocardial infarction in acute coronary syndrome patients receiving coronary stenting are predicted by residual platelet reactivity to ADP detected by a point-of-care assay a 12-month follow-up. *Circulation*, 119(2):237–242, January 2009.

[40] Alex Malinin, Alex Pokov, Malcolm Spergling, Anthony Defranco, Kenneth Schwartz, Dianne Schwartz, Ehtisham Mahmud, Dan Atar, and Victor Serebruany. Monitoring platelet inhibition after clopidogrel with the VerifyNow-P2Y12 rapid analyzer: The VERIfy thrombosis risk ASsessment (VERITAS) study. *Thrombosis Research*, 119(3):277–284, 2007.

[41] Sourav K. Kundu and Ted S. Geiselman. Method for testing coagulation of blood through bioactive porous partition members, December 1998. undefined-Filing Date: Jun 6, 1996 U.S. Classification: 436/69 International Classification: G01N 3386.

[42] Alain Gadisseur, Cedric Hermans, Zwi Berneman, Wilfried Schroyens, Hans Deckmyn, and Jan Jacques Michiels. Laboratory diagnosis and molecular classification of von willebrand disease. *Acta Haematologica*, 121(2-3):71–84, 2009.

[43] C. P. M. Hayward, P. Harrison, M. Cattaneo, T. L. Ortel, and A. K. Rao. Platelet function analyzer (PFA)-100R closure time in the evaluation of platelet disorders and platelet function. *Journal of Thrombosis and Haemostasis*, 4(2):312–319, February 2006.

[44] K. W. von Pape, E. Aland, and J. Bohner. Platelet function analysis with PFA-100 (r) in patients medicated with acetylsalicylic acid strongly depends

on concentration of sodium citrate used for anticoagulation of blood sample. *Thrombosis Research*, 98(4):295–299, 2000.

[45] Birte Fuchs, Ulrich Budde, Andrea Schulz, Craig M. Kessler, Claudine Fisseau, and Christoph Kannicht. Flow-based measurements of von willebrand factor (VWF) function: Binding to collagen and platelet adhesion under physiological shear rate. *Thrombosis Research*, 125(3):239–245, March 2010.

[46] A L Frelinger, Y Li, M D Linden, I Tarnow, M R Barnard, M L Fox, and A D Michelson. Aspirin 'resistance': role of pre-existent platelet reactivity and correlation between tests. *Journal Of Thrombosis And Haemostasis: JTH*, 6(12):2035–2044, December 2008.

[47] Marilena Crescente, Augusto Di Castelnuovo, Licia Iacoviello, Jos Vermylen, Chiara Cerletti, and Giovanni de Gaetano. Response variability to aspirin as assessed by the platelet function analyzer (PFA)-100. a systematic review. *Thrombosis and Haemostasis*, December 2007.

[48] J-L Reny, P De Moerloose, M Dauzat, and P Fontana. Use of the PFA-100 closure time to predict cardiovascular events in aspirin-treated cardiovascular patients: a systematic review and meta-analysis. *Journal Of Thrombosis And Haemostasis: JTH*, 6(3):444–450, March 2008.

[49] Paul A. Gurbel, Kevin P. Bliden, Kathleen Butler, Mark J. Antonino, Cheryl Wei, Renli Teng, Lars Rasmussen, Robert F. Storey, Tonny Nielsen, John W. Eikelboom, Georges Sabe-Affaki, Steen Husted, Dean J. Kereiakes, David Henderson, Dharmendra V. Patel, and Udaya S. Tantry. Response to ticagrelor in clopidogrel nonresponders and responders and effect of switching therapies the RESPOND study. *Circulation*, 121(10):1188–1199, March 2010.

[50] Graeme J Hankey and John W Eikelboom. Antithrombotic drugs for patients with ischaemic stroke and transient ischaemic attack to prevent recurrent major vascular events. *The Lancet Neurology*, 9(3):273–284, March 2010.

[51] Emmanuel J. Favaloro. Clinical application of the PFA-100.

[52] Hans R. Baumgartner. The role of blood flow in platelet adhesion, fibrin deposition, and formation of mural thrombi. *Microvascular Research*, 5(2):167–179, March 1973.

[53] Andrew J. Lucking, Rajesh Chelliah, Alexander D. Trotman, Thomas M. Connolly, Giora Z. Feuerstein, Keith A. Fox, Nicholas A. Boon, Juan J. Badimon, and David E. Newby. Characterisation and reproducibility of a human ex vivo model of thrombosis. *Thrombosis Research*, 126(5):431–435, November 2010.

[54] Gillian Stephens, Ming He, Connie Wong, Marzena Jurek, Hans-Christian Luedemann, Golnaz Shapurian, Kevin Munnelly, Craig Muir, Pamela B. Conley, David R. Phillips, and Patrick Andre. Development of a perfusion chamber assay to study in real time the kinetics of thrombosis and the antithrombotic characteristics of antiplatelet drugs. *Thrombosis Journal*, 10(1):11, August 2012. PMID: 22852789.

[55] RM Barstad, HE Roald, Y Cui, VT Turitto, and KS Sakariassen. A perfusion chamber developed to investigate thrombus formation and shear profiles in flowing native human blood at the apex of well- defined stenoses. *Arteriosclerosis, Thrombosis, and Vascular Biology*, 14(12):1984 –1991, December 1994.

[56] Shunichi Usami, Hsuan-Hsu Chen, Yihua Zhao, Shu Chien, and Richard Skalak. Design and construction of a linear shear stress flow chamber. *Annals of Biomedical Engineering*, 21(1):77–83, January 1993.

[57] Warwick S Nesbitt, Erik Westein, Francisco Javier Tovar-Lopez, Elham Tolouei, Arnan Mitchell, Jia Fu, Josie Carberry, Andreas Fouras, and Shaun P Jackson. A shear gradient-dependent platelet aggregation mechanism drives thrombus formation. *Nature Medicine*, 15(6):665–673, June 2009.

[58] Francisco Javier Tovar-Lopez, Gary Rosengarten, Erik Westein, Khashayar Khoshmanesh, Shaun P. Jackson, Arnan Mitchell, and Warwick S. Nesbitt. A microfluidics device to monitor platelet aggregation dynamics in response to strain rate micro-gradients in flowing blood. *Lab on a Chip*, 10:291, 2010.

[59] A. Para, D. Bark, A. Lin, and D. Ku. Rapid platelet accumulation leading to thrombotic occlusion. *Annals of Biomedical Engineering*, 39(7):1961–1971, March 2011.

[60] Edgar Gutierrez, Brian G. Petrich, Sanford J. Shattil, Mark H. Ginsberg, Alex Groisman, and Ana Kasirer-Friede. Microfluidic devices for studies of shear-dependent platelet adhesion. *Lab on a Chip*, 8(9):1486, 2008.

[61] Ashley Kita, Yumiko Sakurai, David R. Myers, Ross Rounsevell, James N. Huang, Tae Joon Seok, Kyoungsik Yu, Ming C. Wu, Daniel A. Fletcher, and Wilbur A. Lam. Microenvironmental geometry guides platelet adhesion and spreading: A quantitative analysis at the single cell level. *PLoS ONE*, 6(10):e26437, October 2011.

[62] Michelle Tsai, Ashley Kita, Joseph Leach, Ross Rounsevell, James N. Huang, Joel Moake, Russell E. Ware, Daniel A. Fletcher, and Wilbur A. Lam. In vitro modeling of the microvascular occlusion and thrombosis that occur in hematologic diseases using microfluidic technology. *Journal of Clinical Investigation*, 122(1):408–418, January 2012.

[63] K. B. Neeves, S. F. Maloney, K. P. Fong, A. A. Schmaier, M. L. Kahn, L. F. Brass, and S. L. Diamond. Microfluidic focal thrombosis model for measuring murine platelet deposition and stability: PAR4 signaling enhances shear-resistance of platelet aggregates. *Journal of Thrombosis and Haemostasis*, 6(12):2193–2201, December 2008.

[64] Keith B. Neeves and Scott L. Diamond. A membrane-based microfluidic device for controlling the flux of platelet agonists into flowing blood. *Lab on a chip*, 8(5):701–709, May 2008. PMID: 18432339 PMCID: 2612095.

[65] B. Linnemann, J. Schwonberg, H. Mani, S. Prochnow, and E. Lindhoff-Last. Standardization of light transmittance aggregometry for monitoring antiplatelet therapy: an adjustment for platelet count is not necessary. *Journal of Thrombosis and Haemostasis*, 6(4):677–683, April 2008.

[66] B. Savage, F. Almus-Jacobs, and Z. M. Ruggeri. Specific synergy of multiple substrate-receptor interactions in platelet thrombus formation under flow. *Cell*, 94(5):657–666, 1998.

[67] B Lincoln, A Ricco, G Meade, and L.P. Lee. Analysis of whole blood platelet translocation on a vWF-coated microfluidic flow chamber. In *12th International Conference on Miniaturized Systems for Chemistry and Life Sciences (TAS2008)*, pages 453–455, San Diego, CA, October 2008.

[68] D. M. Wootton, C. P. Markou, S. R. Hanson, and D. N. Ku. A mechanistic model of acute platelet accumulation in thrombogenic stenoses. *Annals of Biomedical Engineering*, 29(4):321–329, 2001.

[69] G. Dangas, J. J. Badimon, B. S. Coller, J. T. Fallon, S. K. Sharma, R. M. Hayes, P. Meraj, J. A. Ambrose, and J. D. Marmur. Administration of abciximab during percutaneous coronary intervention reduces both ex vivo platelet

thrombus formation and fibrin deposition - implications for a potential antico-agulant effect of abciximab. *Arteriosclerosis Thrombosis and Vascular Biology*, 18(8):1342–1349, 1998.

[70] A. D. Michelson, A. L. Frelinger, and M. I. Furman. Current options in platelet function testing. *American Journal of Cardiology*, 98(10):4N–10N, 2006.

[71] DN Ku. Blood flow in arteries. *Annual Review of Fluid Mechanics*, 29:399–434, 1997.

[72] Frank M White. *Fluid mechanics*. McGraw-Hill, Boston, MA, 4th edition, 1999.

[73] Andrea N. Para. *Preventing Rapid Platelet Accumulation Under Very High Shear Stress*. PhD thesis.

[74] Brian Kirby. *Micro- and Nanoscale Fluid Mechanics: Transport in Microfluidic Devices*. Cambridge University Press, 2010.

[75] Giovanni Paolo Galdi, Rolf Rannacher, Anne M. Robertson, and Stefan Turek. *Hemodynamical flows: modeling, analysis and simulation*. Birkhuser, April 2008.

[76] M. Faivre, M. Abkarian, K. Bickraj, and H. A. Stone. Geometrical focusing of cells in a microfluidic device: An approach to separate blood plasma. *Biorheology*, 43(2):147–159, 2006.

[77] M. J Davies and A. Thomas. Thrombosis and acute coronary-artery lesions in sudden cardiac ischemic death. *New England Journal of Medicine*, 310(18):11371140, 1984.

[78] E. Falk. Plaque rupture with severe pre-existing stenosis precipitating coronary thrombosis. characteristics of coronary atherosclerotic plaques underlying fatal occlusive thrombi. *British Medical Journal*, 50(2):127, 1983.

[79] D. C. Duffy, J. C. McDonald, O. J. A. Schueller, and G. M. Whitesides. Rapid prototyping of microfluidic systems in poly(dimethylsiloxane). *Analytical Chemistry*, 70(23):4974–4984, 1998.

[80] Lindsey K. Fiddes, Neta Raz, Suthan Srigunapalan, Ethan Tumarkan, Craig A. Simmons, Aaron R. Wheeler, and Eugenia Kumacheva. A circular cross-section PDMS microfluidics system for replication of cardiovascular flow conditions. *Biomaterials*, 31(13):3459–3464, May 2010.

[81] S. E. Nissen, J. C. Gurley, C. L. Grines, D. C. Booth, R. McClure, M. Berk, C. Fischer, and A. N. Demaria. Intravascular ultrasound assessment of lumen size and wall morphology in normal subjects and patients with coronary artery disease. *Circulation*, 84(3):1087–1099, 1991.

[82] Benedetta Enrico, Pal Suranyi, Christian Thilo, Lorenzo Bonomo, Philip Costello, and U. Joseph Schoepf. Coronary artery plaque formation at coronary CT angiography: morphological analysis and relationship to hemodynamics. *European Radiology*, 19(4):837–844, April 2009.

[83] Craig R. Forest, Miguel A. Saez, and Ian W. Hunter. Microforging technique for rapid, low-cost fabrication of lens array molds. *Appl. Opt.*, 46(36):8668–8673, 2007.

[84] J.Y. Kim, J.Y. Baek, K.A. Lee, and S.H. Lee. Automatic aligning and bonding system of PDMS layer for the fabrication of 3D microfluidic channels. *Sensors and Actuators A: Physical*, 119(2):593–598, April 2005.

[85] A. Bernardo, A. L. Bergeron, C. W. Sun, P. Guchhait, M. A. Cruz, J. A. Lpez, and J-F. Dong. Von willebrand factor present in fibrillar collagen enhances platelet adhesion to collagen and collagen-induced platelet aggregation. *Journal of Thrombosis and Haemostasis*, 2(4):660669, 2004.

[86] D. Fuard, T. Tzvetkova-Chevolleau, S. Decossas, P. Tracqui, and P. Schiavone. Optimization of poly-di-methyl-siloxane (PDMS) substrates for studying cellular adhesion and motility. *Microelectronic Engineering*, 85(56):1289–1293, May 2008.

[87] Viscosity of aqueous glycerine solutions. Technical report, Dow Chemical Company.

[88] Density of aqueous glycerine solutions. Technical report, Dow Chemical Company.

[89] L Badimon. Influence of arterial damage and wall shear rate on platelet deposition. ex vivo study in a swine model. *Arteriosclerosis, Thrombosis, and Vascular Biology*, 6(3):312–320, 1986.

[90] David Boas, J. Culver, J. Stott, and A. Dunn. Three dimensional monte carlo code for photon migration through complex heterogeneous media including the adult human head. *Optics Express*, 10(3):159, February 2002.

[91] Lihong Wang, Steven L. Jacques, and Liqiong Zheng. MCML–Monte carlo modeling of light transport in multi-layered tissues. *Computer Methods and Programs in Biomedicine*, 47(2):131–146, July 1995.

[92] W. F Cheong, S. A Prahl, and A. J Welch. A review of the optical properties of biological tissues. *Quantum Electronics, IEEE Journal of*, 26(12):21662185, 1990.

[93] T. Collier, D. Arifler, A. Malpica, M. Follen, and R. Richards-Kortum. Determination of epithelial tissue scattering coefficient using confocal microscopy. *IEEE Journal of Selected Topics in Quantum Electronics*, 9(2):307– 313, April 2003.

[94] Ravikant Samatham and Steven L. Jacques. Determine scattering coefficient and anisotropy of scattering of tissue phantoms using reflectance-mode confocal microscopy. In *Proceedings of SPIE*, pages 718711–718711–8, San Jose, CA, USA, 2009.

[95] C. Bordier, C. Andraud, E. Charron, J. Lafait, M. Anastasiadou, and A. Martino. Illustration of a bimodal system in intralipid-20% by polarized light scattering: experiments and modeling. *Applied Physics A*, 94(2):347–355, July 2008.

[96] Hideto Matsui, Mitsuhiko Sugimoto, Tomohiro Mizuno, Shizuko Tsuji, Shigeki Miyata, Michio Matsuda, and Akira Yoshioka. Distinct and concerted functions of von willebrand factor and fibrinogen in mural thrombus growth under high shear flow. *Blood*, 100(10):3604 –3610, November 2002.

[97] GVR Born. Observations on the change in shape of blood platelets brought about by adenosine diphosphate. *The Journal of Physiology*, 209(2):487, 1970.

[98] P. Harrison. Platelet function analysis. *Blood Reviews*, 19(2):111–123, 2005.

[99] Robert Hoffman and Michael Davidson. Contrast in optical microscopy, 2012.

[100] Herbert M Cullis. Method and apparatus for measuring the hematocrit of blood, 1981.

[101] Flannery Conor. *Thrombus Formation Under High Shear in Arterial Stenotic Flow (MS Thesis)*. PhD thesis, Georgia Institute of Technology, 2005.

[102] G. V. R. Born and M. J. Cross. The aggregation of blood platelets. *The Journal of Physiology*, 168(1):178, 1963.

[103] Matthew K. Runyon, Bethany L. Johnson-Kerner, and Rustem F. Ismagilov. Minimal functional model of hemostasis in a biomimetic microfluidic system. *Angewandte Chemie International Edition*, 43(12):1531–1536, March 2004.

[104] D N Ku and D Liepsch. The effects of non-newtonian viscoelasticity and wall elasticity on flow at a 90 degrees bifurcation. *Biorheology*, 23(4):359–370, 1986. PMID: 3779061.

[105] D. A. Steinman and C. Ross Ethier. The effect of wall distensibility on flow in a two-dimensional end-to-side anastomosis. *Journal of Biomechanical Engineering*, 116(3):294, 1994.

[106] Dehong Zeng, Evangelos Boutsianis, Marc Ammann, Kevin Boomsma, Simon Wildermuth, and Dimos Poulikakos. A study on the compliance of a right coronary artery and its impact on wall shear stress. *Journal of Biomechanical Engineering*, 130(4):041014–11, 2008.

[107] M. H. Friedman, C. B. Bargeron, D. D. Duncan, G. M. Hutchins, and F. F. Mark. Effects of arterial compliance and non-newtonian rheology on correlations between intimal thickness and wall shear. *Journal of Biomechanical Engineering*, 114(3):317–320, 1992.

[108] Hoskins Peter R. Physical properties of tissues relevant to arterial ultrasound imaging and blood velocity measurement. *Ultrasound in Medicine & Biology*, 33(10):1527–1539, October 2007.

[109] Bs Gow and Cd Hadfield. The elasticity of canine and human coronary arteries with reference to postmortem changes. *Circulation Research*, 45(5):588 –594, November 1979.

[110] Christopher Ross Ethier and Craig Alexander Simmons. *Introductory biomechanics: from cells to organisms.* Cambridge University Press, 1 edition, 2007.

[111] K. Hosokawa, T. Ohnishi, T. Kondo, M. Fukasawa, T. Koide, I. Maruyama, and K. A. Tanaka. A novel automated microchip flow-chamber system to quantitatively evaluate thrombus formation and antithrombotic agents under blood flow conditions. *Journal of Thrombosis and Haemostasis*, 9(10):2029–2037, October 2011.

[112] K. Kottke-Marchant, J. B. Powers, L. Brooks, S. Kundu, and D. J. Christie. The effect of antiplatelet drugs, heparin, and preanalytical variables on platelet function detected by the platelet function analyzer (PFA-100). *Clinical And Applied Thrombosis/Hemostasis: Official Journal Of The International Academy Of Clinical And Applied Thrombosis/Hemostasis*, 5(2):122–130, 1999.

[113] Thomas V. Colace, Ryan W. Muthard, and Scott L. Diamond. Thrombus growth and embolism on tissue factor-bearing collagen surfaces under flow role of thrombin with and without fibrin. *Arteriosclerosis, Thrombosis, and Vascular Biology*, 32(6):1466–1476, June 2012.

[114] Melissa Li, David N. Ku, and Craig R. Forest. Microfluidic system for simultaneous optical measurement of platelet aggregation at multiple shear rates in whole blood. *Lab Chip*, 12(7):1355–1362, February 2012.

[115] Stephen R. Hanson and Kjell S. Sakariassen. Blood flow and antithrombotic drug effects. *American Heart Journal*, 135(5, Supplement):S132–S145, May 1998.

[116] P. Whittaker, R. A. Kloner, D. R. Boughner, and J. G. Pickering. Quantitative assessment of myocardial collagen with picrosirius red staining and circularly polarized light. *Basic Research in Cardiology*, 89(5):397–410, 1994.

[117] Markus Velten, Kathryn M. Heyob, Lynette K. Rogers, and Stephen E. Welty. Deficits in lung alveolarization and function after systemic maternal inflammation and neonatal hyperoxia exposure. *Journal of Applied Physiology*, 108(5):1347–1356, May 2010.

[118] M. Mertig, U. Thiele, J. Bradt, G. Leibiger, W. Pompe, and H. Wendrock. Scanning force microscopy and geometric analysis of two-dimensional collagen network formation. *Surface and Interface Analysis*, 25(7-8):514521, 1997.

[119] Mark R. Looney, John X. Nguyen, Yongmei Hu, Jessica A. Van Ziffle, Clifford A. Lowell, and Michael A. Matthay. Platelet depletion and aspirin treatment protect mice in a two-event model of transfusion-related acute lung injury. *Journal of Clinical Investigation*, October 2009.

[120] Matthew J. Price, Peter B. Berger, Dominick J. Angiolillo, Paul S. Teirstein, Jean-Franois Tanguay, David E. Kandzari, Christopher P. Cannon, and Eric J. Topol. Evaluation of individualized clopidogrel therapy after drug-eluting stent implantation in patients with high residual platelet reactivity: Design and rationale of the GRAVITAS trial. *American Heart Journal*, 157(5):818–824.e1, May 2009.

[121] J D Hellums. 1993 whitaker lecture: biorheology in thrombosis research. *Annals of biomedical engineering*, 22(5):445–455, October 1994. PMID: 7825747.

[122] J.R Vane and R.M Botting. The mechanism of action of aspirin. *Thrombosis Research*, 110(56):255–258, June 2003.

[123] Gerrit Veen, Albert Meyer, Freek W.A. Verheugt, Christ J.P.J. Werter, Hans de Swart, Kong I. Lie, Joop M.J. van der Pol, H.Rolf Michels, and Machiel J. van Eenige. Culprit lesion morphology and stenosis severity in the prediction

of reocclusion after coronary thrombolysis: Angiographic results of the APRI-COT study. *Journal of the American College of Cardiology*, 22(7):1755–1762, December 1993.

[124] RM Barstad, U Orvim, MJ Hamers, GE Tjnnfjord, FR Brosstad, and KS Sakariassen. Reduced effect of aspirin on thrombus formation at high shear and disturbed laminar blood flow. *Thrombosis and Haemostasis*, 75(5):827–832, May 1996.

[125] JL Moake, NA Turner, NA Stathopoulos, L Nolasco, and JD Hellums. Shear-induced platelet aggregation can be mediated by vWF released from platelets, as well as by exogenous large or unusually large vWF multimers, requires adenosine diphosphate, and is resistant to aspirin. *Blood*, 71(5):1366 –1374, May 1988.

[126] Shaun P Jackson, Warwick S Nesbitt, and S Kulkarni. Signaling events underlying thrombus formation. *Journal of Thrombosis and Haemostasis*, 1(7):1602–1612.

[127] C. M. Helgason, K. M. Bolin, J. A. Hoff, S. R. Winkler, A. Mangat, K. L. Tortorice, and L. D. Brace. Development of aspirin resistance in persons with previous ischemic stroke. *Stroke*, 25(12):2331–2336, December 1994.

[128] David Bark and D. N. Ku. ScienceDirect - journal of biomechanics : Wall shear over high degree stenoses pertinent to atherothrombosis. http://www.sciencedirect.com.proxy.library.emory.edu/science?_ob=ArticleURL&_udi=B6T8 50V0FBY-1&_user=655046&_coverDate=11%2F16%2F2010&_rdoc=1&_fmt=high&_orig=sea

[129] Keith B. Neeves, Abimbola A. Onasoga, Ryan R. Hansen, Jessica J. Lilly, Diana Venckunaite, Meghan B. Sumner, Andrew T. Irish, Gary Brodsky, Marilyn J.

Manco-Johnson, and Jorge A. Di Paola. Sources of variability in platelet accumulation on type 1 fibrillar collagen in microfluidic flow assays. *PLoS ONE*, 8(1), January 2013. PMID: 23355889 PMCID: PMC3552855.

Microfluidic system for thrombosis under multiple shear rates and platelet therapies

Melissa Li

174 Pages

Directed by Professor Craig R. Forest